Tampere University

Jani Patrakka

AZOBENZENE PHOTOISOMERISATION IN HUMIDITY SENSING

Master's thesis
Faculty of Engineering and Natural Sciences
Examiners: Prof. Arri Priimägi, Dr. Matti Virkki
June 2020

ABSTRACT

Jani Patrakka: Azobenzene photoisomerisation in humidity sensing
Master's thesis
Tampere University
Degree Programme in Science and Engineering
June 2020

Azobenzenes are organic molecules with the ability to photoisomerise, to switch upon illumination between two molecular structures with the same atoms but in a different conformation. Typically, only one of the structures, the rod-like *trans*-azobenzene, is stable and thus molecules in the *cis* form spontaneously relax back to energetically more favourable *trans*-isomer over time. The amount of time required for the relaxation depends on the ambient conditions, such as temperature, humidity, and molecular environment. To be more precise, the relaxation rate depends exponentially on temperature, and in some cases humidity, so if the temperature and relaxation rate can be measured, ambient humidity can be determined.

As the electron configuration of the molecule changes in photoisomerisation, so does the optical response, and hence *cis* and *trans* isomers differ by absorption spectra, for example. In this thesis, azobenzenes self-assemble into supramolecular complexes with hydrogen-bonding polymers to form thin films. Absorption spectra are then periodically measured to detect changes in isomer populations. The films can be illuminated with light causing photoisomerisation and the time needed to recover to initial state can be determined from the change in absorption.

Substituents in azobenzene affect the isomerisation behaviour. In this work, eight azobenzenes were selected to study their isomerisation at various humidity levels. One hydroxyazobenzene was also chosen for two additional set of experiments: (i) the first explored the effects of molecular environment factors such as polymer chain length and mole fraction on isomerisation, and (ii) the second studied whether isomerisation behaviour and material optical properties change over time due to aging effects.

Molecular comparison revealed interesting details about the effects of substitution on isomerisation behaviour. Higher electron density at the azo bond reduced humidity sensitivity, whereas lower electron density produced more humidity sensitive isomerisation behaviour. Weak push-pull substitution led to fast relaxation, while strong push-pull substitution appears to be insensitive or slightly negatively sensitive to humidity. Optimal combination for humidity sensing across the humidity range from the studied molecules is azobenzene para-substituted with cyano and hydroxy groups in both ends of the azobenzene for low humidity measurements, while an azobenzene with para-substituted dimethylamino and hydroxy groups was most suited for high humidity measurements. Azobenzene para-substituted with nitro and amino groups was optimal for temperature sensing.

No aggregation was observed in aging studies but both absorption and isomerisation rate changed over time. Optimal combination for commercial sensor applications would be to use 1:4 mole fraction between azobenzene and 60 000 g/mol molar weight poly(4-vinylpyridine) polymer with 24 h annealing time at 80 °C. These thin films can be used reliably in humidity sensing about 4 weeks after film preparation. However, more research is needed on the effect of the choice of polymer and mole fraction for comprehensive understanding of the aging effects.

Based on the results of this thesis, azobenzene-based humidity sensing has a market potential in both cost-effective sensors and high-end sensors for high sensitivity or extreme conditions. The demand for both exists but further research is needed in order to understand the mechanism of azobenzene humidity sensing as well as to continue mapping potential molecules for humidity sensing purposes.

Keywords: absorption, azobenzene, humidity sensing, lifetime, photoisomerisation, thin film

TIIVISTELMÄ

Jani Patrakka: Atsobentseenien valoisomerisaatio ilmankosteuden mittauksessa
Diplomityö
Tampereen yliopisto
Teknis-luonnontieteellinen DI-tutkinto-ohjelma
Kesäkuu 2020

Atsobentseenit ovat orgaanisia molekyylejä, joilla on kyky valoisomeroitua, eli vaihtaa molekulaarista rakennettaan kahden muodon välillä, joissa ovat samat atomit mutta eri järjestyksessä. Tyypillisesti vain toinen muodoista, sauvamainen *trans*-atsobentseeni, on vakaa, ja siksi molekyylit palautuvat spontaanisti takaisin energeettisesti kannattavimpaan isomeeriin ajan kuluessa. Palautumiseen kuluva aika riippuu ympäristön olosuhteista, kuten lämpötilasta, ilmankosteudesta ja molekulaarisesta ympäristöstä. Tarkemmin sanottuna palautumisnopeus riippuu eksponentiaalisesti lämpötilasta ja joissain tapauksissa ilmankosteudesta, joten jos lämpötila ja palautumisnopeus voidaan mitata, ympäristön ilmankosteus voidaan määrittää.

Kun molekyylin elektronikonfiguraatio muuttuu valoisomeraatiossa, myös molekyylin optinen vaste muuttuu, ja siten *cis* ja *trans*-isomeerit eroavat esimerkiksi absorptiospektrien perusteella. Tässä työssä atsobentseenit järjestyvät supramolekulaarisiksi komplekseiksi vetysidoksia muodostavien polymeerien kanssa muodostaakseen ohutkalvoja, joista mitataan absorptiospektrejä tasaisin väliajoin havaitakseen muutoksia isomeeripopulaatioissa. Kalvoja valaisemalla voidaan aiheuttaa valoisomeraatio, josta palautumiseen kuluva aika määritetään absorption muutoksesta.

Substituentit vaikuttavat isomeroitumiskäyttäytymiseen atsobentseeneissä. Tässä työssä tarkasteltavaksi valittiin kahdeksan atsobentseeniä isomeraatiotutkimuksiin eri ilmankosteuksissa. Yksi hydroksiatsobentseeni valittiin myös kahteen muuhun koesarjaan: (i) ensimmäisessä tutkittiin molekulaarisen ympäristön tekijöiden, kuten polymeeriketjun pituuden tai mooliosuuden, vaikutuksia isomeraatioon, ja (ii) toisessa tutkittiin, muuttuvatko isomeraatiokäyttäytyminen ja materiaalin optiset ominaisuudet tietyllä aikavälillä ikääntymisvaikutusten vuoksi.

Molekyylien vertailu paljasti mielenkiintoisia yksityiskohtia substituution vaikutuksesta isomeroitumiskäyttäytymiseen. Suurempi elektronitiheys atsosidoksessa vähensi ilmankosteusriippuvuutta, kun taas alhaisempi elektronitiheys tuotti ilmankosteudelle herkempää käyttäytymistä. Heikko varausepäsymmetria johti nopeaan palautumiseen, kun vahva varausepäsymmetria vaikuttaa olevan epäherkkä tai hieman negatiivisesti herkkä ilmankosteudelle. Paras yhdistelmä ilmankosteuden mittaamiseen koko ilmankosteusalueella oli tutkittuja molekyylejä käyttäen syano- ja hydroksyyliryhmällä para-substituoitu atsobentseeni alhaisen ilmankosteuden mittauksiin, kun taas dimetyyliamino- ja hydroksyyliryhmällä atsobentseeni soveltui parhaiten korkean ilmankosteuden mittauksiin. Nitro- ja aminoryhmällä atsobentseeni oli soveltuvin lämpötilan mittaamiseen.

Aggregoitumista ei havaittu ikääntymismittauksissa, mutta sekä absorptio että isomeroitumisnopeus muuttuivat ajan kuluessa. Paras yhdistelmä kaupalliseen sensoriin olisi 1:4 mooliosuus atsobentseenin ja 60 000 g/mol moolimassan poly(4-vinyylipyridiini)-polymeerin välillä sekä 24 tunnin lämpökäsittely 80 °C:ssa. Näitä ohutkalvoja voidaan käyttää luotettavasti ilmankosteuden mittaamiseen noin neljän viikon kuluttua valmistuksesta. Kuitenkin lisätutkimusta kaivataan polymeerin valintaan sekä mooliosuuteen ymmärtääksemme kattavasti ikääntymisen vaikutuksia.

Näiden tulosten perusteella atsobentseenipohjaisille ilmankosteuden sensoreille on kysyntää markkinoilla sekä kustannustehokkaan sensorin että korkealaatuisen sensorin eli korkean tarkkuuden tai ääriolosuhteiden parissa. Kysyntää molemmille löytyy, mutta lisätutkimusta tarvitaan ymmärtääkseen atsobentseenien ilmankosteuden havaitsemisen mekanismia sekä jatkaakseen mahdollisten ilmankosteuden havaitsemiseen soveltuvien molekyylien kartoittamista.

Avainsanat: absorptio, atsobentseeni, elinaika, ilmankosteuden mittaus, ohutkalvo, valoisomerisaatio

PREFACE

What a journey! 10 months ago when I started working on my thesis I could not have imagined how fascinating sensor applications can be, but then again I would not have guessed I would find such an amazing group of people and brilliant researchers at Smart Photonic Materials. To image I heard Arri give a presentation about light robotics by chance in 2016, got excited and ended up joining the gang. One of the best decisions of my life for sure. And now, almost four years later, it all culminated to this thesis which was funded by European Research Council Proof of Concept Project "OPTOSENSE: Optical Humidity Sensing via Azobenzene Photoisomerization."

I wish to thank my outstanding supervisors: the talented and inspiring Dr. Matti Virkki, with whom I had the pleasure to work with these past 10 months, and the one and only professor Arri Priimägi, the best boss I have ever had or seen. I could not have asked for better examiners, Arri and Matti were always there when I needed help or advice and they kept me motivated even through the most repetitive aging measurements. Luckily no day in the lab was dull, thanks to the wonderful coworkers at Red Labs – thank you all lovely SPMers and other Sähkötalo folk alike!

A huge thanks goes to my friends and family, I could not have done this without your support. Thank you Aleksi and Ivan for peer support in our thesis struggles, thank you mum for your infinite support, and thank you Survivor for your Eye of the Tiger, the motivational theme song that carried me through the writing process. Thank you Dr. Neill Booth for igniting the spark of academy in me, and finally, thank you Emma. Your encouragement and compassion made my day every day.

Tampere, 29th June 2020

Jani Patrakka

CONTENTS

LIST OF FIGURES

LIST OF TABLES

LIST OF SYMBOLS AND ABBREVIATIONS

A	Absorbance
K	Reaction equillibrium constant
P	Vapour pressure
T	Temperature
γ	Mass concentration
k	Isomerisation rate constant
λ	Wavelength
λ_{exc}	Excitation wavelength
λ_{iso}	Wavelength of the isosbestic point
λ_{max}	Wavelength of the absorption maximum
λ_{mon}	Monitoring wavelength
μ	Dipole moment
ρ	Reaction constant
σ	Substituent constant
t	Time
τ	Lifetime of *cis* state
2PAP	4-Ethyl-4'-hydroxyazobenzene
CN-OH	4-Cyano-4'-hydroxyazobenzene
DMA-OH	4-Dimethylamino-4'-hydroxyazobenzene
MeO-OH	4-Methoxy-4'-hydroxyazobenzene
NH_2-NH_2	4,4'-azodianiline
NO_2-NH_2	4-(4-Nitrophenylazo)aniline
NO_2-OH	4-Nitro-4'-hydroxyazobenzene
Pyr-OH	4-Pyridyl-4'-hydroxyazobenzene
P4VP	Poly(4-vinylpyridine)
HOMO	Highest occupied molecular orbital
LUMO	Lowest unoccupied molecular orbital
RH	Relative humidity
UV	Ultraviolet

1 INTRODUCTION

Photonics often brings to mind semiconductors and other inorganic compounds. Silicon and group IV photonics in general have undeniably shaped our economy, community, and lives for decades through technological advancements in communications, computation, imaging and lighting [1], to name a few. However, organic materials have become an increasingly interesting alternative for conventional photonic materials due to their high functional tunability through synthetic chemistry, low manufacturing costs thanks to solution processing and competitive mechanical properties such as flexibility [2]. Moreover, organic materials enable a wide range of applications in photonics due to the unique ability to tune the optical response of the material, such as in-situ changes in absorbance, refractive index or anisotropicity.

As one example from the domain of polymer-based organic photonic materials, photoresponsive thin films can be fabricated by mixing the photoresponsive molecules with suitable polymers, adding organic solvent and forming a thin film from the solution through rotation and evaporation method known as spin coating. *Photoswitches*, or molecules capable of reversibly switching between at least two conformational states in response to light, have proven particularly interesting in recent years. One classic example of a photoswitch is *azobenzene*, a molecule capable of photoisomerising between *trans* and *cis* isomers after exposure to suitable light. This intrinsic property allows for photocontrol on a molecular level for applications ranging from data storage and energy harvesting to ambient sensing and drug delivery.

Although azobenzenes have been thoroughly studied as dyes for over a hundred years and their prominent photoresponsive properties have been equally well researched, there is still much to be understood about their photoresponsive behaviour as well as potential applications in the field of photonics. The purpose of this thesis is to unravel a new utilisation for azobenzenes in humidity sensing with the potential for commercial applications, and in the process demonstrates that despite its extensive and versatile history, azobenzene remains a topical and fruitful source for new discoveries and solutions. The demand for accurate humidity sensing in extreme conditions exists, and azobenzene-based sensors have a realistic possibility to deliver.

Chapter 2, Theory and background presents the theory necessary to discuss azobenzene thin films for humidity sensing purposes. Azobenzene classification is presented along with their essential features and a short overview of different strategies of producing azobenzene-containing thin films. Lastly, commercially available humidity sensing solu-

tions are discussed and compared to azobenzene thin films in humidity sensing. Chapter 3, Sample fabrication and analysis methods, elaborates thee process of sample preparation and data processing as well as the experimental setup used for the measurements. Results of the measurements are presented in Chapter 4 along with the discussion of their significance, and finally conclusions of the thesis along with an outlook on future research is presented in Chapter 5.

2 THEORY AND BACKGROUND

This chapter presents the theory necessary to discuss azobenzene thin films for humidity sensing purposes. Theory section will classify azobenzenes along with their features essential for the scope of this thesis, present a short overview of different strategies of producing azobenzene-containing thin films and discuss modern commercially available humidity sensing solutions, finishing by elaborating how azobenzene thin films can be utilised in humidity sensing.

2.1 Azobenzenes

Azobenzenes are diazene derivative organic molecules with two benzene rings linked by an *azo bond* (-N=N-), a double bond between a pair of nitrogen atoms [3]. In this thesis, the term "azobenzene" is used interchangeably for both unsubstituted azobenzene and substituted azobenzene derivatives. Since its first description in 1834 [4] and synthesis two decades later [5], azobenzenes have aroused interest for dye and pigment applications for various industries due to their strong UV/Vis absorption bands and consequential colours, nowadays covering over 60 % of the global disperse dyes market [6, p. 135].

As photostability is a requirement for industrial dye applications, azobenzene photoisomerisation was initially a vexatious discovery leading to efforts to reduce the *cis*-isomer stability [7], but ultimately the research focus moved to unravelling the photonics applications of utilising the photoisomerisation process [8]. In the past decades, azobenzenes have been elevated from chromophores in common dye and pigment-related research to a prototype molecular photoswitch in the forefront of organic photonics [9, p. 94].

The photoresponsivity driving the research on azobenzenes stems from the electron density distribution across the molecule: The elongated azobenzene molecule illustrated in 2.1 (a) forms a *conjugated* system where π bond electrons are delocalised across the conjugation length, leading to significant electron density in the entire region and *aromaticity* in the benzene rings with resulting higher stability, planarity and less bond length alternation in the ring [10]. Aromaticity is here simply defined with Hückel's rule: a conjugated planar ring is aromatic if it has $4n + 2$ π electrons [11]. Extending the π-conjugated system with suitable substituents can be used to red shift the strong absorption band to visible spectrum and hence the wavelength range of excitation for photoisomerisation [9] as elaborated in section 2.1.1.

Substituting electron donor and acceptor groups into the benzene ring also allows for tailoring the nonlinear optical response [12]. Perhaps the most prominent optical feature in azobenzenes generated through photoisomerisation is their ability to show photoinduced *anisotropy*, meaning material properties like refractive index differ when observed along one axis compared to another [13]. Through this anisotropy, material can exhibit optical effects such as *birefringence* and *dichroism* where refractive index or absorption of the material depends on the polarisation of incident light with respect to anisotropic material axes, respectively.

2.1.1 Spectral classification

Azobenzenes are typically divided into three distinct spectroscopic classes differing by their HOMO-LUMO gap: azobenzene-type molecules, aminoazobenzenes, and pseudostilbenes [14, pp. 4–5]. Division into these classes is based on the energy of the *trans*-isomer transitions from the highest occupied molecular orbital (HOMO) to lowest unoccupied molecular orbital (LUMO), corresponding $\pi \rightarrow \pi^*$ transitions in their azo bond [7]. The energy of transition determines at which wavelength λ_{max} absorption maximum lies and thus the observed colour of the bulk [15, pp. 426–427]. Change in electron density distribution causes shift in the electronic absorption and thus in the transition energy, meaning electron-donating or electron-withdrawing substituents in benzene rings results in considerable changes in light absorption in the UV-Visible wavelength region. Azobenzenes can thus be spectrally engineered for absorption at a desired wavelength range with suitable choice of substituents [16]. Differences between azobenzene classes in terms of molecular structure, colour and spectral features are illustrated in Fig 2.1.

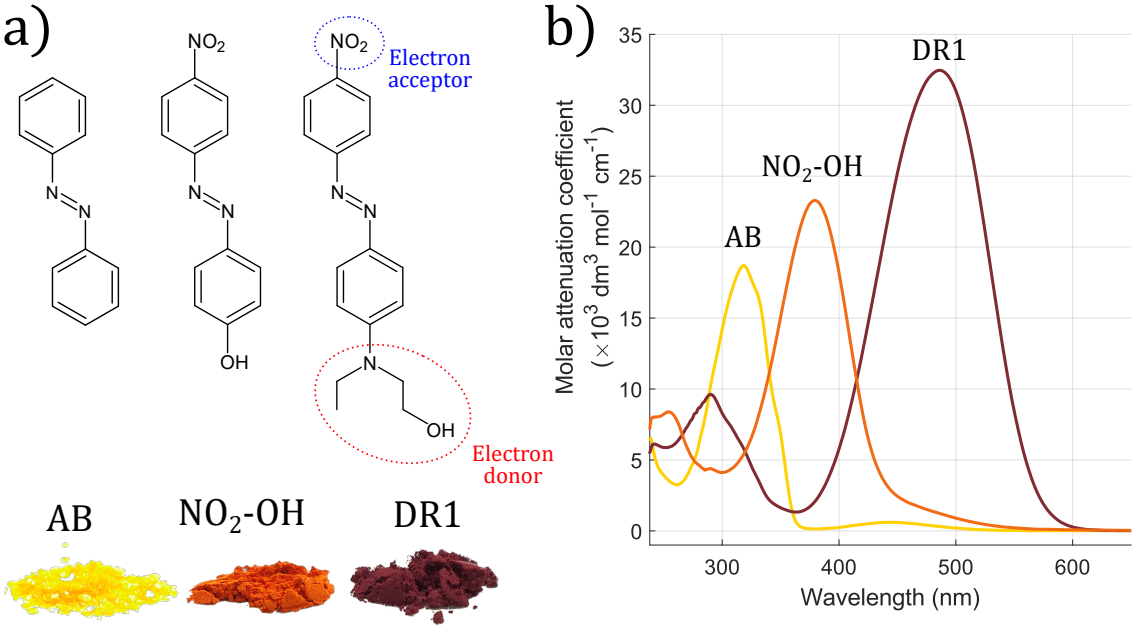

Figure 2.1. Three classes of azobenzenes. *a) Molecular structures of azobenzene-type (AB), aminoazobenzene-type (NO_2-OH), and pseudostilbene-type (Disperse Red 1, DR1) azobenzenes, images of their stock powder and b) their absorption spectra in 50 µM tetrahydrofuran solutions. Adapted from [17].*

Azobenzene-type molecules are spectrally similar to the unsubstituted azobenzene with symmetry-allowed $\pi \rightarrow \pi^*$ transition at a considerably higher energy than symmetry-forbidden $n \rightarrow \pi^*$ transition producing an absorption spectrum similar to that visible at 2.1 (b) for azobenzene [16]. Very low-intensity $n \rightarrow \pi^*$ absorption band can be observed in the visible region around 440 nm and notably higher intensity $\pi \rightarrow \pi^*$ absorption band in the UV region with the peak around 320 nm in 50 μM THF solution as shown with unsubstituted azobenzene in Fig 2.1. With a relatively stable *cis* isomer, azobenzene-type azobenzenes typically have *cis* lifetimes in the order of hours [18]. Given the absorption spectrum, azobenzene-type molecules are typically yellow as can be seen in the image of unsubstituted azobenzene powder.

Aminoazobenzene-type molecules are ortho- or para-substituted azobenzenes with an electron-donating group like amino or hydroxyl groups [19, p. 6]. Electron-donating substituent causes changes in the electron density distribution and thus a red shift of the $\pi \rightarrow \pi^*$ transition while the $n \rightarrow \pi^*$ transition remains unaffected. This reduces the energy difference of the transitions, bringing the prominent $\pi \rightarrow \pi^*$ band very close to lower-intensity $n \rightarrow \pi^*$ band and effectively overshadowing it. The shift in electron density makes the *cis* isomer more unstable, reducing typical *cis* lifetimes of aminoazobenzenes to the order of minutes [18]. Absorption peak can be observed in 2.1 (b) for NO_2-OH around 380 nm in 50 μM THF solution causing the orange colour of aminoazobenzene-type molecules as can be seen in the image of NO_2-OH powder.

Pseudo-stilbene-type molecules are para-substituted azobenzenes in both ends of the azobenzene with electron-donating and electron-withdrawing groups, resulting in lower electron density at electron donor and consequently higher electron density at electron acceptor [19, p. 6]. This is commonly known as the *push-pull* substitution pattern [12, p. 4]. The electron density distribution over the conjugated system causes even further red shift of the $\pi \rightarrow \pi^*$ transition while the $n \rightarrow \pi^*$ transition remains unaffected. For pseudo-stilbenes, $\pi \rightarrow \pi^*$ absorption band is at lower energy and thus higher wavelength than $n \rightarrow \pi^*$ band. The strong push-pull substitution pattern renders the *cis* isomer very unstable with typical *cis* lifetimes of pseudo-stilbenes in the order of mere seconds [18]. Absorption peak can be observed in 2.1 (b) for Disperse Red 1 (DR1) around 490 nm in 50 μM THF solution, overshadowing the lower intensity $n \rightarrow \pi^*$ band and causing the red colour of pseudostilbene-type molecules as can be seen in the image of DR1 powder.

Despite the class names, aminoazobenzenes can have a hydroxyl group as electron-donating substituents, too, in addition to any other substituents in the benzene rings. Similarly, pseudo-stilbenes are not stilbenes as the linkage combining benzene is an azo bond, not an ethylene bridge. Furthermore, pseudo-stilbenes can have versatile electron-donating and electron-withdrawing substituents, for example amino or hydroxy groups and nitro or cyano groups.

Substituent	σ_{meta}	σ_{para}
H	0	0
NO_2	0.71	0.78
CN	0.56	0.66
Pyr (C_5H_5N)	0.27	0.44
C_2H_5	-0.07	-0.15
MeO (OCH_3)	0.12	-0.27
OH	0.12	-0.37
NH_2	-0.16	-0.66
DMA ($N(CH_3)_2$)	-0.15	-0.83

Table 2.1. Substituent constants. *For substituents used in this thesis, negative values indicate electron donor and positive values electron acceptor character [24].*

2.1.2 Substituents and electron density

Substituent groups on aromatic rings influence the reaction rate of the molecule through asymmetric electron density distribution [20, pp. 206–207]. Two effects dictating how electron distribution in a π conjugated system is altered are *mesomeric* effects (also know as resonance effect) and *inductive* effects [20, p. 58]. Inductive effects are present in a sigma bond and arise from differences in electronegativity of bonded substituent atom while mesomeric effect eventuates through interaction of two π bonds or between a π bond and lone pair of electrons as polarity produced in the molecule [20, pp. 206–207].

Mesomeric effects can extend through the molecule in π conjugated systems, accounting for stabilisation or destabilisation depending on substituent electron-donating or withdrawing character. Electron donors produce more *nucleophilic* π conjugated systems, reducing stability and vice versa [20, pp. 206–207], although steric effects can reduce substituent's mesomeric impact of the system. The effects of *meta* and *para*-position substituents can be estimated from linear free energy relationship of benzoic acid dissociation reactions using the Hammett equation [21, p. 6]

$$log\frac{K}{K_0} = log\frac{k}{k_0} = \sigma\rho, \tag{2.1}$$

where K and K_0 are the equilibrium constants for substituted and unsubstituted benzyl group containing molecules, respectively, and k and k_0 and the corresponding rate constants, σ is the *substituent constant* solely depending on substitution and ρ is the *reaction constant* depending on the specific reaction but independent of substitution. Performing different reactions for substituted and unsubstituted azobenzenes reveals a linear dependence of $log\frac{K}{k_0}$ term from ρ which in turn yields substituent constant from the slope [22]. Negative σ values correspond to electron donor character, and for electron-withdrawing groups $\sigma > 0$. Table 2.1 presents the substituent constants essential for this thesis [23].

As can be seen from table 2.1, substituent constants are normalised for hydrogen $\sigma_H = 0$. Based on substituent constants in *para*-position, electron-donating groups are hydroxy, ethyl, DMA and methoxy groups, while cyano and nitro groups are electron-withdrawing.

2.1.3 Photoisomerisation

The defining feature of azobenzenes is their reversible photoisomerisation[1] between thermally stable planar *trans*-isomer and metastable bent *cis*-isomer with benzene rings not in plane [15, p. 426]. Because of the difference in isomer stability and large energy barrier of isomerisation, most azobenzenes are in *trans*-isomer in the dark [12, pp. 4–5]. Upon illumination with a wavelength within the *trans*-azobenzene absorption band, some azo bond electron absorbs the photon, $\pi \rightarrow \pi^*$ or $n \rightarrow \pi^*$ transition occurs and azobenzene isomerises efficiently into *cis*-isomer [9, pp. 92–94]. This light-induced interconversion is illustrated in Fig 2.2.

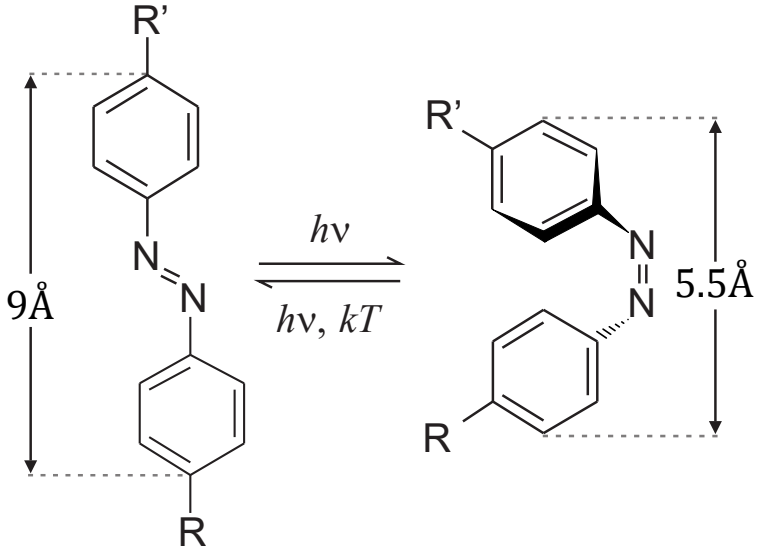

Figure 2.2. *a)* ***Photoisomerisation of azobenzene.*** *Photoexcitation causes* trans $\rightarrow$ cis *isomerisation, while reverse isomerisation can occur thermally or via excitation at* cis*-isomer absorption band, twisting benzenes rings out of plane and reducing distance between their tips. Adapted from [17].*

The isomerisation process of azobenzenes has been studied since the 30's [26] and visually observed using scanning tunneling microscopy [27]. As can be seen from Fig 2.2, isomerisation affects the azobenzene properties considerably: benzene rings are rotated from plane to about 57° angle [28], distance between benzene ring tips reduces from 9 Å to 5.5 Å and dipole moment increases from 0 to 3.0 Debye [29] as the geometry changes causing loss of symmetry. Other observable effects include a change in colour known as *photochromism* [30, pp. 209–210].

Photochromism is defined as molecules having reversible forms with different spectral

[1] Alternative, IUPAC recommended notation of *cis-trans* isomerism is *E-Z* isomerism originating from German words *entgegen* (opposite) and *zusammen* (together) [25].

features and thus different colour [31, pp. 227–229]. Transitions between these forms are induced, and therefore controlled, with light. Parts of the molecule with absorption in the visible spectrum are analogously called *chromophores* as they give colour to the material they are in. For azobenzene-type azobenzenes, isomerisation causes red shift in absorption spectrum and is thus called *positive photochromism*, whereas blue shift in absorption would be considered *negative photochromism* [30, p. 210].

The exact mechanism of azobenzene isomerisation has been a subject of debate for over half a century [16]. The two main mechanisms proposed are *rotation* and *inversion*. In rotation isomerisation mechanism the azo π bond ruptures, allowing for benzene rings to rotate freely about the single (-N-N-) bond while maintaining 120° (C-N-N) angle [32]. Inversion mechanism, on the other hand, involves one of the (C-N=N) angles straightening to 180° into a semilinear transition state while the double bond remains intact [33]. A mechanism where both benzene ring (C-N=N) angles straighten to 180° into a linear transition state has also been proposed and consequently designated *concerted inversion*. Additionally, a combination of both inversion and rotation mechanism called *inversion-assisted rotation* where both (C–N=N–C) dihedral angle and (C-N=N) angles change simultaneously has been suggested. Despite continuous attempts, so far no single proposed mechanism has been able to cover all aspects of even unsubstituted azobenzene isomerisation [19, p. 8].

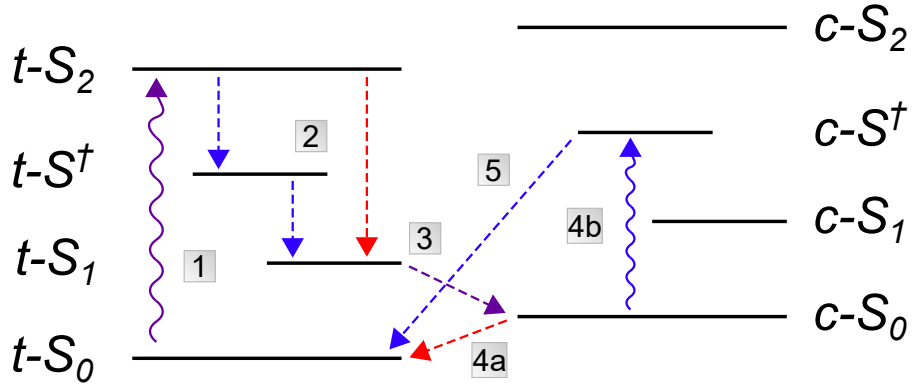

Figure 2.3. Isomerisation mechanism of azobenzenes. *Energy levels for* trans *(t-S) and* cis *(c-S) are presented with solid black lines, radiative transitions with curvy lines and non-radiative transitions with dashed lines. Transitions of two relaxation pathways are indicated with red and blue colours, while purple transitions occur in both. Adapted from [34].*

Fig 2.3 presents an energy and transition diagram of azobenzene isomerisation mechanism for two examples to elucidate the process. One example is indicated with red arrows and another with blue arrows. Transitions which occur for both examples (**1** and **3**) are drawn in purple. A noteworthy detail is that *cis* states are from the HOMO $t - S_0$ to LUMO $t - S_2$ states of the azo bond. As can be seen in Fig 2.3, *cis* isomer states are at higher energy than the corresponding *trans* states but with similar gaps between energy levels, thus *cis* states are energetically less favourable.

State S_0 represents ground state and **1** represents photon absorption and $\pi \rightarrow \pi^*$ excitation to excited $t - S_2$ state [34]. There are multiple ways this excitation can relax back

to *trans* state. In the first example in red, relaxation is non-radiative via **2** to intermediate $t - S_1$ state represented in Fig 2.3 with a red dashed line prior to isomerising to *cis* via **3** with purple dashed line, and as *cis* is thermally unstable, eventually relaxing non-radiatively back to *trans* state of $t - S_0$ along the **4a** red dashed line. This photoisomerisation cycle presented with purple and red arrows represents the inversion mechanism. Quantum yields at each transition determine the likely relaxation route, although isomerisation mechanism seems to be highly dependent on its environment and difficult to characterise in general terms [19, p. 8].

Another presented alternative is non-radiative relaxation from $t - S_2$ via the blue dashed arrow in **2** to intermediate state $S^\dagger$ and from there $t - S_1$ and eventually along **3** in purple dashed arrow to *cis*, corresponding to rotation mechanism. In this cycle, another mechanism for *cis* $\rightarrow$ *trans* isomerisation is illustrated. Transition **4b** from $c - S_0$ ground state to intermediate $c - S^\dagger$ state represents photon absorption at *cis* absorption band, resulting in relaxation to *trans* ground state $t - S_0$ via **5** nonradiative transition in blue dashed line. This photoisomerisation mechanism is typically faster than thermal relaxation and allows for photocontrolling *cis* $\rightarrow$ *trans* isomerisation. This photocontrol is particularly applicable for long *cis* lifetimes with pseudostilbene azobenzenes and called *photoswitching*. Molecules that can be switched between two or more states that are thermally stable in the time frame of the application are known as *photoswitches* with various applications discussed in more detail in the following section [35].

2.1.4 Azobenzene applications

As the defining feature of azobenzenes is their efficient and reversible photoisomerisation, research endeavours aim to optimise different aspects of it. High thermal relaxation rate is crucial especially for biological applications of transmitting information and chemical and electrical stimulation. On the other hand, research is also focused on prolonging the *cis* lifetime in azobenzenes indefinitely to ensure thermal stability for both *trans* and *cis* form. In addition to tuning the photoisomerisation process, aromatic substitution has opened new possibilities for fabricating azobenzene-containing functional materials.

Fast-switching azobenzenes aim to minimise the thermal isomerisation rate constant and ensure *cis* population relaxes back to *trans* efficiently. Femtosecond time-resolved absorption and emission spectroscopy has enabled the study of ultrafast isomerisation processes and demonstrated that azobenzenes show great promise in ultrafast photoswitching applications [36, pp. 237–238]. First under 100 fs thermal isomerisation were recorded as bridged azobenzene in hexane solution isomerising efficiently and reversibly within $t < 1$ ps timescale [37]. By bridging diazocine with a more stable *cis* isomer, azobenzene *cis*-isomer lifetime was greatly reduced and the potential for photoswitchable molecular tweezer applications proposed.

Ultrafast photoswitching has also been realised in biological context: azopyrimidine exhibited high photostability and *cis* lifetime of 40 ns in physiological conditions, enabling

biomedical applications for transmitting information [38]. Key element for biological applications is to operate the switching within visible light spectrum, motivating research to focus on creating photoswitches operating at longer wavelengths in the visible spectrum. One approach has been to red shift the stable isomer absorption spectrum to longer wavelengths through negative photochromism [9]. Some promising alternatives include spiropyranes [39], binaphthyl-bridged imidazole dimers [40], and so-called donor–acceptor Stenhouse adduct "DASA" photoswitches [41, 42].

Meanwhile the opposite race of extending the *cis* lifetime continues. For these *bistable* azobenzenes, an important distinction between two types of *photochromism* arises: chromophores with one isomer being thermally unstable and thus relaxing rapidly to energetically more viable isomer are described to exhibit *T-type photochromism* [9, p. 95]. Relaxation to thermally stable isomer occurs eventually within a time span from seconds to hours. Another, *P-type photochromism*, is defined as all isomers exhibiting thermal stability and thus a bistable switch with *cis-trans* isomerisation. Thermal relaxation can take up to years, but reverse isomerisation can be triggered with excitation within isomer's absorption band. Defining between photochromism types is lifetime τ of thermally less stable isomer.

One strategy for prolonging *cis* lifetime is through addition of halogen substituents or *halogenation*. Bléger and Hecht *et al* reported in 2012 [43] that *ortho*-fluorine substituents caused a significant red shift in the absorption band to the visible spectrum, and combining this with electron-withdrawing substituents enhanced the effect. Fluorination and amination could be used to tune the *cis* lifetime by several orders of magnitude as demonstrated by Ahmed *et al* in 2015 [44]. High thermal *cis* isomer stability can also be achieved using chlorine and bromine substituents [9, pp. 98–100].

Another example of a P-type photochromism was reported four years ago: azobenzene-containing bistable photoswitches managed to transport Urea d-Aminoglucose units and release the cargo upon illumination [45]. Bistability gives rise to a plethora of similar applications ranging from chemical industry to biomedical drug-delivery solutions. In recent years, solar power has risen topical for azobenzene research as efforts are made to utilise photoisomerisation in solar energy harvesting and storage through bistable photoswitching [46]. Beyond azobenzenes, P-type photochromism can also be achieved with *diarylethenes*, compounds similar to azobenzenes but instead of the azo bond, aromatic groups are connected via carbon–carbon double bond, such as stilbenes. Using five-carbon rings, diarylethenes can exhibit bistability with *cis* lifetime exceeding thousands of years [47].

2.2 Effects of molecular environment

In addition to the substitution pattern, azobenzene photoisomerisation is also susceptible to environmental effects ranging from temperature and humidity to the chemical environment azobenzenes are in. Isomerisation has been reported in liquid and gas phase

[48] but majority of azobenzene-related research is conducted in solution or condensed phases [49, p. 16]. This section presents the theory relevant for polymer thin films within the scope of this thesis, particularly from the perspective of providing a chemical environment for azobenzene photoisomerisation. Here azobenzenes are often referred to as chromophores as they cause the colour to a given material or solution.

2.2.1 Azobenzenes in solution

Photoisomerisation in solution is typically faster compared to condensed phases [49, p. 16]. As azobenzene geometry changes from planar *trans* to three-dimensional *cis*, the interconversion is limited by the free volume available for isomerisation. By definition, condensed phases involve less free space and hence isomerisation occurs more rapidly in solutions. Similarly, steric hinderance results from densely occupied volume and non-bonding repulsive electric interactions, reducing the rate of isomerisation in condensed phases. Multiple factors determine the isomerisation rate in solution, including solvent polarity, viscosity, and concentration.

Solvent polarity is directly proportional to *trans-cis* isomerisation quantum yield and inversely proportional *cis-trans* isomerisation quantum yield for electron donor or acceptor substituted azobenzenes [19, p. 16], so polarity can be used to adjust *trans* and *cis* relative populations. While unsubstituted azobenzenes are insensitive to solvent polarity, aminoazobenzenes exhibit a red shift in polar solvents [12, p. 4] and pseudostilbene-type azobenzenes are particularly sensitive to solvent polarity [49, p. 6]. For example, pseudostilbene-type 4-(diethylamino)-4'-nitroazobenzene thermally relaxes from *cis* to *trans* almost 6 orders of magnitude faster in highly polar N-methylformamide solution compared to non-polar hexane as solvent [50]. Less research has been conducted on the effects of solvent viscosity, but higher viscosity appears to be linked to higher isomerisation quantum yield in both directions [51].

Isomerisation rate in solutions can also be tailored with nanoparticles. In recent years, gold nanoparticles have attracted attention with regard to azobenzenes as the rate of thermal relaxation could be reduced by up to 3 orders of magnitude in gold nanoparticle aggregates [52] and in aqueous solution in the presence of gold nanoparticles [53]. Last year, gold nanoparticulate platforms were used to enable azobenzene water-solubility and increase their thermal relaxation rate over 6000 times [54].

2.2.2 Guest–host polymer system

Research concerning azobenzenes is typically conducted using thin films containing azobenzenes [49, p. 10]. Polymer films are often used due to their versatile and affordable availability and easy processability, mechanical flexibility and high chemical resistance [55, p. 1]. They also possess suitable physical properties including being lightweight, owing to the macromolecular nature of *polymers* consisting of numerous repeat-

ing units called *monomers*. Commercially available polymers typically consist of hundreds of monomers per molecule, resulting in high molecular masses [55, p. 2].

Azobenzene-containing films can be fabricated in numerous ways, perhaps the simplest being formation of a *guest-host* polymer system: azobenzene is simply mixed with a polymer in a solution and fabricated into a film, for example using spin coating as elaborated in section 3.1.3. This fabrication strategy produces *amorphous thin films*, material consisting of molecular mixture lacking long-range order due to random orientation of molecules [56, pp. 3, 119]. Heating amorphous films leads to irreversible thermal rearrangement of the structure employed for example in heat treatment or *annealing* discussed in more detail in section 3.1.3. Guest-host polymer system is illustrated in Fig 2.4, where the orange line represents the polymer chain and rod-shaped pieces are para-substituted hydroxyazobenzene molecules.

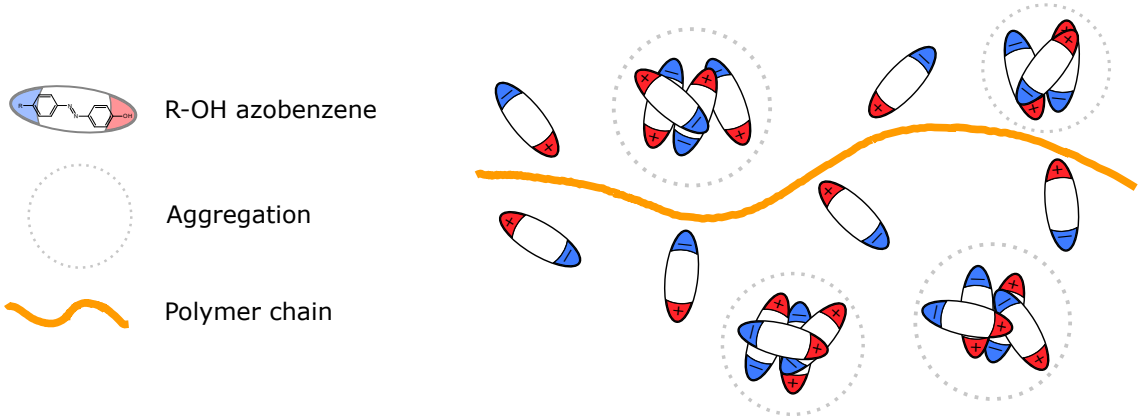

Figure 2.4. Guest-host polymer system. *Weak intermolecular interactions between host polymer and guest hydroxyazobenzene are insufficient to immobilise azobenzenes, leading to aggregation highlighted with a dashed line circle.*

Despite its ease of fabrication, guest-host polymer systems are far from desired in many photonics applications due to detrimental effects with only weak intermolecular interactions. Without bonding between the polymer and the chromophore, molecules are scattered in the film at random, giving rise to challenges in reproducibility. Weak dispersion forces between chromophores and polymers are insufficient to immobilise chromophores [9]. Guest mobility limits applications requiring high chromophore concentration or alignment due to thermal instability. While viable photonics applications typically call for high chromophore concentration to ensure strong optical response, sufficient chromophore concentration and guest mobility can lead to aggregation effects. As chromophore-chromophore interactions grow predominant over chromophore-polymer interactions, aggregation depicted in Fig 2.4 occurs, ultimately leading to macroscopic phase separation in high guest concentration which often impact negatively on the material optical properties [49]. This poses a challenge especially for azobenzenes with dipolar nature. For example, aggregation can lead to detrimental effects such as photoisomerisation quenching, increased optical scattering or fluorescence emission, while azobenzene derivatives are typically nonfluorescent [12, p. 4].

2.2.3 Azobenzene aggregation

Intermolecular interactions between azobenzenes affect their spectral properties and can be adequately understood with the *exciton model* introduced by Kasha *et al* over half a century ago [57, p. 379]. Exciton model approximates tightly packed azobenzenes as point dipoles and describes how molecular packing influences their photophysical properties though Coulombic coupling. These electrostatic interactions result in excitonic band splitting of the electronic transitions into states with an energy difference ΔE, causing energetic shifts in the absorption and emission spectra [58]. For identical molecules with parallel transition dipole moments $\boldsymbol{\mu}_{eg}$, this energy difference ΔE of the exciton band splitting can be estimated from [57]

$$\Delta E = \frac{2|\boldsymbol{\mu}_{eg}|^2}{r^3}(1 - 3\cos^2\theta), \tag{2.2}$$

where r is the distance between centres of molecules and θ is the inclination angle as illustrated in Fig 2.5. As the energy gap between the states is proportional to the square of the transition dipole moments, for azobenzenes ΔE is marginal for weak $n \rightarrow \pi^*$ transitions and thus only $\pi \rightarrow \pi^*$ transitions are affected by aggregation.

In the event that molecules align to in-line position with $\theta = 0°$, energy difference ΔE reaches maximum as the allowed state energy is at a minimum. As θ increases, the energy difference reduces until split states are in phase and hence at equal energy $\Delta E = 0$. This occurs at $\theta \approx 54.7°$ according to equation 2.2, dividing aggregation in the exciton model into two distinct regions as illustrated in Fig 2.5. For $\theta < 54.7°$, transition energies are lower for excitonic coupling compared to isolated chromophores leading to accelerated radiative decay rate and a red shift in the absorption band [12, p. 4]. This shift is known as known as *bathochromic shift* and occurs due to parallel alignment of transition dipole moments in the dimer designated *J-type dimers* after their discoverer Edwin E. Jelley in 1936 [59]. In case these dipoles are parallel or "head-to-tail" aligned, the altering electron density strongly affects higher order multipole moments, allowing tuning of molecule's nonlinear response through inducing anisotropy by applying an electric field known as *poling* [60]. For example, azobenzenes with push–pull substitution pattern yield noteworthy nonlinear response due to their strongly asymmetric electron density distribution [12, p. 4].

For $\theta > 54.7°$, transition energies are higher for excitonic coupling compared to isolated chromophores leading to blue shift or *hypsochromic shift* in the absorption band and a reduction in radiative decay rate [12, p. 4]. This shift occurs due to "side-by-side" alignment of transition dipole moments in the dimer designated *H-type dimers*. Planar molecules such as *trans*-azobenzenes form typically H-type dimers, particularly with dipolar push-pull substitution [58] with limited free volume as in condensed phases, rendering H-aggregating pseudostilbenes challenging for NLO applications. This aggregation can be averted through stronger intermolecular interaction between pseudostilbenes

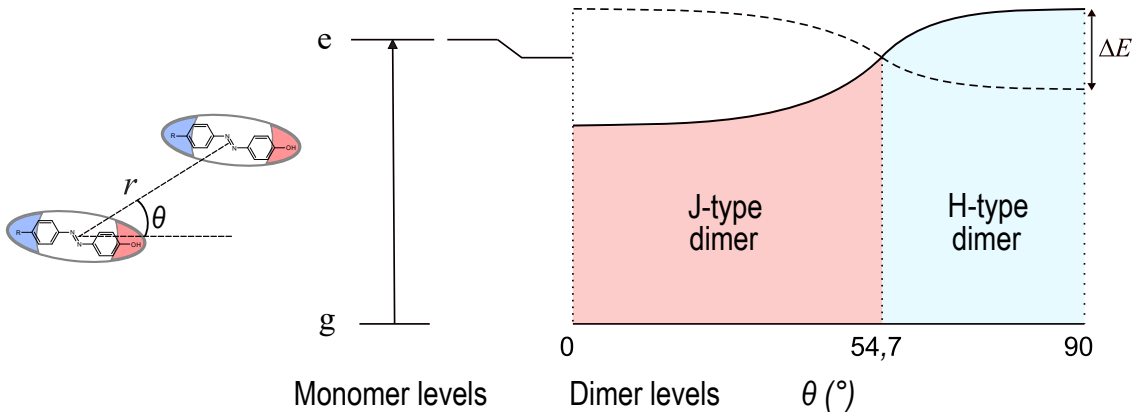

Figure 2.5. Exciton model band diagram. *Illustration of the dimerisation of parallel azobenzenes molecules with inclination angle θ and the exciton band energy as a function of θ. Dashed line represents the energy of the symmetry forbidden state. Redrawn from [57, p. 379].*

and polymers as discussed in the upcoming sections. Multiple extensions to the exciton model have been proposed to explain aggregates indescribable with Kasha's model, most recently in 2017 [58], to accommodate for unconventional (non-Kasha) packing geometries.

2.2.4 Covalent polymer system

One strategy to resolve issues with azobenzene-containing guest-host polymer system is to incorporate azobenzene molecules into the polymer chemically. This removes any issues with azobenzene diffusion into the polymer system and limitation to azobenzene concentration due to aggregation and phase separation [36, pp. 237–239]. As demonstrated in Fig 2.6, covalently bound chromophores are immobilised yet functional, and with negligible chromophore-chromophore interactions, phase separation related issues prevalent in guest-host polymer systems are eliminated [55, pp. 130–131]. Furthermore, covalent bonding allows for site-specific engineering where chromophores are attached: with suitable polymer and azobenzene substituents, azobenzene can become side chain or main chain constituent [61] as show in Fig 2.6. Combined with the significant change in geometry during photoisomerisation, covalent polymer system azobenzene films can be used to functionalise materials into various applications such as molecular zippers [62].

The drawback of covalently bonding azobenzenes into a rigorous polymer matrix is the complexity of the process. For each new azobenzene-polymer combination, a strenuous multistep synthesis is required, rendering covalent bonding time-consuming, expensive, and thus undesirable strategy [15, pp. 427–428]. Covalent bonding also changes the chemical environment and available free space of azobenzene, reducing the thermal relaxation rate from excited *cis*-state dramatically [36, pp. 237–238].

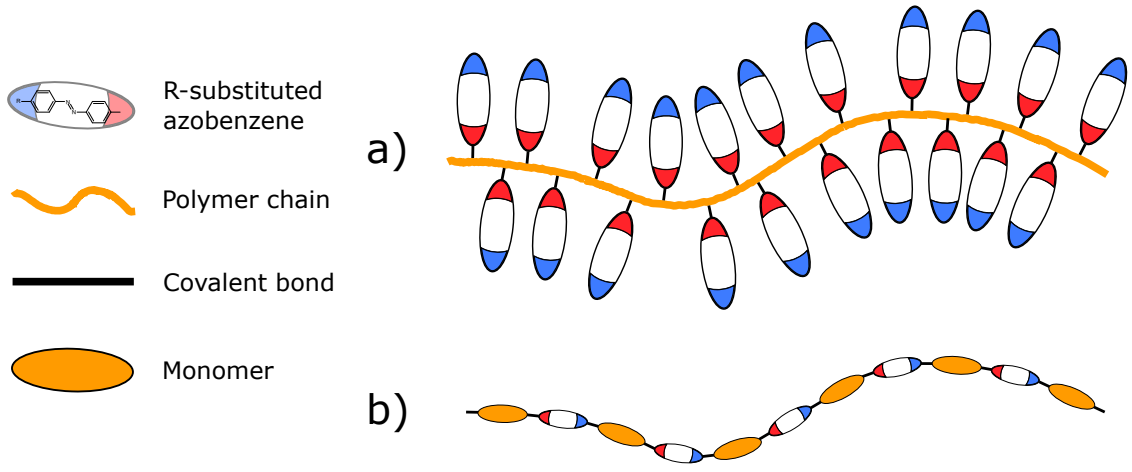

Figure 2.6. Covalent polymer system. *Azobenzenes can be (a) side chain (b) or main chain in the polymer system connected via covalent bonds illustrated as black lines.*

2.2.5 Supramolecular polymer

Supramolecular chemistry [63] offers a strategy to combine the enhanced optical performance of covalent azobenzene-containing polymer system and the ease of fabrication involved in guest-host systems. With compatible substituents in the azobenzene and the polymer repeating unit, intermolecular interaction between chromophore molecules and polymer chain monomers are sufficient to noncovalently bind azobenzene into a *supramolecular polymer* as shown in Fig 2.7. Functioning as a side chain, azobenzenes are relatively immobile and chromophore-chromophore interactions are restricted enough to allow high chromophore concentration without risking aggregation, up to equimolar concentration with noncovalently bonding monomer. Sufficiently strong intermolecular interaction can be achieved via hydrogen bonding, metal coordination or electrostatic interactions [64, p. 302]. In a supramolecular polymer system, simple mixing of the constituents self-assembles the polymer with spontaneous non-covalent bonding between appropriate functional groups [65].

In this thesis, the polymer of choice is poly(4-vinylpyridine) designated P4VP and illustrated in Fig 2.8. P4VP has the ability to form non-covalent intermolecular bonds via hydrogen bonding [66]. Provided a suitable hydrogen bond donor substituent on azobenzene molecules, pyridyl group in P4VP operates as hydrogen bond acceptor, noncovalently bonding azobenzenes into the polymer system. Azobenzenes can be engineered for a specific environmental interaction through aromatic substitution. Perhaps the most applicable substituent, hydroxy group enables strong intermolecular interactions with other molecules containing electron-withdrawing groups [9, pp. 92–94].

Hydroxyazobenzenes

Hydroxyazobenzenes are characterised by their hydroxy group and have been studied for versatile applications ranging from carbon dioxide capture and conversion [67] and

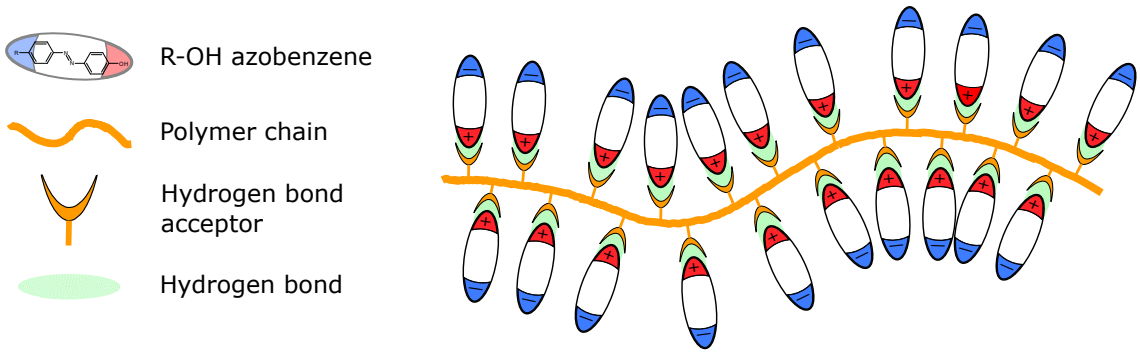

Figure 2.7. Supramolecular polymer system. *Polymer capable of hydrogen bonding forms a supramolecular system with para-substituted hydroxyazobenzene (symbolised with R-OH) via hydrogen bonding. In this thesis, hydrogen bond between P4VP and hydroxyazobenzenes forms between the hydroxy (hydrogen bond donor) and pyridyl (hydrogen bond acceptor) groups.*

nanostructured surface patterning [68] to data storage utilising two-photon process to create erasable polarisation [65]. Hydrogen bonds can form between a hydrogen atom bound to a strongly electronegative atom and another electronegative atom. Hydrogen bond donor substituents in molecules used in this thesis are hydroxyl and amino groups. Hydrogen bonding between these groups and P4VP is illustrated in Fig 2.8.

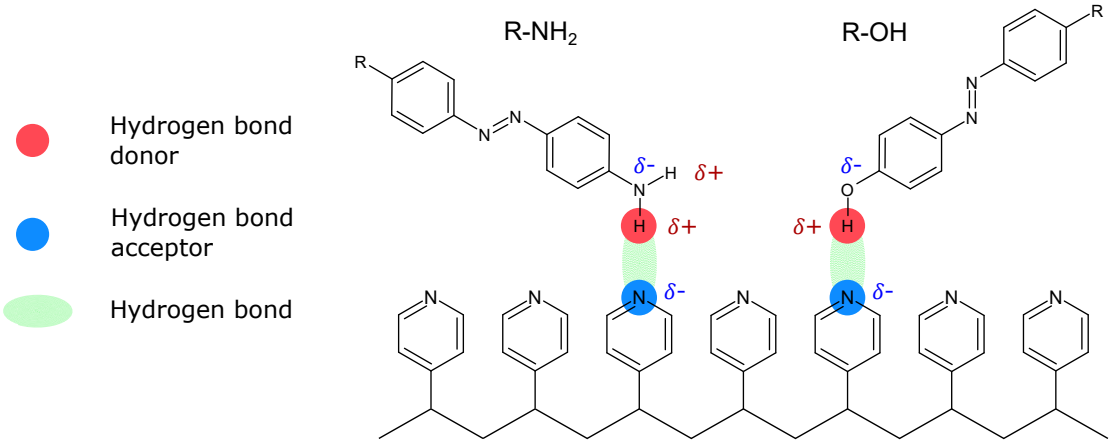

Figure 2.8. Hydrogen bonding. *Hydroxyl and amino groups in azobenzenes function as hydrogen bond donors while nitrogen atom in P4VP pyridyl group is the hydrogen bond acceptor. Partial charges in the vicinity of the hydrogen bonds are indicated with δ.*

Hydrogen bonds allow for comparably strong noncovalent bonding between molecules without chemical reactions involving forming sigma bonds, giving rise to self-assembly in materials containing hydroxyazobenzene, granted a suitable hydrogen bond acceptor is available. Most notably for hydroxyazobenzenes, hydrogen bonding between hydrogen in hydroxyl group and nitrogen in azo bond of two hydroxyazobenzene molecules brings further instability to *cis* isomer, making *cis* $\rightarrow$ *trans* thermal relaxation process rapid [16]. Hydroxyazobenzenes also exhibit hydrogen-bond assisted *tautomerisation* with orders of magnitude change in *cis* $\rightarrow$ *trans* relaxation rate depending on solvent polarity [69].

Tautomerisation is chemical reaction and a form of structural isomerisation where the structure of a molecule changes through interconversion [70, pp. 1-2]. Often tautomerisation involves proton relocation as illustrated in Fig 2.9 and is thus called prototropic tautomerism. Distinction between resonance structures and tautomers is worth noting: resonance structures only describe electron relocation and do not actually exist, while tautomerisation changes the molecular structure and hence the chemical nature of the molecule [71, p. 142].

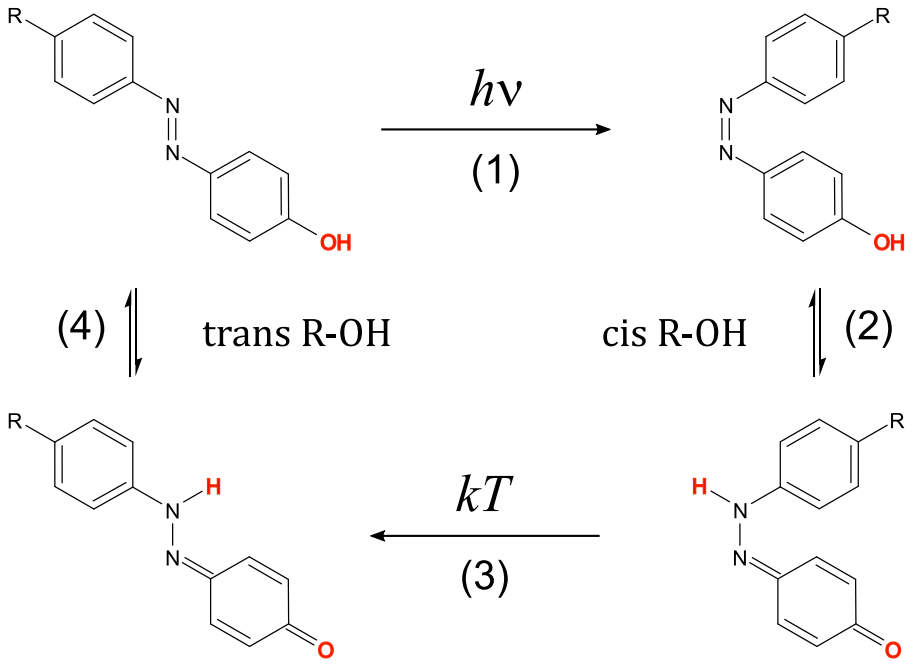

Figure 2.9. Azobenzene tautomerisation. ***(1)*** trans *Hydroxyazobenzene denoted R-OH photoisomerises to* cis*,* ***(2)*** *tautomerises into hydrazone,* ***(3)*** *thermally relaxes into* trans *and* ***(4)*** *tautomerises back to* trans *R-OH. Hydroxy group of relocating proton is highlighted in red.*

An example of azobenzene tautomerisation is given in Fig 2.9. In the example, a hydroxyazobenzene with an arbitrary substituent R is denoted as R-OH and presented at first as *trans* isomer. R-OH is photoisomerised into *cis* isomer **(1)**, which in turn tautomerises into hydrazone **(2)**. This prototropic tautomerisation involves proton relocation from the hydroxy group to the azo bond breaking the π bond. The tautomerised *cis* isomer then relaxes thermally to *trans* **(3)** and eventually tautomerises back to *trans* R-OH. As tautomerisation removes the π bond from the azo bond, *cis* $\rightarrow$ *trans* isomerisation via rotation mechanism becomes favourable and occurs rapidly.

The effect of tautomerisation on *cis* $\rightarrow$ *trans* relaxation rate was demonstrated by Poutanen *et al* in 2016 [72]. Hydroxyazobenzenes were fabricated into supramolecular side-chain polymer complexes as thin films and by varying the hydroxyazobenzene concentration in the complex the relaxation rate constant changed by two orders of magnitude. This was due to the hydrogen bonding between hydroxyazobenzene molecules and consequent tautomerisation. As the π bond was removed from the azo bond, it enabled easier isomerisation via rotation mechanism and quickening the overall thermal isomerization rate.

2.2.6 Other azobenzene matrices

In addition to amorphous polymers, azobenzenes have been studied in other condensed phases including gels, dendrimers, molecular glasses, liquid crystals and functional monolayers. Each new material is an endeavour to optimise optical performance for smarter applications, and azobenzene photoswitching is an integral part of it. For biomedical applications, azobenzene-containing *hydrogels* have surfaced as an alternative in drug delivery and mechanical signalling [73]. As a three-dimensional network of hydrophilic polymers capable of swelling and thus accommodating relatively large amount of water, hydrogels can be engineered to be nontoxic, porous, pH or temperature sensitive and thus marvel in applications targeted for biological environment [74, p. 20].

Similarly, for cargo delivery purposes, azobenzene-containing dendrimers have been studied for a few decades for the combination of photoresponsivity of azobenzenes and box-like geometry of highly branched macromolecules [75]. Dendrimer–azobenzene complexes show promise for large biomolecule transport within globular supramolecular structures, and azobenzenes are used to operate the open-close mechanism upon illumination [76]. Contrast to globular geometry, azobenzenes monolayers are studied for surfaces responsive to stimuli such as light, mechanical stress, pH, or electric fields [49, p. 5]. Azobenzene monolayer surfaces have proven promising for applications ranging from biosensors to memory devices [77].

The disadvantage of polymer matrices is variation in molecular mass and structure, limiting reproducibility. An alternative to long polymer chains is to use small molecules capable of forming stable amorphous structures known as *molecular glasses* [78]. Fabricating azobenzene-containing films from molecular glasses improves repeatability without compromising nonlinear optical response, indicating superior performance for molecular glasses in all-optical poling applications compared to polymer alternatives [79].

2.3 Humidity

As the most valuable, indispensable, and abundant natural resource on our planet, water is present in our atmosphere as well as oceans and glaciers. *Humidity* is used to describe the amount of water vapour present in a gas phase, typically air, and it is one of the most commonly measured physical quantities [80]. Humidity is a crucial environmental parameter to monitor and control for a plethora of fields of industry and science ranging from electronics, chemical, pharmaceutical, paper, textile and construction industry to meteorology, agriculture, aerospace, semiconductors and food production [81, pp. 57–58]. This section illuminates the concept of humidity and its impact on society, presents an overview of commercially available solutions for humidity sensing and provides a comparison of these alternatives.

2.3.1 Humidity terminology

Humidity is often discussed in either absolute or relative terms. *Absolute humidity* (AH) is expressed as water mass or in a unit volume of gas or parts per million in gas, whereas *relative humidity* (RH) is defined as the ratio of the water vapour pressure present in the gas P_w to the water vapour pressure at saturation P_s in a given temperature [81, pp. 16–17]. This ratio is expressed as [82]

$$\text{RH} = \frac{P_w}{P_s} \times 100\%, \tag{2.3}$$

where RH is relative humidity and P_w and P_s vapour and saturation pressures, respectively. As vapour pressure is a function of temperature, higher temperature means higher saturation pressure and thus lower relative humidity with same absolute humidity. Vapour pressure can be estimated using Clausius–Clapeyron relation, although more accurate empirical correlations between saturation vapour pressure of water and temperature have been formulated, most recently the Arden Buck equation [83]. Ideal gas approximation cannot accurately describe water vapour due to strong intermolecular hydrogen bonding. Vapour pressure of water as a function of temperature is presented in Fig 2.10 along with Clausius–Clapeyron relation and Arden Buck equation fitting. As is visible in the graph, Arden Buck equation describes water vapour pressure more realistically.

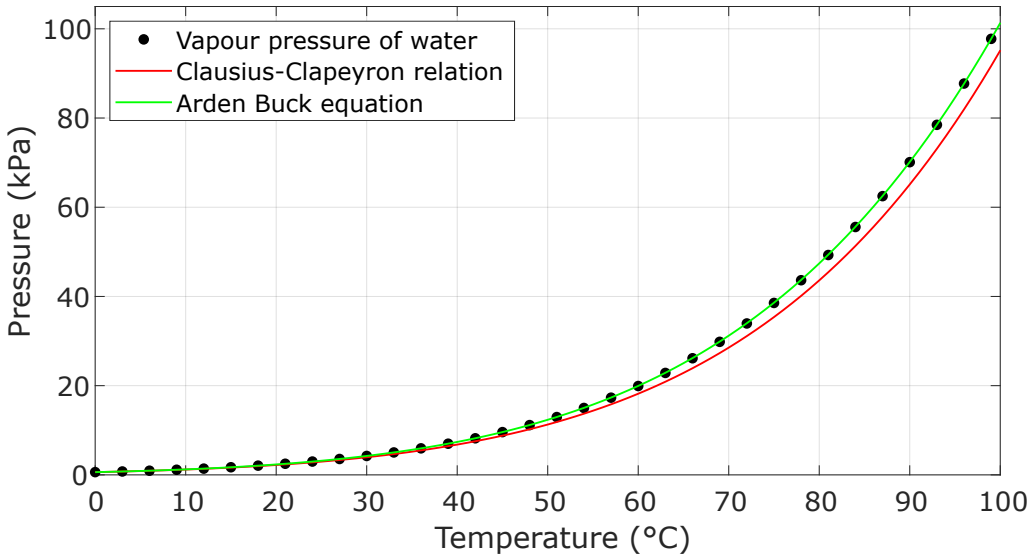

Figure 2.10. Vapour pressure of water. *Black dots represent experimental results, red line Clausius–Clapeyron relation fit and green line Arden Buck equation fit. Data from [84, p. 6-10].*

Although absolute humidity provides a more comparable measure of humidity, relative humidity is predominant expression for humidity as it is in percentage. Another common way to describe humidity is *dew point*, defined as the temperature at which current water vapour pressure equals saturation vapour pressure $P_w = P_s$ [81, p. 13]. In other words, dew point T_d indicates the temperature below which current humidity causes wetting or dewing [85, p. 659]. For $T_d < 0°$C, dew point is called *frost point* [86].

2.3.2 Existing humidity sensors

Simplest instrument for humidity measurement is called *psychrometer*. Also known as the wet-bulb and dry-bulb hygrometer, its operating principle revolves around two temperature sensors with one exposed in measured gas and another wrapped in soaked wick [85, p. 659]. As gas is blown at the sensors, evaporation from the wick cools the sensor, ensuing in a temperature difference between the sensors, which in turn is used to determine relative humidity using the following equation [82]:

$$P_w = P_s - P_{tot}A(T_{dry} - T_{wet}), \tag{2.4}$$

where P_{tot} is total gas pressure, A is instrument-specific constant related to structural geometry and gas flow rate, T_{wet} and T_{dry} are temperatures measured at wet and dry sensors, respectively. Despite its simplicity, psychrometer remains a simple yet effective method of estimating humidity and one of the three major instruments used for measuring humidity, although measurement accuracy is low with lowest uncertainty attainable is $\pm$4 % [85].

Most commercially available humidity sensors are relative humidity sensors [86], although competitive absolute humidity sensors are on the market for a specific purpose. The following subsections delve into different humidity sensing solutions and recent advances in research by sensor type: capacitive, resistive, optical, and gravimetric humidity sensors or *hygrometers* are introduced, as well as some novel piezoresistive and magnetoelastic sensors.

Capacitive sensors

Capacitive sensors covered over 75 % of the relative humidity sensing market share 30 years ago [87], and undoubtedly similar trend has continued to this day. Sensors are typically comprised of two interdigitated noble metal electrodes (IDE) covered by a dielectric humidity-sensitive layer [82]. Water vapour interacts with the dielectric layer, causing a change in its dielectric constant ϵ_r and thus in the system capacitance, forming a measured signal. Capacitance can be nonlinearly related to humidity and depends on the material used, selection ranging from polymers to porous ceramics and silicon. Cross-linked polymer networks hinder swelling and ceramics can withstand high operating temperatures, which enhance long-term sensor stability. Illustration of a typical capacitive humidity sensor is shown in Fig 2.11.

Most capacitive sensors operate comfortably within 5-95 % RH range with lowest attainable uncertainty around $\pm$2 % RH [85, p. 657], making them suitable for a wide range of applications. Some limitations are brought by chemically contaminable materials and aging effects, however. Furthermore, lack of calibration extends uncertainty 2–3 times due to drift caused by contaminants and saturation, giving rise to need for frequent calibrating

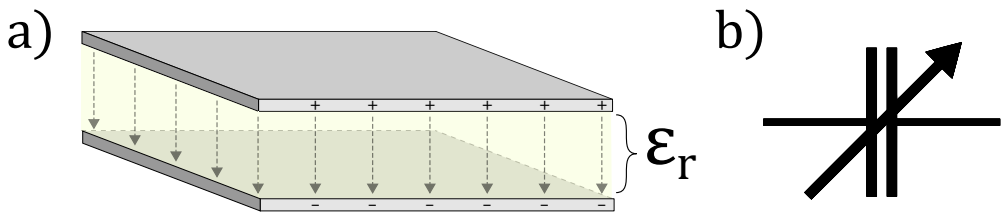

Figure 2.11. Capacitive humidity sensor. *a) Gray plates represent IDEs and yellow area in between the dielectric humidity-sensitive layer ϵ_r. b) Variable capacitor symbol indicating variance in capacitance due to changes in humidity.*

[86]. Another challenge with capacitive sensors is *hysteresis* or history dependence of physical systems: measurement result depends on the gradient of the time-dependent humidity change [81, p. 43]. As measured reading is different for increasing and decreasing humidity, sensor reliability can be compromised.

Recent advances in capacitive sensors research have aimed at reducing hysteresis effects, increasing sensitivity, and tailoring linear dependence between capacitance and humidity. Some promising concepts include a ZnO nanopowder/PVP-RGO multilayer [88], where high surface-to-volume ratio resulted in small hysteresis and improvements in both sensitivity and linearity while maintaining long-term stability and fast-response in sensor materials. Polymer-oriented approach from last year yielded similar results with a polyimide-based sensor [89]. A linear correlation was observed between measured capacitance and RH in the range of 5–85 % while also exhibiting extraordinarily low hysteresis. Third sensor concept from earlier this year comprised of mesoporous silica and poly (3, 4-ethylenedioxythiophene) composites outperforming their bulk counterparts in terms of sensing range, sensitivity, and response speed [90].

Resistive sensors

In resistive humidity sensors, the change in electrical resistance is measured. This transduction mechanism involves absorption of water vapour onto sensor material, typically conducting ceramics, polymers, or electrolytes, which causes the change in conductivity [82, p. 7]. Benefits of resistive sensing involve simple electrical circuits operating at low power, high sensitivity and good linearity between resistivity and humidity. Simple circuits and humidity-sensitive materials have led to affordable instruments, although resistive sensors are typically not as sensitive as capacitive sensors.

Resistive response of sensor materials depends on both humidity and temperature, so for humidity sensing applications instrument requires a temperature sensor to operate in practice [81, pp. 98–100]. Temperature effects generating signal drift encompass majority of problems limiting resistive humidity sensor usage. Moreover, condensation issues pose challenges with more sensitive material options. With multiple materials employed for different humidity ranges, resistive sensors can measure up to 10-90 % RH with lowest attainable uncertainty around $\pm$3 % RH [85, p. 657].

Research in resistive sensor materials has been recently focused on durability and sensitivity with heavy condensation of water vapours in high humidity. Three years ago, a water durable resistive humidity sensor was fabricated using a rigid sulfonated polybenzimidazole [91]. Durability and stability at a high humidity and temperature was greatly improved by cross-linking and consequently anchoring the film to the substrate. Another approach to enhance resistive humidity sensor sensitivity was the use of platinum decorated MoS_2 nanoflakes to fabricate a low power yet extremely sensitive humidity sensor [92]. Various composites were fabricated, and optimal sample composition yielded unprecedented high response in high humidity compared to other nanomaterial-based resistive sensors.

Optical sensors

Optical humidity sensing is a versatile field with numerous innovative concepts. Fiber-optic humidity sensors are based on humidity-induced refractive index change [82]. A suitable humidity-sensitive material is immobilized on the surface of the fiber, and with a change in ambient humidity the refractive index of the material changes, creating a detectable signal in the transmitted intensity. Fibers are often preferred method for humidity sensing in applications requiring electromagnetic insensitivity, high temperature and pressure ranges or sensor placement in tight spaces [93]. However, current fiber fabrication methods are limited by repeatability as well as relatively high cost of spectrometers and other associated equipment, which poses challenges in competing electronic humidity sensors on the market.

Another variation of measuring humidity through transmittance is based on IR-absorption. Tungsten disulfide based humidity sensor was reported to be particularly promising with 35–85 % RH measurement range and 1–5 s response time using 1550 nm laser [94]. With the measuring principle dating back almost a hundred years [95], copious similar sensor concepts have been developed where humidity from gas is determined by measuring attenuation of light between emitter and detector in a volume of gas at wavelengths within water UV absorption bands [81, pp. 112–113]. An example instrument is the krypton hygrometer using 123.58 nm light emitted by krypton.

Perhaps the most popular type of optical hygrometers is the *dew point meter* [96], where gas sample is analysed with an electrically cooled Peltier module mirror surface. After cooling the mirror surface to dew point of water in gas sample, condensation occurs, and relative humidity can be determined. Dew point meters are commonly used as a calibration standard due to their high precision and accuracy [85, p. 657]. Instrument often includes a microscope setup for condensate thickness and quality observation. While commendable for their high sensitivity, optical sensors requiring optical setup are relatively bulky and expensive, require high power and frequent decontamination on mirror surfaces. They also suffer from hysteresis similar to capacitive and resistive sensors. Notwithstanding these drawbacks, optical humidity sensing is superior in sensitivity and especially at low humidity, so for laboratory conditions they are optimal.

Optical humidity sensing research has involved new mechanisms for humidity sensing along with faster sensing and improved stability. Rapid humidity measurements were realised last year with hydrogel thin film expansion [97]. Measuring thickness change in the thin film interferometrically and relating it to humidity according to Flory–Huggins theory allowed for up to three times faster humidity measurements than any commercially available sensors with a setup suitable for explosive or corrosive environments. Another group in France created a humidity sensor using 2D hybrid networks of gold nanoparticles [98]. Humidity-sensitive plasmonic coupling caused prominent shifts in the SPR band enabling humidity sensing with promising stability. Similarly, a highly stable optical humidity sensor was demonstrated with Au nanoparticles deposited on 3-mercaptopropionic acid capped CdTe quantum dots [99]. Material proved highly stable over an impressive 5–97 % RH range with a fairly fast response recovery time.

Other humidity sensors

Gravimetric sensors are based on surface acoustic waves (SAW) converted from electrical signals with an interdigitated transducer (IDT) [82]. SAWs are used to measures the mass of a gas sample compared to a dry sample by cooling the device and condensing water vapour. Acoustic waves are mechanical and thus influenceable by physical phenomena such as mass accumulation from condensation, reducing wave velocity and causing a measurable time-delay or phase-shift. Gravimetric sensors are considered to be the most accurate method to determine absolute humidity, meaning Gravimetric sensors are mainly used to calibrate less accurate instruments [100].

2.3.3 Humidity sensing with photoisomerisation

As discussed in section 2.1.3, photoisomerisation causes changes to azobenzene geometry, dipole moment and electron density distribution. Due to these factors *trans* and *cis*-isomers have prominent differences in their absorption spectra. As azobenzenes are illuminated with a wavelength within *trans* absorption band, photoisomerisation occurs, converting *trans* population to *cis* and causing changes in the spectral features. These changes are visualised in Fig 2.12.

Fig 2.12 illustrates spectral changes in *cis-trans* thermal relaxation. Prior to photoisomerisation, the azobenzene-containing material is purely *trans* populated (>99 $\%$) and prominent $\pi \rightarrow \pi^*$ transition absorption band can be observed between 300–400 nm with a peak around 360 nm. Similarly, less prominent yet detectable $n \rightarrow \pi^*$ transition absorption band can be observed around 450 nm. *trans*-rich spectrum corresponds to blue line in Fig 2.12. Upon illumination within this band with 365 nm light, *trans* azobenzenes are excited into *cis* with a different spectral profile.

Measuring absorption spectrum right after photoisomerisation reveals a notable reduction in absorption within the *trans* absorption band and a slight but noticeable increase in the *cis* absorption band between 450-500 nm. *cis*-rich spectrum corresponds to red line in

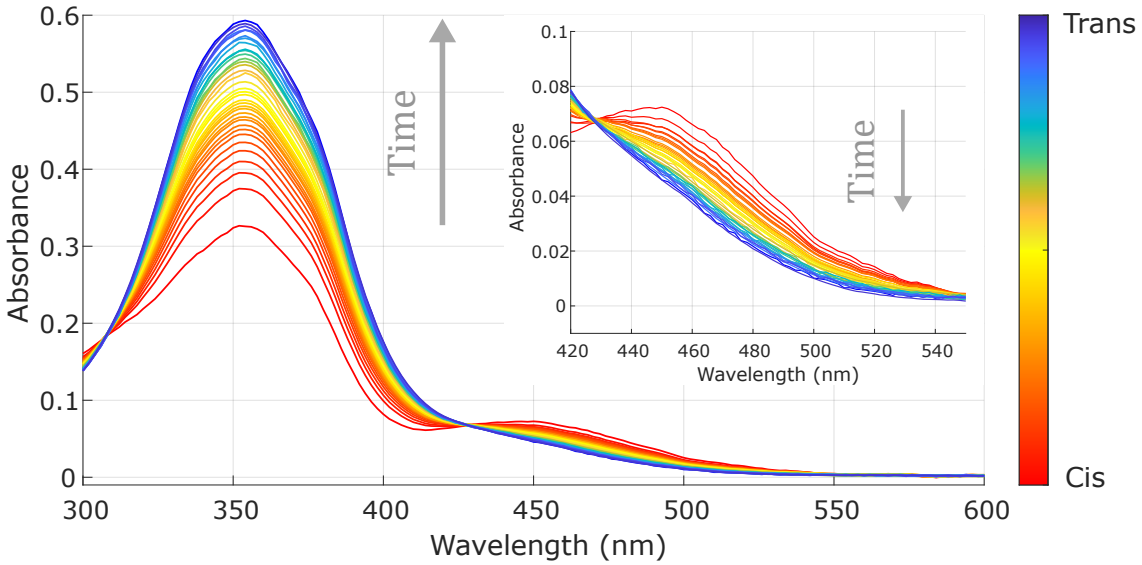

Figure 2.12. **cis-trans** ***Thermal relaxation.*** *Spectral changes in equimolar poly(4-vinylpyridine) and 4-ethyl-4'-hydroxyazobenzene thin film prior to UV illumination with 365 nm light and at regular time intervals after. Spectra were measured at 21.3 °C and 36.1 % RH. Absorbance peak is at 353 nm and isosbestic points at 308 nm and 428 nm.*

Fig 2.12. Periodic measurements reveal how *cis*-isomers are thermally relaxing back to *trans* as absorption at *trans* band region recovers and simultaneously reduces at *cis* absorption band. For the system in question, after eight minutes virtually all *cis* population has interconverted into relaxed *trans*-isomer. $n \rightarrow \pi^*$ band is highlighted in a separate inset to illustrate an increase in absorption as azobenzene population shifts from *trans* to *cis*. Moreover, two wavelengths at which absorption does not depend on isomerisation can be observed at intersections of spectra. These *isosbestic points* lie at 308 nm and 428 nm for 2PAP.

The thermal relaxation rate is highly dependent on environmental factors. As the relaxation occurs via thermal non-radiative relaxation, increased thermal motion exponentially grows the rate constant [101]. Poutanen *et al.* demonstrated two years ago that certain exponential relation also holds for humidity for hydroxyazobenzenes. They studied thermal relaxation rate constant for thin films of poly(4-vinylpyridine) (P4VP) and 4-Ethyl-4'-hydroxyazobenzene (2PAP) in various humidities and detected that the rate constant varies exponentially as a function of humidity. Furthermore, they showed a similar dependence for ethanol vapour in the atmosphere surrounding the studied film. From this they concluded that an optical humidity sensor could be devised from azobenzene-containing thin film and light sources within and without its *trans*-isomer absorption band for excitation and monitoring light, respectively.

Type	Range	Accuracy	Resolution	Response time	Cost
Capacitive	5–95 %	±2 %	±1 %	10–100 s	Low–medium
Resistive	10–90 %	±3 %	±2 %	10–50 s	Low
Optical	5–97 %	<±1%	±1 %	1–10 s	High

Table 2.2. Comparison of common commercial humidity sensing methods.

2.3.4 Photoisomerisation versus existing humidity sensors

Table 2.2 summarises the key features of the most common commercial humidity sensors in terms of sensing range, accuracy, resolution, response time and relative cost. Majority of these are capacitive with benefits of portability, temperature tolerance, relatively low cost and fair accuracy across a wide RH range but require frequent calibration. Resistive sensors are more affordable and very compact but cannot compete in terms of sensitivity and require a second sensor for temperature reference. Commercially available optical humidity sensors are by far most sensitive and accurate but often stationary and expensive. All sensor types face challenges when taken to the extreme: none of the commercially available options are very reliable at very low (<10 %) or very high (>90 %) RH. Pharmaceutical, food processing, storage and electronic manufacturing industries pose a high demand for humidity sensors both in terms of sensitivity and reliable sensing at RH extremes, which presents a potential niche market for suitable humidity sensing solutions.

In order to provide a competitive azobenzene-based humidity sensor application, the sensor would have to improve on one or more of the current limitations set by demand on the market. One option would be to find azobenzene materials suitable for low or high RH measurements and compete through providing a previously unavailable service. Another edge to compete with could be to provide equal range of measurement with superior accuracy or faster response time. Moreover, reducing the cost compared to an established equally good sensor is an alternative: azobenzene-containing thin films are inexpensive as sensor materials as long as no tedious synthesis is involved.

This thesis studies eight hydrogen-bonding azobenzene molecules for possible commercial humidity sensing applications. The following chapter elaborates on the methods of azobenzene-containing thin film fabrication and consequent characterisation. Each material is investigated in terms of reliability, accuracy and range in humidity sensing in order to improve on the limitations of currently available commercial solutions. The results of the study involving eight studied azobenzenes are presented in chapter Results and discussion with analysis of each molecule's potential for humidity sensing applications.

3 SAMPLE FABRICATION AND ANALYSIS METHODS

This chapter includes all the information about sample fabrication and data analysis methods. The chapter is divided into three distinct sections illuminating different parts of the process leading to measurements and ultimately results. First section delves into sample fabrication by presenting molecules, solvents and methods used to produce azobenzene-containing thin films, second section presents polarised light microscopy and absorption spectroscopy setup used to study the samples and third section elaborates data processing methods with MATLAB.

3.1 Sample preparation

This section explains the process of how solid-state poly(4-vinylpyridine) (P4VP) and azobenzenes formed supramolecular side chain polymer complex on glass substrates. Materials and instruments used and different parameters affecting the resulting sample quality are presented in detail.

3.1.1 Studied azobenzenes

In order to study the effects of substitution on humidity sensitivity in hydrogen-bonding azobenzenes, eight molecules were selected for testing. Ethyl-substituted hydroxyazobenzene 4-ethyl-4'-hydroxyazobenzene designated 2PAP was used as a reference because its humidity sensitivity has been thoroughly reported in 2018 [101]. Five other hydroxyazobenzenes were selected based on their availability and diversity in substituents. In addition, two other azobenzene molecules without a hydroxy group were selected as reference molecules to confirm the hypothesis of humidity dependence being a property of specifically hydroxyazobenzenes. The selected molecules and their molar masses are presented in Fig 3.1.

DMA-OH, molecule **2** in Fig 3.1, is substituted with a strong electron-donating dimethylamino group of $\sigma_{DMA} = -0.83$ in addition to hydroxy group of $\sigma_{OH} = -0.37$ as presented in table 2.1 [23]. With two electron-donating groups symmetrically in the para positions of both benzene rings, electron density at the π conjugated azo bond is increased. Similarly to DMA-OH, the third molecule in 3.1 has a methoxy group instead of DMA group and is hence designated MeO-OH. Methoxy group is electron-donating but weaker than DMA

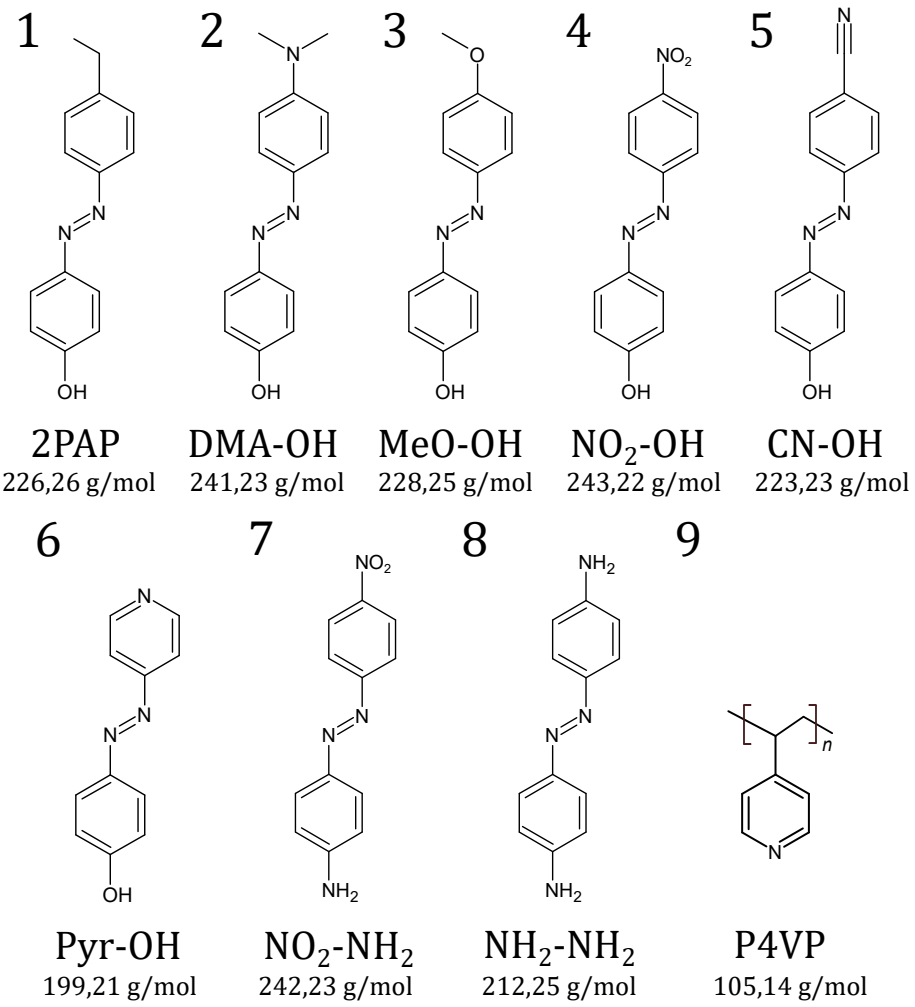

Figure 3.1. Studied molecules. *The structures of eight para-disubstituted azobenzenes studied in this thesis designated 2PAP (**1**), DMA-OH (**2**), MeO-OH (**3**), NO_2-OH (**4**), CN-OH (**5**) and Pyr-OH (**6**). Two azobenzenes not containing a hydroxy group were NO_2-NH_2 (**7**) and NH_2-NH_2 (**8**). Polymer used to fabricate sample films was P4VP (**9**).*

with $\sigma_{MeO} = -0.27$, so MeO-OH is expected to behave similarly with regard to humidity as DMA-OH.

The fourth molecule in Fig 3.1, designated NO_2-OH, has a push-pull substitution pattern with a strong electron-withdrawing nitro group of $\sigma_{NO_2} = 0.78$ pulling electron density through the π conjugated system from electron-donating hydroxy group. The fifth molecule is similar to NO_2-OH, substituted with a slightly weaker electron-withdrawing cyano group of ($\sigma_{CN} = 0.66$) and thus designated CN-OH.

With electron-donating and withdrawing groups at either end of the benzene rings, electron density at the π conjugated azo bond is altered in the push-pull substitution, although the fairly weak electron-donating hydroxy group is not enough to classify either molecule into strong push-pull molecules. Pyr-OH differs from the other five studied molecules as azo bond is not between two symmetrically substituted benzene rings, but as pyridine is electron-withdrawing, push-pull type behaviour can be expected [102, pp. 247–250].

Two studied azobenzenes did not contain a hydroxy group and were selected to confirm the hypothesis of humidity dependence being a property of specifically hydroxyazobenzenes. These molecules were 4-(4-nitrophenylazo)aniline, commercially known as Disperse orange 3 and here designated as NO_2-NH_2, and 4,4'-azodianiline designated as NH_2-NH_2. With two strong electron-donating amino groups of $\sigma_{NH_2} = -0.66$, substitution pattern brings a considerable increase in electron density to NH_2-NH_2 azo bond. NO_2-NH_2, on the other hand, is the only molecule studied in this thesis with strong push-pull character. Having both amino group as electron donor and nitro group as electron acceptor, NO_2-NH_2 is expected to isomerise with a lifetime of in the order of seconds due to high electron density at the azo bond [27].

As azobenzene derivatives are classified into toxic solids with combustible nature, can cause irritation to eyes, skin and respiratory system and are considered a potential carcinogen [103, pp. 330-331], standard laboratory safety was followed by wearing laboratory coat, nitrile gloves and safety goggles. Fume hood and local exhaust ventilation were utilised when preparing stock solutions and samples. Gloves were also used to prevent sample contamination from hands. Furthermore, solvents used in sample fabrication are moderately toxic and suspected carcinogen, necessitating extra care when dealing with solutions. Chloroform can cause permanent eye damage or fainting, [103, pp. 773-776], whereas DMF can cause liver damage and absorbs readily through the skin [104].

3.1.2 Polymer-azobenzene complexes

Sample fabrication began with preparing 2 ml stock solutions of P4VP and each studied azobenzene. For 2PAP, stock solutions with *mole fractions* χ of 1:1, 1:2, 1:4 and 1:10 were produced. Here, mole fraction is the ratio of how many 2PAP molecules are in solution per P4VP repeating unit, *e.g.* 1:1 refers to a solution with equimolar amount of 2PAP molecules and P4VP monomers. For other azobenzenes, stock solutions were made with 1:4 mole fraction. Furthermore, 2PAP samples were studied using two sets of stock solutions: one set with heavier long-chain P4VP polymer of average molar weight $M_w \approx$ 60 000 g/mol and thus approximately 570 monomers per polymer, and another using lighter short-chain polymer with $M_w \approx$ 1 200 g/mol or around 10 repeating units.

Table 3.1 presents desired and realised mole fractions χ_{calc} and χ_{real}, mass concentration γ, masses of P4VP m_p and azobenzene m_a, azobenzene mass percentage w_a and polymer molar mass M_w. Solvent for all 2PAP stock solutions was chloroform. It has been reported to dissolve both 2PAP and 4PVP without issues [101] and its high vapour pressure (21.3 kPa at 20 °C [105]) ensures rapid evaporation during spin coating.

MeO-OH, CN-OH, NO_2-NH_2 and NH_2-NH_2 stock solutions were also prepared in chloroform but DMA-OH, NO_2-OH and Pyr-OH were dissolved in dimethylformamide (DMF) due to solubility issues with chloroform. DMF was chosen after solubility tests between DMF, tetrahydrofuran and acetonitrile because of its highly polar aprotic nature (nearly four times higher dipole moment than chloroform). Unfortunately DMF has extremely

Stock ID	χ_{calc}	γ (mg/ml)	m_p (mg)	m_a (mg)	w_a	M_w (g/mol)	χ_{real}
T1	1:1	15	9.6	20.5	68.1%	60 000	1:1.01
T2	1:4	15	19.6	10.6	35.1%	60 000	1:3.98
T3	1:10	25	61.8	13.3	17.7%	60 000	1:10.0
T4	1:1	15	9.5	20.6	68.4%	1 200	1:0.99
T5	1:4	15	19.5	10.5	35.0%	1 200	1:4.00
T6	1:10	25	61.8	13.4	17.8%	1 200	1:9.93
T7	1:2	15	14.5	15.5	51.7%	60 000	1:2.01
T8	1:2	15	14.5	15.5	51.7%	1 200	1:2.01
T9	1:1	15	9.4	20.48	68.5%	60 000	1:0.99

Table 3.1. Stock solutions for 2PAP samples. *Each stock was dissolved into 2 ml chloroform.*

Molecule	χ_{calc}	γ (mg/ml)	m_p (mg)	m_a (mg)	w_a	χ_{real}
DMA-OH	1:4	75	95.3	54.6	36.4%	1:4.01
MeO-OH	1:4	20	13.1	7.0	34.8%	1:3.97
NO_2-OH	1:4	50	25.3	14.6	36.6%	1:4.01
CN-OH	1:4	20	13.1	6.9	34.5%	1:4.12
Pyr-OH	1:4	56	30.4	14.4	32.1%	1:4.00
NH_2-NH_2	1:4	20	13.2	6.9	34.3 %	1:3.86
NO_2-NH_2	1:4	20	12.8	7.4	36.6 %	1:3.99

Table 3.2. Stock solutions for studied hydroxyazobenzenes. *For MeO-OH, CN-OH, NH_2-NH_2 and NO_2-NH_2 stock solvent was chloroform, but DMA-OH, NO_2-OH and Pyr-OH were dissolved in DMF.*

low vapour pressure (490 Pa at 20 °C [106]), so 2-3 times higher mass concentration was used to achieve sufficient sample thickness and extra steps were taken in sample preparation to ensure complete solvent evaporation.

Masses were weighted with the laboratory scale Fisher Scientific PAS214 Analytical Balance with $\Delta m = 0.1$ mg repeatability and solvent was added with Thermo Scientific Finnpipette F1 1000 µl Variable Volume Pipette with $\Delta V = 6$ µl $\pm$0.6 % inaccuracy and reported 2 µl $\pm$ 0.2 % imprecision. Stock solutions were stored in Supelco 27001-U 4 ml clear vials with PTFE sealing on caps to prevent solvent corrosion and consequent evaporation. Stock solutions were filtered to remove any insoluble contaminants with 200 nm pore size PTFE syringe filters and films were fabricated immediately after within hours of making solutions. Example of stock solution is shown in Fig 3.2.

Prior to sample preparation, glass substrates suitable for film deposition were prepared. The used substrate glass was Menzel-Gläser Thermo Scientific microscope slides in accordance with the ISO 8037/1 standard and 26 x 76 x 1 mm dimensions. Microscope

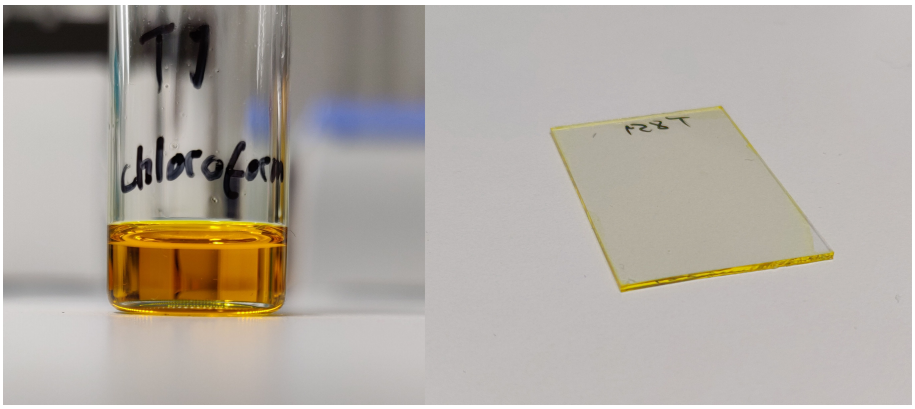

Figure 3.2. Stock solution and thin film.

slides were split in half with a glass cutter and cleaned from any contaminants with *sonication*, a method of converting electrical signal into mechanical vibrations generally to agitate particles in a liquid medium chemically and physically [107, p. 153]. Sonication utilises ultrasonic frequencies of over 20 kHz to generate microscopic vacuum bubbles and bursting them in a process coined *cavitation* to disrupt intermolecular interactions within the medium. Sonication can be employed in degassing solutions, facilitating aggregate dissolving, or removing contaminants from surfaces [108].

For thorough surface contaminants removal, sonication was performed with Elma Elmasonic P sonicator at 37 kHz and 30 °C for 20 min in three solutions: acetone, isopropyl alcohol and finally highly purified water. After third sonication, excess water was briefly removed from clean glass substrates with nitrogen gas flow and placed in an oven at 80 °C for 2 hours to evaporate any remnant water. Clean glass substrates were subsequently used for spin coating or stored in a sample holder protected from dust and air contaminants.

3.1.3 Film fabrication

Sample films were fabricated from stock solutions presented in table 3.1 using *spin coating*, a fabrication method where organic materials dissolved in volatile solvent form a thin film on substrate via centrifugal force and the process of evaporation [109, pp. 50–51]. Spin coating involves four steps which are illustrated in Fig 3.3. First, a small volume of solution is deposited on a substrate stationed on a rotating chuck. This step is known as *deposition* and it can be a defining step in film fabrication involving highly volatile solvents as even a brief moment between deposition and spinning can allow for significant solvent evaporation and result in uneven film thickness [110].

Second step, spin up, involves rapid angular acceleration of the chuck. In this step, excess solution is ejected from the surface of the substrate due to centrifugal force, followed by a period of rotation at a constant speed [111, pp. 204—206]. Third and fourth steps involve spin off and evaporation, although for highly volatile solvents majority of evaporation takes place during constant rotation. Dark grey block in Fig 3.3 represents the rotating

chuck, black part is the rubber seal for vacuum suction and light grey block is the glass substrate.

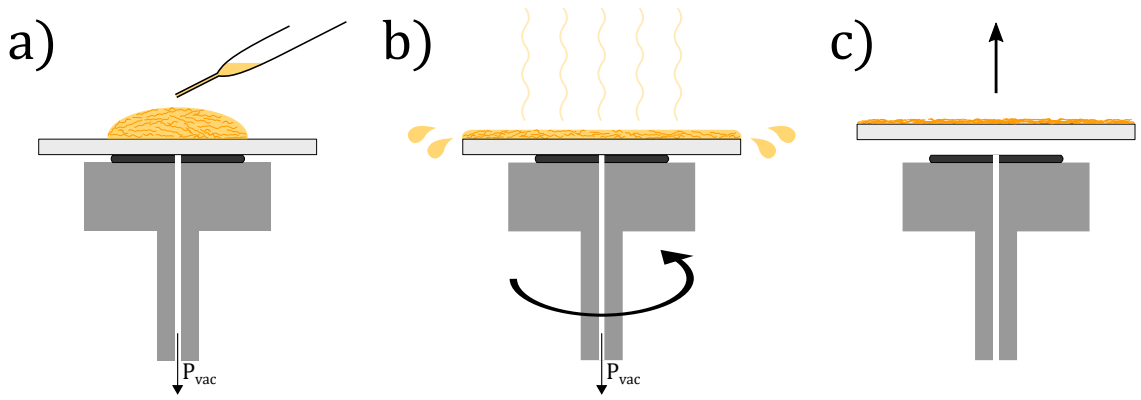

Figure 3.3. Thin film spin coating. *a) Solution is deposited on a substrate held in place on a rotating chuck with vacuum suction P_{vac}. b) Rotating chuck is accelerated rapidly causing excess solution to be ejected. Prolonged rotation at constant angular speed promotes solvent evaporation without ejecting further solution from substrate. c) Once solvent has evaporated, rotation and vacuum suction is stopped, allowing sample removal.*

Spin coating is often the preferred method in organic thin film fabrication on account of method simplicity and affordability [112, p. 56]. Main parameters defining spin coated film thickness are angular velocity of rotation ω and solution viscosity η, but other factors have an effect such as spin time, solution density, solvent evaporation rate and surface wettability. Thickness of the film produced via spin coating can be determined numerically from the following equation [111, pp. 204-–206]:

$$h = \left(1 - \frac{\rho_A}{\rho_{A_0}}\right) \cdot \left(\frac{3\eta m}{2\rho_{A_0}\omega^2}\right)^{1/3}, \tag{3.1}$$

where h is the film thickness, ρ_A is solvent density, η is viscosity of solution, m is rate of solvent evaporation, and ω is the angular velocity of rotation. As rate of evaporation is determined experimentally, calculating numerical film thickness values are out of scope of this thesis. Instead, assuming linear dependency between absorption in film and film thickness $A \propto h$, a simpler expression can be used to approximate the relation between absorption and speed of rotation ω in spin coating [110]

$$A \propto \omega^{-1/2}, \tag{3.2}$$

which correlates well with experimental results. Spin coating was conducted with Laurell Technologies WS-650-23 spin coater at 21 $\pm$ 0.5 °C ambient temperature. A clean glass substrate was placed on the rotating chuck of the spin coater where vacuum suction secured it during spinning. 160 µl volume of stock solution was discharged on the substrate and immediately spun to avoid inhomogeneous film formation. To ensure solvent evaporation, substrates were spinned for 20 s each. First film from T4 stock solution was fabricated using specifications for a similar solution from [101], and based on the ab-

sorbance of the resulted sample speed of rotation was adjusted to produce samples with absorbance maximum around $A_{max} \approx 0.6$. Thicker samples were required for lower mole fraction samples to compensate for the chromophore scarcity. For each stock solution, eight samples were fabricated and are presented in table 3.3. Absorbance maxima were determined from absorption spectra with second degree polynomial fitting to peak region to reduce the effect of noisy data.

Stock ID	ω (rpm)	A_{max}	λ_{max} (nm)
T1	2500−3500	0.55−0.61	353
T2	700	0.56−0.59	358
T3	500−600	0.54−0.67	361
T4	2300−2500	0.59−0.65	353
T5	500−700	0.55−0.63	359
T6	500	0.52−0.61	360
T7	2000	0.63−0.66	356
T8	2000	0.57−0.62	356
T9	2300−2500	0.70−0.80	353

Table 3.3. 2PAP samples. *Higher angular velocity resulted in lower absorbance maximum. Spinning time was 20 s for each sample.*

Stock ID	χ_{real}	ω (rpm)	**Solvent**	A_{max}	λ_{max} (nm)
DMA-OH	1:4.01	2500-2800	DMF	0.68-0.77	412
MeO-OH	1:3.97	1000-1500	Chl	0.72-0.84	364
NO_2-OH	1:4.01	800	DMF	0.64-0.65	385
CN-OH	1:4.12	1000	Chl	0.68-0.69	385
Pyr-OH	1:4.00	800-1000	DMF	0.65-0.74	365
NH_2-NH_2	1:3.86	700	Chl	0.68-0.69	412
NO_2-NH_2	1:3.99	700	Chl	0.58-0.60	455

Table 3.4. Studied molecules samples. *For MeO-OH and CN-OH, spinning time 20 s, while DMA-OH, NO_2-OH and Pyr-OH were first spun for 20 s at reported angular velocity and subsequently 5 min at 800 rpm.*

Spin coating DMF solution on a stock microscopy glass substrate proved challenging as surface wettability was insufficient and virtually all DMF solution was ejected from the surface of the substrate due to centrifugal force. As surface wettability can be enhanced [113, pp. 72–79] by removal of surface contaminants including particles, organic or inorganic thin film or molecular contamination and microbial contamination, *UV-O_3* cleaning was applied on the surfaces using BioForce ProCleaner^{TM}Plus single drawer tray UV-O_3 cleaning unit with 15 min treatment time for glass substrates.

UV-O_3 cleaning is an efficient, ecological, and inexpensive method of surface contaminants removal for achieving near-atomically clean surface [113, p. 94]. UV light of $\lambda = 184.9$ nm is used to convert molecular oxygen into ozone and atomic oxygen and

in turn $\lambda = 253.7$ nm UV light dissociates ozone into molecular and atomic oxygen. The strongly oxidising atomic oxygens react with the contaminants, desorbing organic mass as volatile gaseous compounds and inorganic mass in highly oxidised states. The most typical contaminants on microscopy glass substrates are volatile organic and sulphur compounds, [113, pp. 91–92] which proved effortless to remove with UV-O_3 cleaning.

As most of the surface contaminants were removed through sonication, main benefit in surface wettability resulted from changes in the chemical properties of the glass surface. UV-O_3 treatment leads to formation of hydrophilic hydroxyl groups and thus enhanced wettability with polar DMF. DMF solutions also involved an additional spin coating step. DMA-OH, NO_2-OH and Pyr-OH samples were first spun for 20 s at angular velocity reported at table 3.4 and subsequently for 5 min at 800 rpm. The purpose of the extended spinning step with lower angular velocity was to ensure sufficient evaporation without further thinning the film while rotational motion prevented the volume from retracting from flat film into a drop.

After spin coating, samples were kept on a heat plate at 60 °C for 5 min to ensure solvent evaporation, after which initial absorption spectra were measured and samples were thereafter placed on an 80 °C heat plate in vacuum for 2 h time period. Longer heat treatment was particularly important for samples fabricated from DMF solutions due to its slower evaporation rate. Heat plate and oven treatments are called *annealing*, meaning a process where the material is exposed to moderate heat treatment for a time in order to change material properties, often to relieve internal stresses introduced during film fabrication [114].

Possible annealing effects were monitored with repeated absorption spectra measurements to determine if heat treatment had an effect on absorption through thickness change, for example. When spectral changes were observed due to annealing, samples were kept additionally overnight on an 80 °C heat plate in vacuum. 80 °C temperature was chosen as it is below P4VP glass transition temperature T_g but above solvent boiling point $T_b = 61.2$ °C [105]. For samples fabricated from DMF solution, annealing time was at least 24 h to ensure sufficient time for solvent evaporation.

3.2 Experimental setup

This section elaborates the experimental setup used for measurements with images or schematics of equipment used as well as details about measurement conditions and parameters. Microscope setup was used to examine visible microstructures in samples while spectrophotometer setup allowed for investigating static and dynamic light absorption. The section will also discuss possible instrumental, environmental, or procedural sources of error in measurements.

3.2.1 Polarised light microscopy

Polarised light microscopy involves polarised light as a means to study materials [115, pp. 774–777]. Instruments utilising polarised lights are referred to as polarising optical microscopes (POM), and their operating principle relies on optical filters called *polarisers* which limit light transmission through it to a specific polarisation, effectively filtering out light not matching its polarisation. Polarisers can be absorptive or beam-splitting, meaning they can filter light be absorbing it or reflecting it. POM operates with two crossed *linear polarisers* which block all other light except that which is linearly polarised along polariser axis. When these linear polarisers are positioned so that their polariser axes are crossed or perpendicular to each other, no light can pass through their combination. This phenomenon is illustrated in Fig 3.4 (b).

Crossed linear polarisers enable viewing *birefringent* materials with high contrast to their surroundings: birefringent material causes double refraction where light is split based on polarisation into ordinary and extraordinary beam along and perpendicular to the optical axis of the material, respectively [115, p. 776]. As a result of beam splitting, polarisation of light propagating through birefringent material is altered and some nonzero component of polarisation is along the analyser axis, allowing light to pass through. The amount of light passing through the analyser depends on the angle θ presented in Fig 3.4 can be estimated from Malus's law.

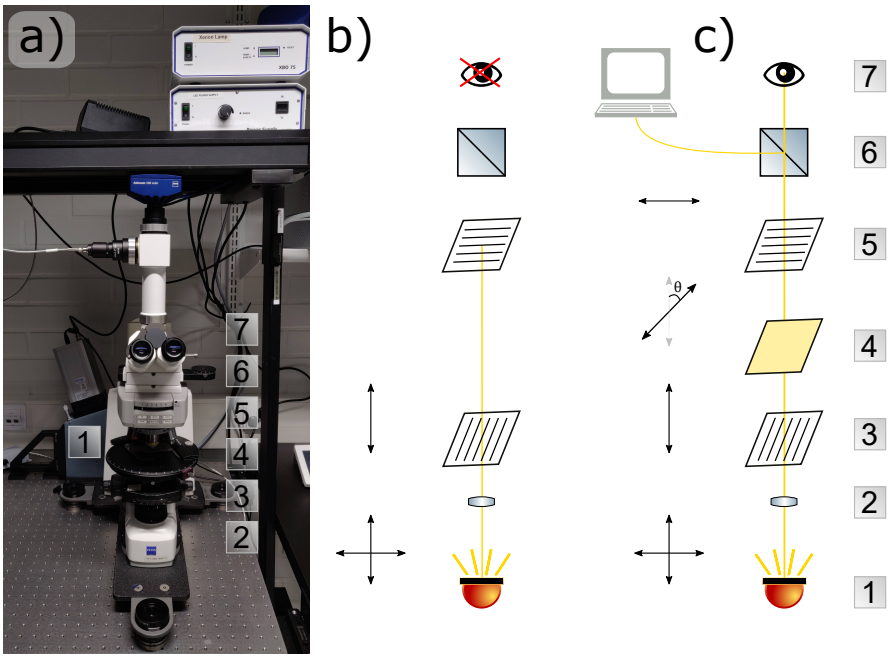

Figure 3.4. Polarised light microscope. *a) Image of POM from laboratory, b) illustration of cross-polarised light not propagating to the observer and c) birefringent sample rotating linearly polarised light, resulting in detected light.*

Essential components of the POM setup are shown in Fig 3.4. Light propagating from a white light source, here an LED light source behind the microscope (**1**) is directed upward through a lens and an aperture (**2**). Before the light reaches the sample, it passes through

the first linear polariser (**3**). This linearly polarised light propagates through the sample on a rotating microscope stage (**4**) and to the second linear polariser known as *analyser* (**5**). Given that the polariser and analyser are properly crossed, light only propagates through the analyser if something in between is birefringent. After the analyser, light can either be directed with a beam splitter (**6**) to the eyepiece for direct viewing or to the microscope camera for image processing (**7**). Microscope camera is the Axiocam 506 color visible in the Fig 3.4 a) as the blue part at the top of the microscope.

Azobenzenes studied in this thesis would not exhibit birefringence while noncovalently bound to the amorphous polymer as amorphous materials have no long-range order and are thus isotropic. If aggregation occurs, however, aggregating azobenzenes may recrystallize into ordered anisotropic structures exhibiting birefringence. POM imaging can be used to reveal prominent birefringent aggregates within the sample. Therefore, linear and cross-polarised images were taken periodically from a set of samples at a fixed point to study possible aggregation effects over the time span of 9 months. Images were taken with Axio Scope.A1 POM and Axiocam 506 Color microscope camera using 10x objective with 0.25 NA and 1.0x zoom and exposure time set at 30 ms with cross-polarised and linearly polarised light. Additionally, cross-polarised images were taken with 300 ms exposure time for higher sensitivity towards small birefringence.

3.2.2 Absorption spectroscopy

Absorption spectra were measured with Agilent Technologies Cary 60 UV-Vis spectrophotometer between 300–800 nm wavelength range. Wavelength range was chosen as the absorption bands of $\pi \rightarrow \pi^*$ and $n \rightarrow \pi^*$ transitions for studied molecules lie within this range and glass substrates used begin to strongly absorb UV at $\lambda < 300$ nm. Absorption spectra were measured for fully relaxed samples in pure *trans* population (>99 $\%$). In order to avoid unwanted photoisomerisation, measurements were conducted in red lighting at 21 $\pm$ 0.5 $^{\circ}$C ambient temperature using 10 nm/s scanning speed with 1 nm interval. Similarly, *cis* spectra were measured in identical conditions immediately after excitation with Prior Lumen 1600 LED light source within sample absorption band and at regular intervals afterwards with 160 nm/s scanning speed with 2 nm interval, resulting in spectra visualising thermal relaxation as shown in Fig 2.12.

To further study thermal isomerisation at different relative humidities, a setup comprising of two light sources, measurement chamber with humidity controller and a spectrophotometers was utilised. Samples were confined in Linkam LTS420-H measurement chamber which provided an airtight environment of convenient volume. Combined with Linkam RH95 humidity controller, samples could be kept at constant temperature and RH indefinitely. RH95 operated at $\pm$0.5 % stability between 5-90 % RH according to manufacturer specifications, and thus $\pm$0.5 % was elected as the tolerance for variation in humidity measurements.

Monitoring light source was Ocean Optics DH-2000-BAL deuterium and tungsten halogen lamp combination operating between 230–2500 nm. According to manufacturer specifications, monitoring light source involved 25 min warm-up time until drift of optical output was $\leq$ 0.1 %/h, and approximately 30 min warming up time was observed before thermal stability settled and intensity drift ceased. Excitation light source was Prior Lumen 1600 LED light source with 16 available emission wavelengths and 100-step output power adjustment. Monitoring signal passed through Edmund Optics bandpass filter with 10 nm wide transmission band and was collected at the photodetector to Avantes Starline AvaSpec-2048L spectrophotometer with $<$ 0.01 % stray light reported by manufacturer. Bandpass filters used had transmission band at 365 nm, 405 nm, 430 nm, and 470 nm center wavelengths.

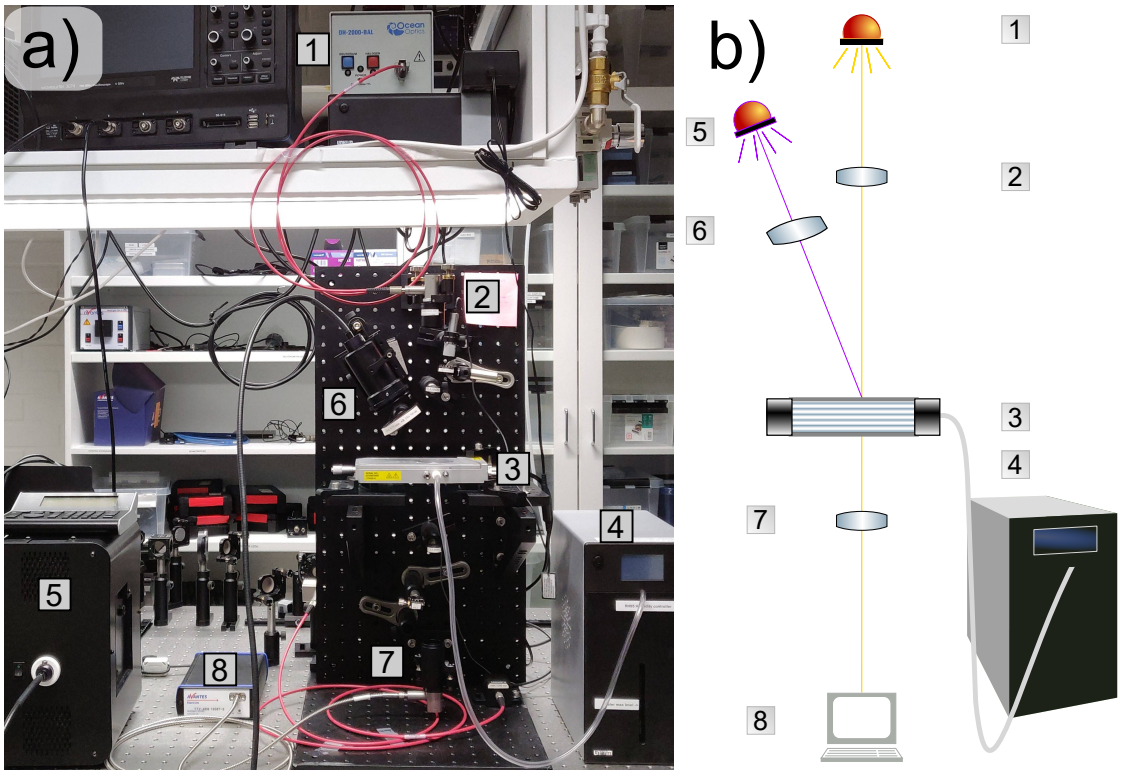

Figure 3.5. Thermal isomerisation setup. *a) Image of thermal isomerisation setup from laboratory and b) illustration of the setup with monitoring (yellow vertical beam) and excitation (purple angled beam) light sources, measurement chamber with humidity controller and spectrophotometer.*

As shown in Fig 3.5, thermal isomerisation measurement setup comprised of eight essential components. Monitoring light (**1**), represented in Fig 3.5 b) as the yellow vertical beam, was guided into the setup via optical fiber and focused onto the sample with a lens setup (**2**). Sample was kept at constant temperature and RH inside the airtight measurement chamber (**3**) where constant humidity was maintained with the computer-operated humidity controller (**4**). Thermal relaxation measurements were initiated with measuring absorbance of pure *trans* population at monitoring wavelength range, followed by 1 s pulse of excitation light. For the studied molecules, excitation wavelengths between 365–405 nm were used. Excitation light was emitted at the LED light source (**5**), repre-

sented in Fig 3.5 b) as the purple angled beam, and guided using a liquid light guide onto a collimator and subsequently through a focusing lens (**6**) onto the sample. Photoisomerisation caused a drop and subsequent rise in monitored absorbance as *cis* population relaxed thermally back to *trans*. Monitoring signal was focused onto an optical fiber (**7**) and analysed at the spectrophotometer (**8**). Measurements were conducted at 23 $\pm$ 0.5 °C and ambient red lighting.

3.3 Data processing

Data collected by Avantes spectrophotometer from thermal isomerisation measurements was further processed to determine *cis-trans* isomerisation rate constants and lifetimes of *cis*-isomers. Spectrophotometer collected data with 25 ms integration time and averaging 4 of these measurements into a data point, so data points were collected every 100 ms. Absorbance was measured as a function of time and plotted into a graph displayed at 3.6 (a). It has been reported that azobenzene thermal isomerisation in polymer films does not follow simple first-order kinetics [101], so a stretched exponential function known as Kohlrausch-Williams-Watts function is employed. Difference between regular and stretched exponential fit is illustrated in Fig 3.6 (b). Absorbance at a given moment in time t is given by [101]

$$A(t) = (A_0 - A_\infty)e^{-(kt)^\beta} + A_\infty, \tag{3.3}$$

where A_0 is absorbance immediately after illumination, A_∞ is absorbance of fully relaxed *trans* population state, k is the thermal isomerisation rate constant and β is the stretching exponent term. A_∞ corresponds to practically pure (>99 $\%$) *trans* population as samples were kept in the dark longer than their lifetimes and measurements were conducted in red lighting. Poutanen *et al* also showed that the *cis* $\rightarrow$ *trans* rate constant can be expressed as exponentially dependent from temperature and humidity according to equation 3.4 [101]

$$k(T, RH) = k_0 \cdot e^{-E_a/RT} \cdot e^{\lambda \cdot \mathrm{RH}}, \tag{3.4}$$

where k_0 is a sample-dependent constant, E_a is the apparent activation energy, R is the molar gas constant, RH is the relative humidity and T the corresponding temperature. In practice this means that in order to measure humidity with an azobenzene-based sensor, ambient temperature must be simultaneously monitored. Optimally both measurements can be conducted optically using a single film, one monitoring wavelength for temperature and another for humidity. Based on the Poutanen's proposition of humidity sensitivity being a property of tautomerisable azobenzenes, most of the studied molecules were selected to be hydroxyazobenzenes. Additionally, two molecules not containing hydroxy group were selected for comparison.

As shown in Fig 3.6 (a), absorbance was measured from the fully relaxed samples for about 10 s prior to illumination to determine A_∞. At $t = 0$, measured absorbance corresponds to A_0 and thus $A(0) = A_0$ as indicated in Fig 3.6 a). The time it takes for the sample population to thermally relax from *cis* to *trans* and hence the from *cis* lifetime can be determined by monitoring absorbance change from A_0 to A_∞.

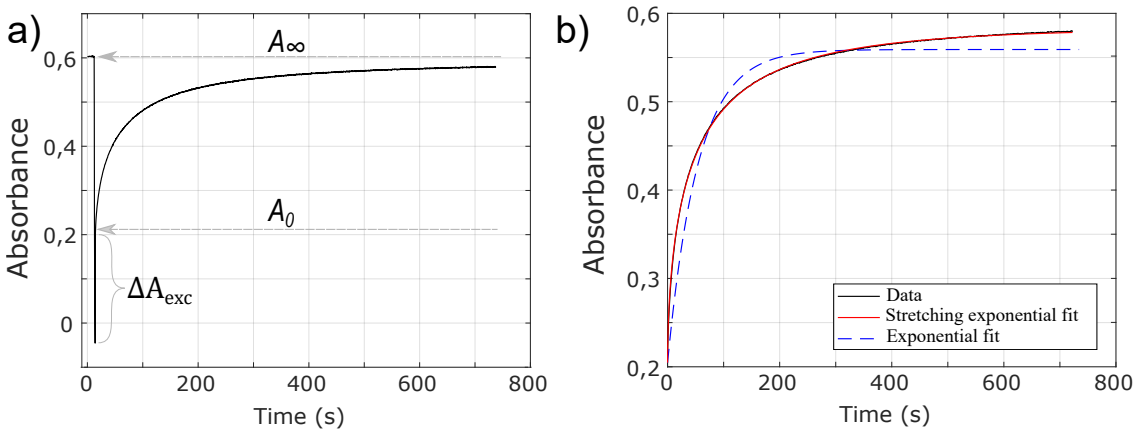

Figure 3.6. Data fitting. *a) Absorbance change over time shows the life cycle of azobenzene photoisomerisation. Absorbance was monitored for $\chi = 1{:}4$ P4VP/2PAP sample 360–370 nm. Prior to photoisomerisation, absorbance of fully relaxed sample with >99 % trans population is A_∞, while A_0 is absorbance after illumination. Additional drop in absorbance is due to detection of excitation wavelength shown in figure with ΔA_{exc}. b) Illustration of fitting equation 3.3 onto the data with $\beta \approx 0.55$ and $R^2 = 0.999$ in red compared to plain exponential fit with $\beta = 1$ and $R^2 = 0.913$ in blue.*

As shown in Fig 3.6 (b), thermal relaxation rate constant k and *cis* lifetime $\tau = 1/k$ can be solved from data after measuring absorbance change over time. The life cycle of azobenzene photoisomerisation is spectrally presented in Fig 3.6 (a). In the example data set, absorbance was monitored for 1:4 molar fraction P4VP/2PAP sample at 360-370 nm monitoring wavelength range. Prior to photoisomerisation, absorbance of fully relaxed sample with >99 % *trans* population is A_∞, while A_0 is absorbance right after illumination. Excitation beam intensity was between 90–600 mW/cm^2 for molecules tested for humidity sensing purposes and 50–70 mW/cm^2 for P4VP/2PAP studies of possible aging effects, while monitoring beam intensity was orders of magnitude weaker and therefore its contribution to photoisomerisation can be considered negligible.

Additional drop in absorbance indicated in Fig 3.6 a) with ΔA_{exc} is due to detection of excitation wavelength of 365 nm being within monitoring wavelength range. Absorbance drops below zero during excitation which would indicate the sample is actually emitting light. However, this is not the case but rather a small portion of the excitation beam is diffracted into the detector in addition to the monitoring beam. As the excitation beam is orders of magnitude more intensive, even a fraction of a percent of the excitation beam intensity is enough to distort the monitoring beam reading. Fortunately, with some molecules monitoring could be conducted at a different wavelength than excitation, effectively eliminating the distortion.

Isomerisation data was processed in MATLAB computing environment using an algo-

rithm. Given suitable limits to data fitting parameters such as $0 < \beta \leq 1$ and $0 < k < 10^3$, equation 3.3 fit extremely well to all data and yielded reproducible results. Fig 3.6 b) illustrates how well fitting equation 3.3 onto the data succeeds with coefficient of determination $R^2 = 0.999$. With coefficient of determination close to unity, the model expressed with equation 3.3 describes the thermal isomerisation phenomenon accurately and shows that the data has high signal-to-noise ratio and is thus of good quality. Furthermore, the significance of using the stretched exponential fit is also evident in Fig 3.6 b). Exponential fit of equation 3.3 with $\beta = 1$ is presented with a blue dashed line and clearly does not adequately describe the thermal relaxation, whereas stretching exponential fit with $\beta \approx 0.55$ yields the accurate fit presented with a red solid line.

Thermal isomerisation measurements were conducted for a set of 2PAP samples over the time span of 9 months alongside with POM imaging to determine possible aging effects on absorption and thermal relaxation. For the studied molecules, thermal isomerisation was measured at various relative humidities to determine the humidity dependence of *cis-trans* relaxation mechanism. Results of the experiments are presented in the following chapter.

4 RESULTS AND DISCUSSION

This chapter presents the results from measurements described in the previous chapter as well as discussion about the significance and implications of the results. First part delves into the effect of substitution and molecular environment on azobenzene thermal relaxation constant, while the second part presents the aging effects of azobenzene thin films on absorption spectra, aggregation, and relaxation rate. Final part summarises these two parts and presents how the results can be used to design a humidity sensor.

4.1 Parameters affecting the isomerisation rate

In addition to ambient conditions such as temperature or humidity, azobenzene isomerisation rate can be tailored by altering the benzene ring substitution pattern or the local environment of azobenzene molecules. As P4VP constitutes the azobenzene local environment in the supramolecular complex of the thin film, the effect of P4VP molar mass M_w and mole fraction χ on the isomerisation rate were studied in addition to electron-donating and withdrawing substituents. This section will present parameters affecting the isomerisation rate and discuss in more detail how hydrogen-bonding azobenzenes behave in humidity sensing.

4.1.1 Azobenzene substitution

Studying the effects of azobenzene substitution on isomerisation was conducted with eight azobenzene molecules in $\chi = 1{:}4$ mole fraction thin films. Absorption spectra between 300–800 nm were measured from these samples before and after excitation with light within $\pi \rightarrow \pi^*$ absorption band, and the *cis* $\rightarrow$ *trans* relaxation rate was measured at various humidities with 15 % RH increments from highest to lowest RH. The following subsections will present the studied molecules individually, discuss the molecular properties affecting the spectral features and isomerisation rate and how these molecules could be used in humidity sensing.

Results are compared to previous work by Poutanen *et al* in 2018 [101] where hydroxyazobenzenes were first proposed for humidity sensing, and therefore 2PAP is the reference molecule. $\chi = 1{:}4$ mole fraction thin films was chosen for this thesis as equimolar films were hypothesised to demonstrate aggregation-related issues and $\chi = 1{:}9$ exhibited inconveniently slow relaxation in the Poutanen's article. Polymer used in thin films

for azobenzene substitution studies was long-chain P4VP with $M_w \approx$ 60 000 g/mol because of its availability and inexpensiveness, while Poutanen used a special short-chain P4VP with $M_w \approx$ 1 200 g/mol. Further reasoning on the choice of polymer is presented in section 4.1.2. Otherwise the samples and measurements were similar to the previously established system by Poutanen *et al* [101].

Reference molecule: 2PAP

As already extensively studied and reported by Poutanen *et al* [72], 2PAP is well known to display humidity dependence and was therefore selected as the reference molecule for comparing other azobenzenes in humidity sensing [101]. With two weak electron donor groups, hydroxy and ethyl groups, 2PAP has lightly red shifted absorption band compared to unsubstituted azobenzene and can be classified as azobenzene-type. Absorption spectrum for pure ($> 99\ \%$) *trans* population 2PAP sample is presented in Fig 4.1 a) with a dashed black line. After excitation with 1 s pulse of 90 mW/cm^2 $\lambda_{exc} = 365$ nm light, a large portion of the *trans* population isomerised into *cis* resulting in notable spectral changes. Excitation light intensities were estimated from LED light source measured output power and beam area at sample surface. A spectrum of this *cis*-rich population state was measured immediately after excitation and is presented in Fig 4.1 a) with a red line.

Absorption spectra were periodically measured from the same spot, illustrating the non-radiative thermal relaxation from *cis* to *trans* over time with spectra varying from orange to teal. The prominent and wide $\pi \rightarrow \pi^*$ transition absorption band can be observed between 330–380 nm with a peak at 353 nm. Note that Fig 4.1 a) shows the absorption spectra from an equimolar sample, while rate constants in varying humidity are from $\chi =$ 1:4 samples. Corresponding λ_{max} for 1:4 mole fraction samples would be 358 nm.

Similarly, weaker but detectable $n \rightarrow \pi^*$ transition absorption band can be observed between 440–520 nm and highlighted as a separate inset graph in Fig 4.1 a). Higher absorbance can be observed for *cis*-rich population at $n \rightarrow \pi^*$ band. Furthermore, two wavelengths at which absorption does not depend on isomerisation can be observed at intersections of spectra. These *isosbestic points* at 308 nm and 428 nm for 2PAP and stand as a strong indication that there are only two energy states with relatively long lifetimes above 1 s, $t - S_0$ and $t - S_0$ as presented in fig 2.3.

Humidity dependence and molecular structure of 2PAP is presented in Fig 4.1 b). Samples were kept in the dark for at least a day prior to measurements to ensure thermal relaxation to pure *trans* population. Measurements were conducted in Linkam RH95 humidity controller to maintain 23 $\pm$ 0.5 °C and constant humidity. Spectrophotometer collected data with 25 ms integration time and averaging 4 of these measurements into a data point, so data points were collected every 100 ms. Relative humidity values selected for a set of measurements were 25 %, 40 %, 55 %, 70 % and 85 % RH with $\pm$0.5 % tolerance for humidity variance.

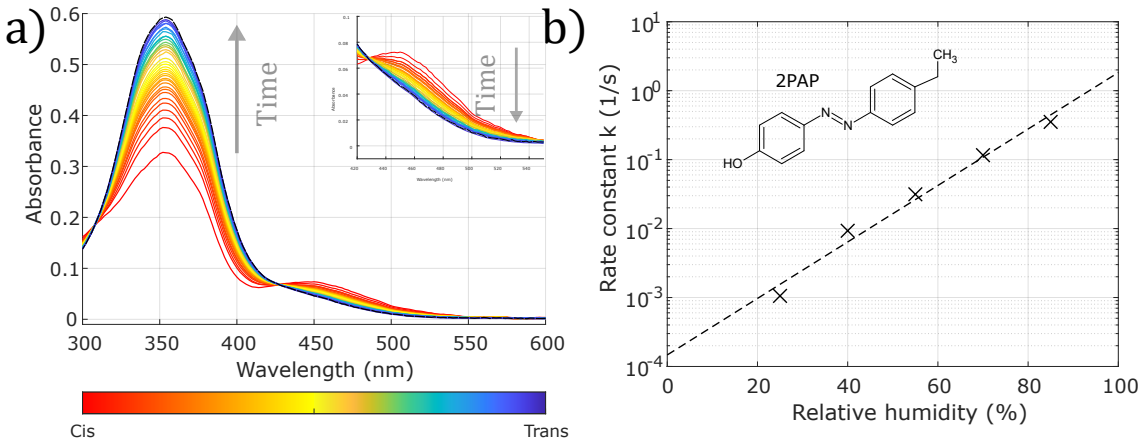

Figure 4.1. 2PAP absorption spectra and humidity dependence. *a) Absorption spectra for* trans*-rich (blue) and* cis*-rich (red) population 2PAP sample with $\tau = 7$ min at $21.3\,^{\circ}$C and $36\,\%$ RH. Dashed black line represents pure trans spectrum. Note: spectra measured from equimolar sample while b) presents rate constant of $\chi = 1{:}4$ 2PAP samples as a function of humidity. Dashed line is linear fits to data. Thermal relaxation rate depends on humidity.*

Once the temperature and humidity had settled, 2PAP sample was excitated with 1 s pulse of 90 mW/cm^2 $\lambda_{exc} = 365$ nm light from Prior LED light source. Excitation wavelength was chosen from the $\pi \rightarrow \pi^*$ band to ensure sufficient absorption while leaving the absorbance maximum for monitoring change in absorbance. As can be seen from Fig 4.1 b), 2PAP *cis* $\rightarrow$ *trans* isomerisation is exponentially humidity-dependent. This exponential RH dependence will be used as a comparison for other studied molecules.

Slow relaxation: DMA-OH

Absorption spectrum for pure ($> 99\,\%$) *trans* population DMA-OH sample is presented in Fig 4.2 a) with a dashed black line. After excitation with 1 s pulse of 90 mW/cm^2 $\lambda_{exc} = 435$ nm light, a large portion of the *trans* population isomerised into *cis* resulting in notable spectral changes. A spectrum of this *cis*-rich population state was measured immediately after excitation and is presented in Fig 4.2 a) with a red line.

DMA-OH substitution involves two electron donor groups in para positions, where hydroxy group is a weak donor while dimethylamino group is a strong donor. Their combination causes a significant shift in the electron density around the azo bond and consequent red shift in the $\pi \rightarrow \pi^*$ band, leading to DMA-OH being spectrally classified as aminoazobenzene. Absorption spectra were periodically measured from the same spot, illustrating the nonradiative thermal relaxation from *cis* to *trans* over time with spectra varying from orange to teal. The prominent and wide $\pi \rightarrow \pi^*$ transition absorption band can be observed between 370–470 nm with a peak at 412 nm.

Similarly, weaker but detectable $n \rightarrow \pi^*$ transition absorption band can be observed between 500–600 nm and highlighted as a separate inset graph in Fig 4.2 a). Although partially overshadowed by the $\pi \rightarrow \pi^*$ band, higher absorbance can be observed for *cis*-rich population at $n \rightarrow \pi^*$ band as well as below 360 nm in the UV shoulder. Furthermore,

two wavelengths at which absorption does not depend on isomerisation can be observed at intersections of spectra. These *isosbestic points* are at 363 nm and 503 nm for DMA-OH.

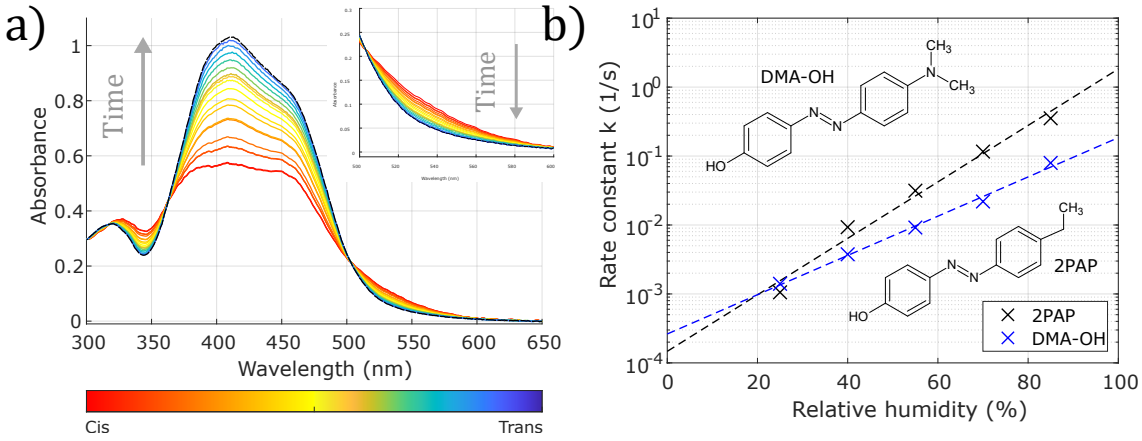

Figure 4.2. DMA-OH absorption spectra and humidity dependence. *a) Absorption spectra for* trans*-rich (blue) and* cis*-rich (red) population DMA-OH sample with $\tau = 16$ min at $21.7\,^{\circ}C$ and $24\,\%$ RH. Dashed black line represents pure trans spectrum. b) Rate constant of DMA-OH samples as a function of humidity. Dashed lines are linear fits to data. Thermal relaxation rate depends on humidity and exhibits slower relaxation than 2PAP for humidities above 20 % RH.*

Humidity dependence and molecular structure of DMA-OH hydroxyazobenzene is presented in Fig 4.2 b). Samples were kept in the dark for at least a day prior to measurements to ensure thermal relaxation to pure *trans* population. Measurements were conducted in Linkam RH95 humidity controller to maintain $23 \pm 0.5\,^{\circ}$C and constant humidity. Spectrophotometer collected data with 25 ms integration time and averaging 4 of these measurements into a data point, so data points were collected every 100 ms. Relative humidity values selected for measurements were 25 %, 40 %, 55 %, 70 % and 85 % RH with $\pm$0.5 % tolerance for humidity variance.

Once the temperature and humidity had settled, DMA-OH sample was excited with 1 s pulse of 90 mW/cm^2 $\lambda_{exc} = 435$ nm light from Prior LED light source. Excitation wavelength was chosen from the $\pi \rightarrow \pi^*$ band to ensure sufficient absorption while leaving the absorbance maximum for monitoring change in absorbance. Moreover, it is noteworthy that excitation wavelength was chosen to be less energetic than absorbance maximum but still from the high absorbance $\pi \rightarrow \pi^*$ band to prevent unwanted photobleaching effects due to sample exposure to intense high energy illumination. Monitoring wavelength range was 400–410 nm for maximum resolution in absorbance change.

As can be seen from Fig 4.2 b), DMA-OH *cis* $\rightarrow$ *trans* isomerisation is exponentially humidity-dependent and the thermal relaxation is slower than for P4VP/2PAP supramolecular polymer above 20 % RH. Slower relaxation in higher humidity most likely results from replacing the ethyl group with dimethylamino group as other conceivable variables remained unchanged. DMA increases the electron density at the azo bond, rendering the *cis* isomer more stable and prolonging its lifetime in high humidity. However, this partially contradicts the mechanism for azobenzene RH dependence proposed by Poutanen *et al*

where water molecules hydrogen bonding with the azo bond reduce the energy barrier of *cis* $\rightarrow$ *trans* isomerisation via rotation mechanism and effectively reduce the *cis* lifetime [101]. As replacing the ethyl group with DMA increases electron density at the azo bond, the bond should become stronger hydrogen bond acceptor and hence the relaxation rate be higher than for 2PAP in higher humidity. For low RH environment there is no contradiction and DMA-OH has shorter *cis* lifetime as can be expected based on its substitution.

Data suggests almost 3 orders of magnitude change in DMA-OH relaxation rate constant whereas the reference 2PAP exhibits an order of magnitude greater rate constant change and thus humidity sensitivity. Therefore DMA-OH cannot compete with 2PAP in terms of sensitivity and resolution, although slower relaxation can be beneficial in measuring higher humidity. 2PAP lifetime is mere seconds in above 90 % RH, potentially compromising humidity measurements with more affordable instruments incapable of precisely measuring such swift relaxations. Sensor setup can be adjusted to measure faster relaxation by reducing spectrophotometer integration time, but monitoring signal must be amplified accordingly to ensure sufficient signal-to-noise ratio, limited by monitoring light source and chromophore optical stability. Excitation pulse must also be shorter than *cis* lifetime for any viable sensing application to ensure sufficient drop in absorbance and thus accuracy in humidity sensing. Conducting higher RH measurements with DMA-OH eliminates this issue as DMA-OH relaxation occurs in high RH with a lifetime in the range dozens of seconds to minutes instead of seconds.

Sensitive relaxation: MeO-OH

Similar spectral features as with DMA-OH can be observed for MeO-OH sample in Fig 4.3 a). Dashed black line represents pure *trans* spectrum and the red line a *cis*-rich spectrum after excitation with 1 s pulse of 160 mW/cm^2 $\lambda_{exc} = 385$ nm light. Absorption spectra were periodically measured from the same spot, illustrating the thermal relaxation from *cis* to *trans* over time with spectra varying from orange to blue. As methoxy group is not as strong electron donor as DMA group, $\pi \rightarrow \pi^*$ transition absorption band is not as red shifted as for DMA-OH. With two weak donor substituents, MeO-OH is borderline aminoazobenzene class molecule with considerable absorption in the UV region. MeO-OH is spectrally fairly similar to 2PAP due to its similar substitution with two weak donor groups.

The prominent and wide $\pi \rightarrow \pi^*$ band can be observed between 330–430 nm with a peak at 364 nm, while $n \rightarrow \pi^*$ band is not overshadowed by $\pi \rightarrow \pi^*$ band but rather distinctly visible between 450–550 nm. As highlighted as a separate inset graph in Fig 4.3 a), higher absorbance can be observed for *cis*-rich population at $n \rightarrow \pi^*$ band as well as below 320 nm in the UV shoulder. Isosbestic points are at 326 nm and 447 nm for MeO-OH.

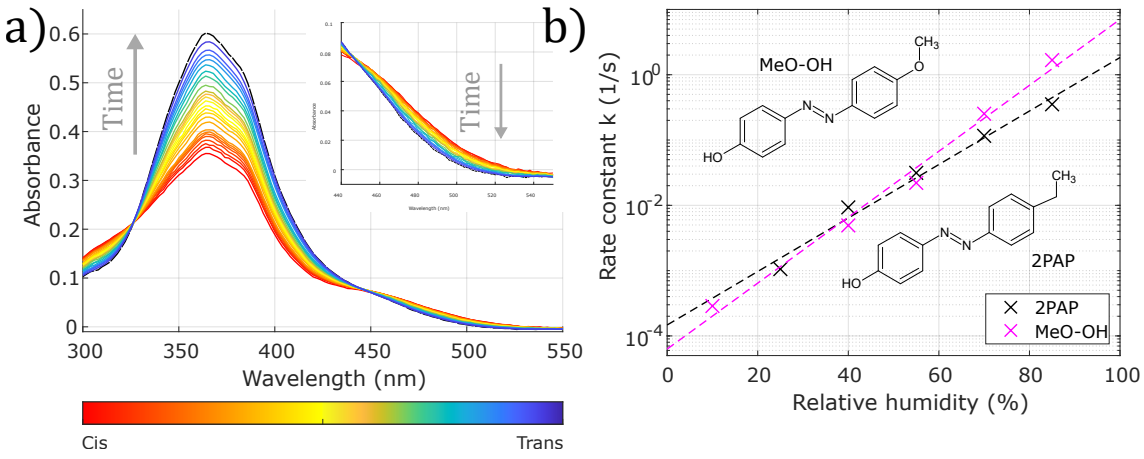

Figure 4.3. MeO-OH absorption spectra and humidity dependence. *a) Absorption spectra for* trans*-rich (blue) and* cis*-rich (red) population MeO-OH sample with $\tau = 3$ min at $22.6\,^{\circ}C$ and $37\,\%$ RH. Dashed black line represents pure trans spectrum. b) Rate constant of MeO-OH samples as a function of humidity. Dashed lines are linear fits to data. Thermal relaxation rate depends on humidity and exhibits slower relaxation than 2PAP in low humidity and faster relaxation in higher humidity.*

Humidity dependence and molecular structure of MeO-OH is presented in Fig 4.3 b). Samples were kept in the dark for a day prior to measurements at 23$\pm$0.5 °C and constant humidity. Six measurements were conducted in 10 %, 25 %, 40 %, 55 %, 70 % and 85 % RH with $\pm$0.5 % tolerance for humidity variance. Photoisomerisation was done with 1 s pulse of 160 mW/cm^2 $\lambda_{exc} = 385$ nm light within $\pi \rightarrow \pi^*$ band but with low enough energy to prevent unwanted photobleaching. Monitoring wavelength range was 360–370 nm for maximum resolution in absorbance change.

As can be seen from Fig 4.3 b), MeO-OH exhibits exponential humidity dependence and the thermal relaxation is slower than for 2PAP below 40 % and faster above 50 % RH. With over 5 orders of magnitude change in relaxation rate constant, MeO-OH demonstrates an order of magnitude greater dynamic range and thus superior sensitivity to humidity compared to the reference 2PAP. MeO-OH is suitable for humidity measurements demanding high sensitivity and resolution, although faster relaxation in higher humidity can be detrimental for sensing applications for instrument limitations discussed with DMA-OH. Given the large dynamic range, MeO-OH is best suited for mid-range humidity measurements demanding high resolution while other azobenzene polymer systems are more optimal for low or high humidity measurements.

In MeO-OH, the weak electron donor ethyl group was replaced with slightly stronger electron-donating methoxy group. With two electron-donating groups, electron density at the azo bond is increased and thus the *cis* isomer becomes more stable. Measurements partially confirm this hydrogen bonding assisted rotation mechanism proposed by Poutanen *et al*: increased electron density at the azo bond makes it a stronger hydrogen bond acceptor and hence the relaxation rate is higher than for 2PAP in higher humidity.

Fast relaxation: NO_2-OH

While DMA-OH and MeO-OH were disubstituted with electron-donating groups, NO_2-OH represents a weak push-pull substitution with a strong electron-withdrawing nitro group in addition to hydroxy group. As hydroxy group is not a strong donor, the weak push-pull system causes only a slight red shift in the $\pi \rightarrow \pi^*$ band. Fig 4.4 a) introduces NO_2-OH spectral features. Dashed black line represents pure *trans* spectrum and the red line a *cis*-rich spectrum after excitation with 1 s pulse of 600 mW/cm^2 $\lambda_{exc} = 405$ nm light. Higher intensity was used to ensure large enough change in absorbance for accurate measurements.

Absorption spectra were periodically measured from the same spot, illustrating the thermal relaxation from *cis* to *trans* over time with spectra varying from orange to teal. The prominent $\pi \rightarrow \pi^*$ transition absorption band can be observed between 350–430 nm with a peak at 385 nm. $n \rightarrow \pi^*$ band is not overshadowed by $\pi \rightarrow \pi^*$ band but barely visible between 480–580 nm. As highlighted as a separate inset graph in Fig 4.4 a), higher absorbance can be observed for *cis*-rich population at $n \rightarrow \pi^*$ band as well as below 340 nm in the UV shoulder. Isosbestic points are at 339 nm and 485 nm for NO_2-OH.

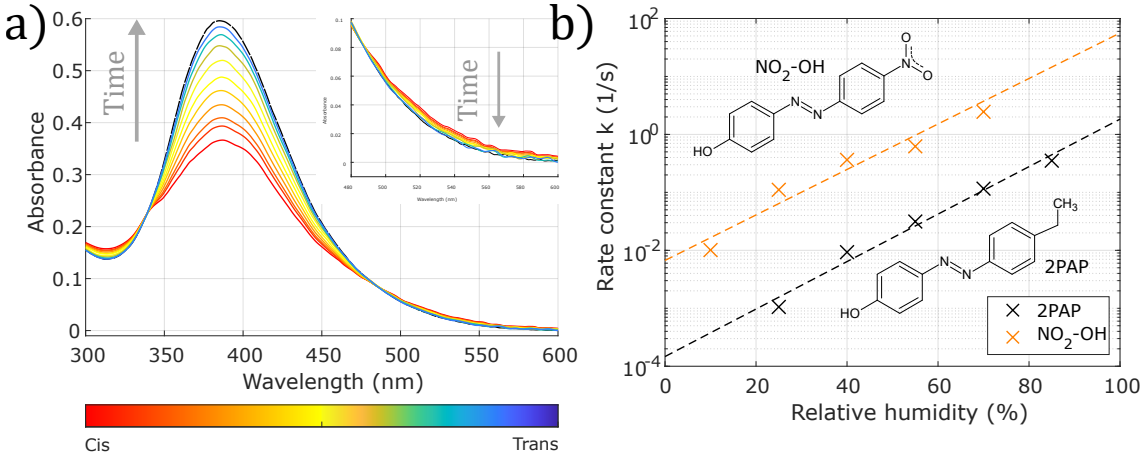

Figure 4.4. NO_2-OH absorption spectra and humidity dependence. *a) Absorption spectra for* trans*-rich (blue) and* cis*-rich (red) population NO_2-OH sample with $\tau = 12$ s at $22.1\,^{\circ}C$ and $23\,\%$ RH. Dashed black line represents pure trans spectrum. b) Rate constant of NO_2-OH samples as a function of humidity. Dashed lines are linear fits to data. Thermal relaxation rate depends on humidity and exhibits 40-50 times faster relaxation than 2PAP across the humidity range.*

Humidity dependence and molecular structure of NO_2-OH is presented in Fig 4.4 b). Five measurements were conducted in similar conditions as described for DMA-OH in 10 %, 25 %, 40 %, 55 % and 70 % RH with ± 0.5 % tolerance for humidity variance. Photoisomerisation was done with 1 s pulse of 600 mW/cm^2 $\lambda_{exc} = 405$ nm light within $\pi \rightarrow \pi^*$ band but with low enough energy to prevent unwanted photobleaching, while monitoring wavelength range was 360–370 nm. Clearly NO_2-OH exhibits exponential humidity dependence with dozens of times faster thermal relaxation than 2PAP across the RH range and a similar DR = 10^4 change in rate constant between 0–100 % RH.

Push-pull substitution causes a shift in the electron density across the π conjugated system from the electron-donating hydroxy group to the electron-withdrawing nitro group, destabilising the *cis* isomer. Despite being weak in push-pull character, the effects of push-pull substitution can be seen in NO_2-OH humidity dependence as drastically reduced *cis* lifetime. Azobenzenes substituted with hydroxy and nitro groups are capable of tautomerising in the presence of polar water, leading to reduced *cis* τ corresponding to increased k. These results are in agreement with the hydrogen-bonding-assisted rotation mechanism proposed by Poutanen *et al*.

With over 4 orders of magnitude change in relaxation rate constant, NO_2-OH demonstrates similar humidity sensitivity as 2PAP, so NO_2-OH is not an alternative for higher resolution humidity sensing. However, notably faster relaxation yields potential for sensor applications in low humidity: even around 10 % RH, NO_2-OH lifetime is mere minutes compared to hours with 2PAP. Given the rapid relaxation at low humidity, NO_2-OH would be best paired with another azobenzene more suitable for high humidity measurements such as DMA-OH.

Fast relaxation: CN-OH

Similar to NO_2-OH, CN-OH represents a weak push-pull substitution with a slightly weaker than nitro electron-withdrawing cyano group in addition to hydroxy group. As hydroxy group is not a strong donor, the weak push-pull system causes even less red shift in the $\pi \rightarrow \pi^*$ band than with NO_2-OH. Fig 4.5 a) introduces CN-OH spectral features. Dashed black line represents pure *trans* spectrum and the red line a *cis*-rich spectrum after excitation with 1 s pulse of 600 mW/cm^2 $\lambda_{exc} = 405$ nm light. Absorption spectra were periodically measured from the same spot, illustrating the thermal relaxation from *cis* to *trans* over time with spectra varying from orange to teal.

The prominent $\pi \rightarrow \pi^*$ transition absorption band can be observed between 330–450 nm with a peak at 385 nm. Weak push-pull substitution pattern brings $\pi \rightarrow \pi^*$ and $n \rightarrow \pi^*$ band close together but is not enough to shift $\pi \rightarrow \pi^*$ band to lower energy. $n \rightarrow \pi^*$ band is visible between 450–550 nm. As highlighted as a separate inset graph in Fig 4.5 a), higher absorbance can be observed for *cis*-rich population at $n \rightarrow \pi^*$ band as well as below 330 nm in the UV shoulder. Isosbestic points are at 326 nm and 452 nm for CN-OH. Humidity dependence and molecular structure of CN-OH is presented in Fig 4.5 b). Eight measurements were conducted in similar conditions as described for DMA-OH in 10 %, 25 %, 40 %, 50 %, 55 %, 70 %, 85 % and 90 % RH with $\pm$0.5 % tolerance for humidity variance. Photoisomerisation was done with 1 s light pulse of 600 mW/cm^2 using $\lambda_{exc} = 405$ nm within $\pi \rightarrow \pi^*$ band but with low enough energy to prevent photobleaching, while monitoring wavelength range was 360–370 nm. CN-OH exhibits similar exponential humidity dependence as NO_2-OH and 2PAP with several times faster thermal relaxation than 2PAP across the RH range. DR = 10^4 change in rate constant is identical to NO_2-OH and 2PAP.

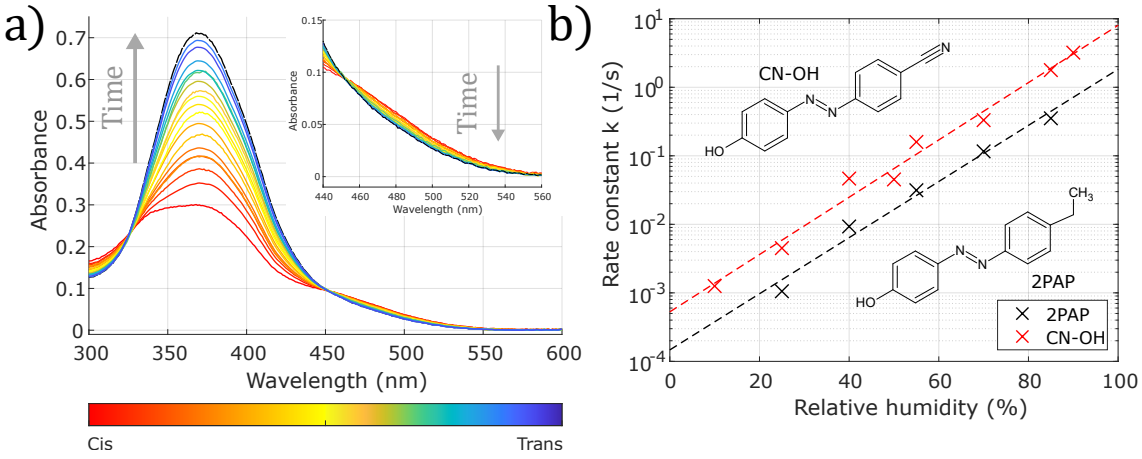

Figure 4.5. CN-OH absorption spectra and humidity dependence. *a) Absorption spectra for* trans*-rich (blue) and* cis*-rich (red) population CN-OH sample with $\tau = 2$ min at $21.3\,^{\circ}C$ and $21\,\%$ RH. Dashed black line represents pure trans spectrum. b) Rate constant of CN-OH samples as a function of humidity. Dashed lines are linear fits to data. Thermal relaxation rate depends on humidity and exhibits faster relaxation than 2PAP in the entire humidity range.*

Similar effects of push-pull substitution can be seen in CN-OH and NO_2-OH humidity dependences in drastically reduced *cis* lifetimes. However, cyano substituted azobenzene is not capable of tautomerising in the presence of polar water like hydroxy group, leading to lower k and thus longer *cis* τ than with NO_2-OH and corresponding to the hydrogen bonding assisted rotation mechanism proposed by Poutanen *et al*. With a fairly similar electron density distribution across the π conjugated system, relative *cis* isomer instability ensues from the reduced ability for the azobenzene to tautomerise.

CN-OH is on a par with NO_2-OH in terms of humidity sensing. CN-OH demonstrates similar humidity sensitivity as 2PAP and NO_2-OH, so is not an alternative for higher resolution humidity sensing either. Faster relaxation in allows for sensors applications in low humidity, although NO_2-OH can achieve similar resolution in measurements ten times faster, rendering NO_2-OH the superior choice for low humidity sensing. CN-OH would be best paired with another azobenzene more suitable for high humidity measurements such as DMA-OH. However, CN-OH and NO_2-OH are superior to 2PAP in spectral features: both can operate with $\lambda_{exc} = 405$ nm, which reduces the cost in sensing applications as UV light sources such as 365 nm are significantly more expensive, emit lower output power and have shorter product lifetime [116]. Furthermore, often optical components are optimised for visible light and hence more suitable for $\lambda_{exc} = 405$ nm.

Leaping relaxation: Pyr-OH

Unlike previous azobenzenes, Pyr-OH is a molecule where phenol and pyridyl are united through an azo bond. With regard to electron density distribution, pyridyl behaves like an electron acceptor with electron-donating hydroxy group at the opposite end of the π conjugated molecule. Fig 4.6 a) introduces Pyr-OH spectral features. Dashed black line represents pure *trans* spectrum and the red line a *cis*-rich spectrum after excitation with

1 s pulse of 240 mW/cm^2 $\lambda_{exc} = 385$ nm light. Absorption spectra were periodically measured from the same spot, illustrating the thermal relaxation from *cis* to *trans* over time with spectra varying from orange to teal. The prominent $\pi \rightarrow \pi^*$ transition absorption band can be observed between 340–400 nm with a peak at 365 nm. $n \rightarrow \pi^*$ band is not overshadowed by $\pi \rightarrow \pi^*$ band but visible between 450–580 nm. As highlighted as a separate inset graph in Fig 4.6 a), higher absorbance can be observed for *cis*-rich population at $n \rightarrow \pi^*$ band as well as below 320 nm in the UV shoulder. Isosbestic points are at 328 nm and 437 nm for Pyr-OH.

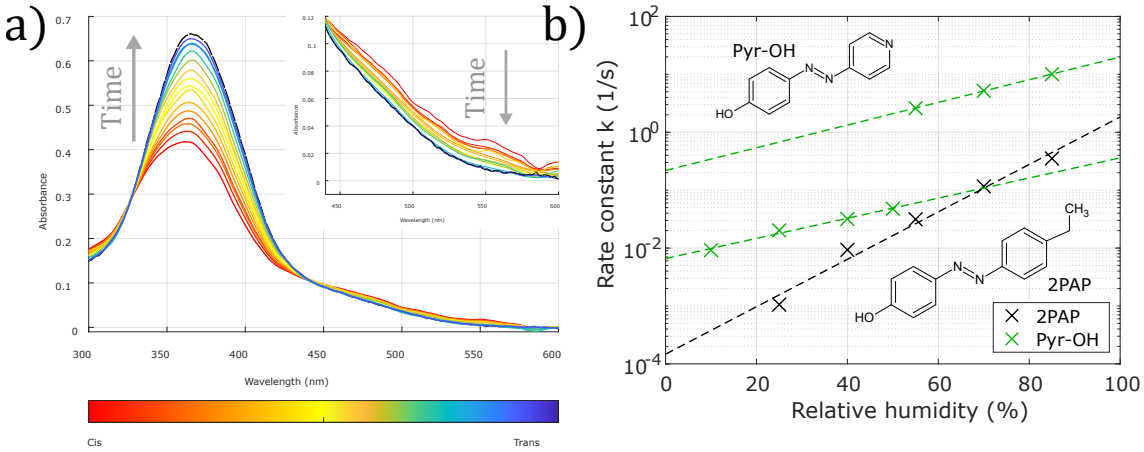

Figure 4.6. Pyr-OH absorption spectra and humidity dependence. *a) Absorption spectra for* trans*-rich (blue) and* cis*-rich (red) population Pyr-OH sample with $\tau = 45$ s at $21.9\,^{\circ}$C and $32\,\%$ RH. Dashed black line represents pure trans spectrum. b) Rate constant of Pyr-OH samples as a function of humidity. Dashed lines are linear fits to data. Thermal relaxation rate depends on humidity and exhibits faster relaxation than 2PAP across the humidity range. Humidity dependence is exponential but a leap in rate constant occurs at around RH $\approx 50\,\%$.*

Humidity dependence and molecular structure of Pyr-OH is presented in Fig 4.5 b). Seven measurements were conducted in similar conditions as described for DMA-OH in 10 %, 25 %, 40 %, 50 %, 55 %, 70 % and 85 % RH with $\pm$0.5 % tolerance for humidity variance. Photoisomerisation was done with 1 s pulse of 240 mW/cm^2 $\lambda_{exc} = 385$ nm light within $\pi \rightarrow \pi^*$ band with monitoring wavelength range was 360–370 nm. Pyr-OH exhibits an exceptional exponential humidity dependence as it can divided into two distinct parts: below 50 % RH Pyr-OH relaxation occurs with $k = (1\text{–}4) \cdot 10^{-2}$ 1/s, but for measurements above 50 % RH there is a sudden leap in relaxation rate constant as *cis* lifetime is reduced by over 60 times between 50 % and 55 % RH measurements. Linear fit was applied for both humidity ranges separately to emphasise this peculiar behaviour.

Pyr-OH demonstrates faster relaxation than 2PAP across the humidity range, although the rate constant only changes for an order of magnitude below 50 % RH and another order of magnitude above 50 % RH, totalling to an over hundred times smaller dynamic range than 2PAP. Fast relaxation can be explained with Pyr-OH push-pull character: the combination of electron-donating hydroxy and electron-withdrawing pyridyl significantly reduces *cis* isomer stability and thus τ, leading to faster relaxation. However, simple substitution pattern interpretations cannot explicitly explain the leaping humidity dependence of Pyr-OH. Perhaps the isomerisation mechanism for Pyr-OH is different in low

RH than high RH and the transition between the mechanisms occurs around 50 % RH. Further research on the topic is required in order to gain a comprehensive understanding of the humidity interaction of pyridyl-containing azobenzenes and thence the underlying mechanism of azobenzene humidity sensitivity.

Extraordinary humidity dependence limits the possible applications for Pyr-OH sensors. Despite relaxing faster from *cis* to *trans* than 2PAP, narrow dynamic range compromises the resolution of humidity sensing. Furthermore, uncertainty revolving around the leap in relaxation rate constant around 50 % RH calls sensor reliability into question. Considering these factors, Pyr-OH seems undesirable as a humidity sensing material. However, with additional research to 40–60 % RH range Pyr-OH may prove valuable in extreme resolution mid-range humidity measurements. If the observed leap can be characterised and modelled, future research may lead to the ability to engineer this region of humidity hypersensitivity into low or high humidity range, unlocking various commercially viable applications.

Slow relaxation: NH_2-NH_2

Differing from the previously studied hydroxyazobenzenes, NH_2-NH_2 is a disubstituted molecule with an electron-donating amino group in para position at either benzene ring. Fig 4.7 a) introduces NH_2-NH_2 spectral features. Dashed black line represents pure *trans* spectrum and the red line a *cis*-rich spectrum after excitation with 1 s pulse of 115 mW/cm^2 $\lambda_{exc} = 435$ nm light. Absorption spectra were periodically measured from the same spot, illustrating the thermal relaxation from *cis* to *trans* over time with spectra varying from orange to teal. The prominent $\pi \rightarrow \pi^*$ transition absorption band can be observed between 380–480 nm with a peak at 412 nm. $n \rightarrow \pi^*$ band is not overshadowed by $\pi \rightarrow \pi^*$ band but visible between 500–580 nm. As highlighted as a separate inset graph in Fig 4.7 a), higher absorbance can be observed for *cis*-rich population at $n \rightarrow \pi^*$ band as well as below 365 nm in the UV shoulder. Isosbestic points are at 365 nm and 495 nm for NH_2-NH_2.

Humidity dependence and molecular structure of NH_2-NH_2 is presented in Fig 4.5 b). Five measurements were conducted in similar conditions as described for DMA-OH in 25 %, 40 %, 50 %, 70 % and 85 % RH with $\pm$0.5 % tolerance for humidity variance. Photoisomerisation was done with 1 s pulse of 115 mW/cm^2 $\lambda_{exc} = 435$ nm light within $\pi \rightarrow \pi^*$ band with monitoring wavelength range of 400–410 nm. NH_2-NH_2 exhibits similar exponential humidity dependence as DMA-OH with slower thermal relaxation than 2PAP above 20 % RH. The DR = 10^2 change in rate constant is similar to Pyr-OH and thus far less sensitive than 2PAP. Both DMA-OH and NH_2-NH_2 have two electron donor substituents and therefore behave similarly with regard to humidity. While the substituents on DMA-OH differ substantially in terms of electron donor strength, NH_2-NH_2 has symmetric substitution pattern.

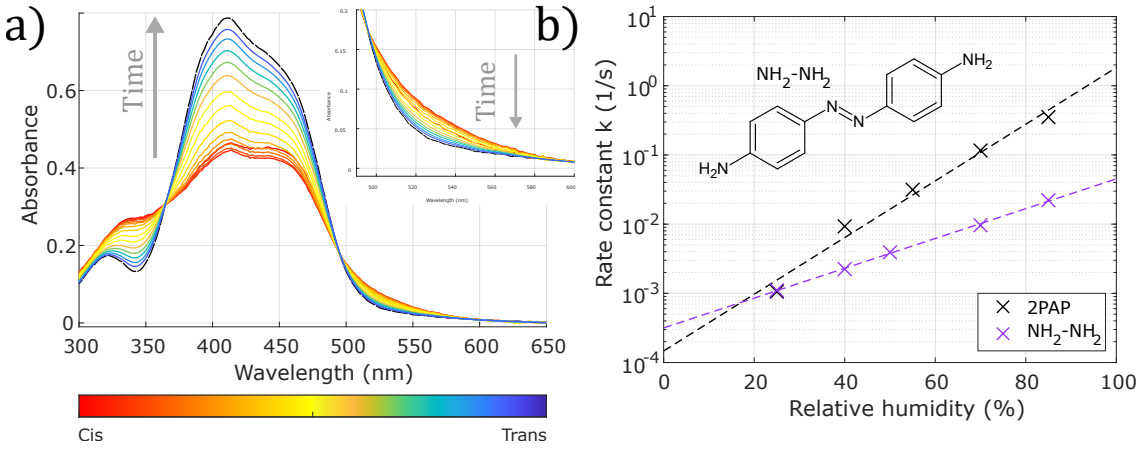

Figure 4.7. NH_2-NH_2 absorption spectra and humidity dependence. *a) Absorption spectra for* trans*-rich (blue) and* cis*-rich (red) population NH_2-NH_2 sample with $\tau = 9$ min at $22.6\,^{\circ}C$ and $37\,\%$ RH. Dashed black line represents pure trans spectrum. b) Rate constant of NH_2-NH_2 samples as a function of humidity. Dashed lines are linear fits to data. Thermal relaxation rate depends on humidity and exhibits slower relaxation than 2PAP across the humidity range.*

With two electron-donating amino groups, electron density at the azo bond and consequently *cis* isomer stability is increased, resulting in drastically increased *cis* lifetimes in above 20 % RH. This does not agree with the hydrogen bonding assisted rotation mechanism for azobenzene thermal relaxation proposed by Poutanen *et al*. With increased electron density at the azo bond, the bond should become stronger hydrogen bond acceptor and hence the relaxation rate should become higher than for 2PAP in higher humidity.

Given that NH_2-NH_2 exhibits only 2 orders of magnitude DR, NH_2-NH_2 is not an attractive candidate for humidity sensing applications. While NH_2-NH_2 could be used to measure high humidity, DMA-OH can do the same with an order of magnitude higher resolution and faster relaxation. However, NH_2-NH_2 is an interesting azobenzene as it demonstrates humidity dependence beyond hydroxyazobenzenes discussed by Poutanen *et al* [101]. NH_2-NH_2 is able to tautomerise as well as form hydrogen bonds with P4VP using its amino groups.

Insensitive relaxation: NO_2-NH_2

Last studied molecule is unlike the previous as NO_2-NH_2 is disubstituted with a strong electron-donating amino group as well as strong electron-withdrawing nitro group. With this potent push-pull character NO_2-NH_2 is the only studied molecule that classifies as pseudostilbene type azobenzene known for short *cis* lifetimes of mere seconds. Fig 4.7 a) introduces NO_2-NH_2 spectral features. Dashed black line represents pure *trans* spectrum and the red line a *cis*-rich spectrum after excitation with 3 s pulse of 320 mW/cm^2 $\lambda_{exc} = 435$ nm light. Absorption spectra were periodically measured from the same spot, illustrating the thermal relaxation from *cis* to *trans* over time with spectra varying from orange to teal. Due to the fast relaxation, *cis*-rich spectrum was measured during excitation and the subsequent spectra immediately after, albeit short *cis* lifetime limited the number of spectra that could be measured before full relaxation.

The prominent and wide $\pi \rightarrow \pi^*$ transition absorption band can be observed between 400–540 nm with a peak at 455 nm. $n \rightarrow \pi^*$ band is completely overshadowed by $\pi \rightarrow \pi^*$ as $\pi \rightarrow \pi^*$ band is at lower energy than $n \rightarrow \pi^*$ for pseudostilbenes. As highlighted as a separate inset graph in Fig 4.7 a), higher absorbance can be observed for *cis*-rich population below the isosbestic point at 387 nm in the UV shoulder, indicating *cis* NO_2-NH_2 absorbs more strongly in UV region than in *trans* form. No second isosbestic point can be found for NH_2-NH_2 as $n \rightarrow \pi^*$ band is completely overshadowed.

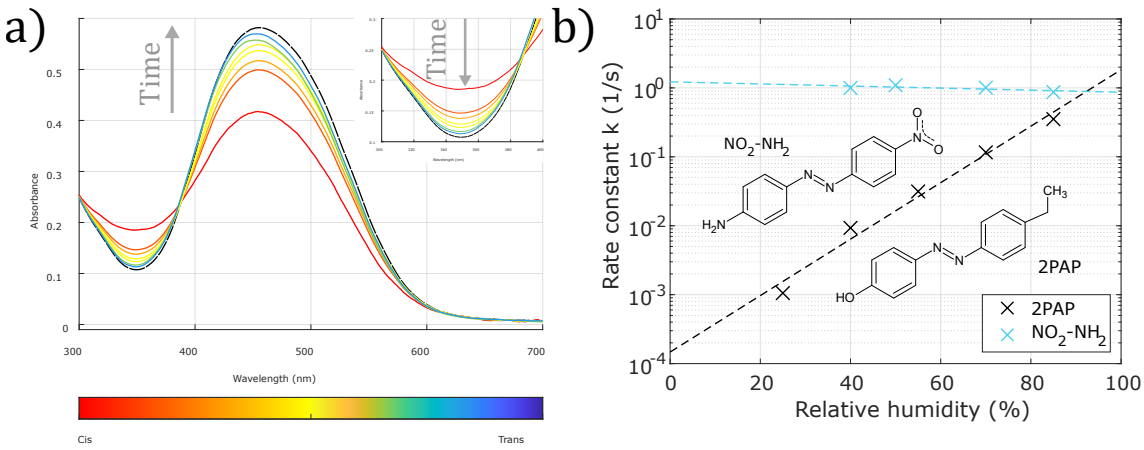

Figure 4.8. NO_2-NH_2 absorption spectra and humidity dependence. *a) Absorption spectra for* trans*-rich (blue) and* cis*-rich (red) population NO_2-NH_2 sample with $\tau = 1$ s at $22.6\ ^\circ$C and $37\ \%$ RH. Dashed black line represents pure trans spectrum. b) Rate constant of NO_2-NH_2 samples as a function of humidity. Dashed lines are linear fits to data. Thermal relaxation rate does not depend on humidity.*

Humidity dependence and molecular structure of NO_2-NH_2 is presented in Fig 4.5 b). Four measurements were conducted in similar conditions as described for DMA-OH in 40 %, 50 %, 70 % and 85 % RH with $\pm$0.5 % tolerance for humidity variance. Photoisomerisation was induced with 1 s pulse of 320 mW/cm^2 $\lambda_{exc} = 435$ nm light within $\pi \rightarrow \pi^*$ band with monitoring wavelength range was 465–475 nm. Due to the expected fast relaxation, detector signal integration time was reduced to 5 ms with 4 times averaging and monitoring signal intensity consequently increased to allow for reliable relaxation measurements with data points collected every 20 ms for subsecond *cis* lifetimes.

NO_2-NH_2 did not exhibit humidity dependence in the humidity range of 40–85 % RH. The change of 70 % in rate constant is miniscule compared to other molecules and can be at least in part explained with the margin of error considering the $\pm$0.5 % RH and $\pm$0.5 $^\circ$C tolerances for humidity and temperature variation within the measurement chamber. However, Poutanen *et al* detected a similar phenomenon with the humidity dependence of 4-Methoxyazobenzene [101, p. 384]. The assumed humidity-insensitive molecule displayed a similar small decrease in rate constant over the studied humidity range which persisted repeatably over multiple measurements. Therefore, these results may be linked and evidence of a group of azobenzenes whose humidity dependence is slightly negative.

NO_2-NH_2 is evidently unsuited for sensitive humidity measurements, but the results are

fascinating, nonetheless. Both amino and nitro groups appear to render azobenzenes humidity sensitive, yet their combined disubstitution in push-pull pattern results in a humidity insensitive azobenzene. Despite this, NO_2-NH_2 can be useful in humidity sensors, for example in temperature sensing. As presented in equation 3.4, rate constant is exponentially dependent on both humidity and temperature, so accurate measurement of both is required for a functional azobenzene-based humidity sensor. Therefore, using a film with multiple azobenzenes with suitable spectral differences allows for humidity sensing with one wavelength and temperature sensing with another, provided the temperature sensing azobenzene is humidity insensitive, such as NO_2-NH_2.

Considering the shift in electron density around the azo bond caused by push-pull substitution, NO_2-NH_2 should resemble NO_2-OH and CN-OH in having short *cis* lifetime but still demonstrate humidity dependence, even more so than NO_2-OH or CN-OH due to the strong push-pull character of the molecule. However, no such humidity dependence is visible in Fig 4.5 b). One possible explanation is that the NO_2-NH_2 thermal relaxation comprises of combination of mechanisms, one sensitive and the other insensitive to humidity. Majority of the *cis* population relaxes via the humidity-dependent pathway and faster than could be detected with the setup used in this thesis, while the humidity-independent nonradiative isomerisation mechanism exhibits only $\tau \sim 1$ s *cis* lifetime. Lowered monitoring signal integration time led to lower signal-to-noise ratio, although fitting equation 3.3 onto the data was successful with $R^2 \sim 0.95$.

It is plausible that only one of the possible azobenzene isomerisation mechanisms with different activation energies is humidity dependent, and as changes in substitution pattern affects the mechanisms differently, the studied molecules exhibit differences in humidity dependence. Further research with higher temporal resolution with respect to relaxation rate measurements is needed to determine whether NO_2-NH_2 relaxation truly is independent of humidity and to adequately describe its isomerisation mechanism. Results from NO_2-NH_2 goes to show how limited our understanding of the mechanism of humidity sensitivity in azobenzenes still is.

Molecular comparison in humidity sensing

Most suitable azobenzenes for water vapour sensing in high humidity based on the results presented above are summarised in Fig 4.9. As DMA-OH relaxation occurs in high RH with a lifetime in the range dozens of seconds to minutes instead of seconds like 2PAP, DMA-OH thin films are more suitable for high RH sensing in applications where resolution of threefold change in rate constant per 10 % RH is sufficient. DMA-OH films are also applicable in sensors with limitations in monitoring signal intensity or detector signal integration time: slower relaxation above 25 % RH allows for longer integration times and hence lower monitoring signal intensity with similar signal-to-noise ratio, albeit with lower resolution.

For measurements requiring higher sensitivity to humidity, MeO-OH thin films are the op-

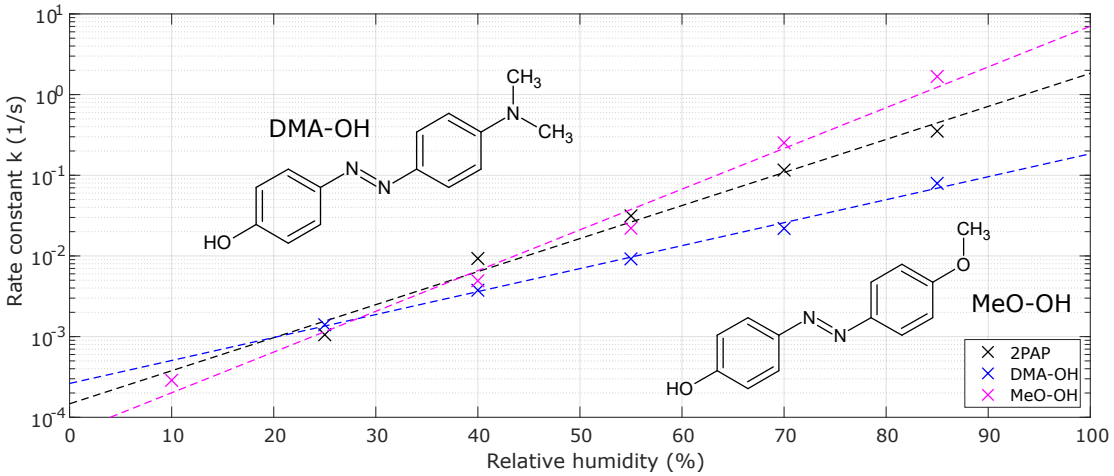

Figure 4.9. Comparison of azobenzenes suitable for high humidity sensing.

timal choice. Given the high resolution of approximately fivefold change in rate constant per 10 % RH, MeO-OH is twice as sensitive to humidity as DMA-OH while differing from 2PAP by less than an order of magnitude in relaxation rate. However, subsecond lifetime for above 85 % RH measurements can prove challenging in sensor applications as acceptable signal-to-noise ratio would require higher monitoring signal intensity and could result in photo-oxidative degradation or other photobleaching effects.

Conversely, most suitable azobenzenes for low humidity measurements are reiterated in Fig 4.10. While 2PAP humidity dependence has been thoroughly studied and reported by Poutanen *et al*, relaxation lifetime of half an hour to several hours below 20 % RH is unacceptable for on-demand humidity sensing as an extended period of waiting for the reading is objectionable in commercial use. Therefore, utilising azobenzenes with faster relaxation is aspirable for measuring low RH. Two hydroxyazobenzenes, CN-OH and NO_2-OH, proved suitable for this purpose. Both exhibit similar dynamic range as 2PAP with fourfold change in rate constant per 10 % RH while thermally relaxing back to *trans* faster across the humidity range.

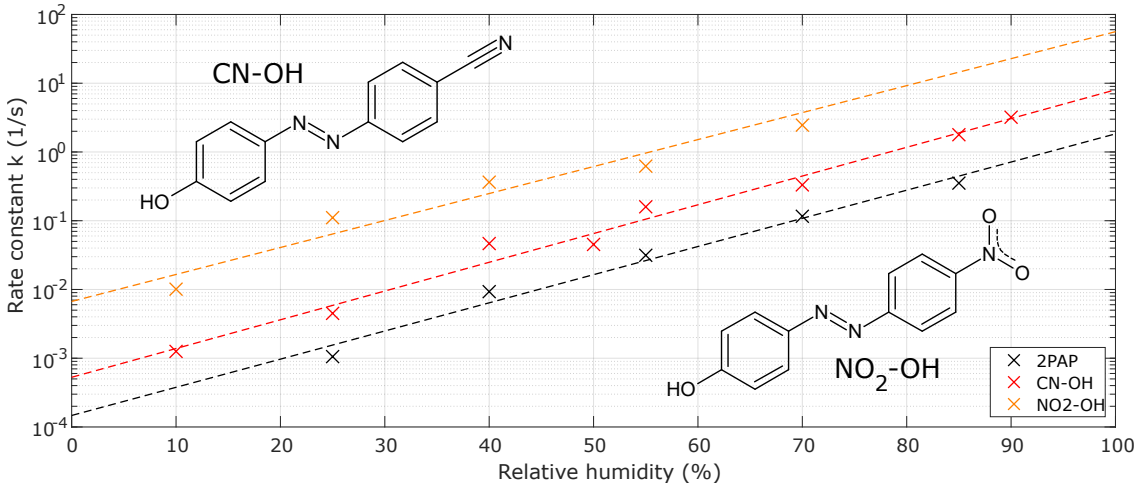

Figure 4.10. Comparison of azobenzenes suitable for low humidity sensing.

Molecule	λ_{max} (nm)	τ	λ_{iso} (nm)	**DR**	**Suitable for (RH)**
2PAP	358	1 min	308, 428	10^4	20–90 %
DMA-OH	412	2.4 min	363, 503	10^3	25–100 %
MeO-OH	364	48 s	326, 447	10^5	25–85 %
NO_2-OH	385	3 s	339, 485	10^4	0–55 %
CN-OH	385	15 s	326, 452	10^4	10–90 %
Pyr-OH	365	21 s	328, 437	10^2	0–50 %
NH_2-NH_2	412	5.7 min	365, 495	10^2	25–100 %
NO_2-NH_2	455	1 s	387	–	unsuitable

Table 4.1. Summary of studied molecules for humidity sensing. cis *lifetimes were measured at 23 °C and 50 % RH. DR stands for dynamic range. Pyr-OH may be most suited for hypersensitive humidity measurements between 50–55 % RH, further research needed to confirm this.*

Both CN-OH and NO_2-OH have sufficiently fast thermal relaxation to qualify for low RH measurements. For extremely low humidity measurements, NO_2-OH is far superior with its *cis* lifetime of mere minutes below 10 % RH. However, subsecond lifetime for humidity above 55 % RH poses limitations for sensing higher RH, whereas CN-OH *cis* lifetime drops below 1 s only around 80 % RH and reaches a minimum of $\tau_{100\,\%} = 125$ ms. Therefore CN-OH could be a viable alternative for humidity sensing across the full RH range, given the sensor can measure relaxation rate of $k \sim 10$ 1/s with sufficient signal-to-noise ratio.

Summary of the essential features of the studied molecules for humidity sensing are presented in Table 4.1. Wavelength of pure *trans* spectrum absorbance maxima λ_{max} illustrate how red shifted the absorption spectra are compared to unsubstituted azobenzene while dynamic range and *cis* lifetimes measured at 23 °C and 50 % RH describe the molecule's aptness for humidity sensing. Table 4.1 also presents for which RH range the molecule is most suitable in sensor applications. Given the small red shift from unsubstituted azobenzene, 2PAP, MeO-OH and Pyr-OH are limited to monitoring wavelengths in the UV region while other azobenzenes can be operated within visible light spectrum, reducing the sensor cost as visible spectrum light sources are more affordable.

Azobenzene-based humidity sensor could contain multiple azobenzene molecules in the same film as long as they can be excited and monitored separately. For this purpose, the isosbestic points λ_{iso} are crucial as they represent wavelengths upon irradiation with which the photostationary states do not change, meaning the rate of photoisomerisation is equal in both directions. With multiple azobenzenes in the same film one can be used to probe ambient temperature and another for humidity, for example. Given the λ_{iso} in Table 4.1, optimal combination of azobenzenes in a film would be CN-OH or NO_2-OH with DMA-OH. CN-OH can measure low humidity fast enough for sensing applications while similarly DMA-OH has short enough *cis* lifetime in high RH. CN-OH has an isosbestic point at 452 nm, while DMA-OH strongly absorbs around 450 nm, meaning DMA-OH can

be excited without interference from CN-OH absorption.

NO_2-OH has an isosbestic point at 485 nm, also well within DMA-OH absorption band. Both NO_2-OH and CN-OH can hence be used with DMA-OH in a single humidity sensor film without mutual interference. Furthermore, both combinations can be enhanced with NO_2-NH_2, a strong push-pull azobenzene that seems to be insensitive to humidity. DMA-OH has an isosbestic point at 503 nm where NO_2-NH_2 still greatly absorbs, while neither CN-OH nor NO_2-OH has strong absorption above 500 nm. Thus 503 nm could be used to measure temperature with NO_2-NH_2 while 452 nm is used for high RH measurements with DMA-OH and 363 nm, the second isosbestic point of DMA-OH, is used for low RH measurements with CN-OH. Whereas CN-OH strongly absorbs at 363 nm, NO_2-NH_2 has sufficiently low absorption there for sensing purposes.

Based on the results summarised in Table 4.1, optimal azobenzene-based humidity sensor would utilise multiple thin films with azobenzenes for different humidity ranges. For below 50 % RH, optimal sensor material would be a NO_2-OH thin film, while measurements above 50 % RH could be conducted with a DMA-OH thin film. Sensor could also involve a MeO-OH thin film for enhanced resolution setting or replace DMA-OH in high RH sensing altogether if measuring relaxation rates up to $k \sim 10^1$ 1/s feasible. For sensors comprising of a single thin film, CN-OH demonstrates tolerable relaxation lifetime in low humidity while remaining below $k \sim 10$ 1/s relaxation rate in saturated humidity.

4.1.2 Molecular environment

Although azobenzene substitution profoundly determines the thermal relaxation behaviour of the material, molecular environment greatly affects the *cis* $\rightarrow$ *trans* isomerisation mechanism and thus delimits the humidity sensing applications of the system. In order to study the environmental aspects of azobenzene photoisomerisation, P4VP/2PAP thin films of different mole fraction χ and polymer molar mass M_w were fabricated.

Poutanen *et al* used an exceptionally short chain 1 200 g/mol P4VP to characterise 2PAP humidity dependence in supramolecular P4VP complex [101], so $M_w = 1\,200$ g/mol P4VP, designated $P4VP_{1.2k}$, was chosen as reference. To explore the concept's viability in commercial applications, $M_w \sim 60\,000$ g/mol P4VP, designated $P4VP_{60k}$, was chosen for comparison. Being a common and widely available polymer, heavier P4VP is also roughly 50 times cheaper, making it a desired constituent in azobenzene-containing thin films over its special short-chain yet costly version. Both short-chain and heavier P4VP were fabricated into thin films with 2PAP with mole fractions of 1:1, 1:2, 1:4 and 1:10, from which relaxation rate constants were measured at 23 °C and 50 % RH similarly as described in section 4.1.1. Results of the comparison are presented in Fig 4.11.

For each (χ, M_w) combination, three samples were chosen from a set of eight and the mean rate constant of these samples is presented in Fig 4.11. As can be seen from the figure, equimolar samples had the highest rate constants with $P4VP_{1.2k}$ relaxing back to *trans* more than twice as fast as equimolar $P4VP_{60k}$ samples. Conversely, for other

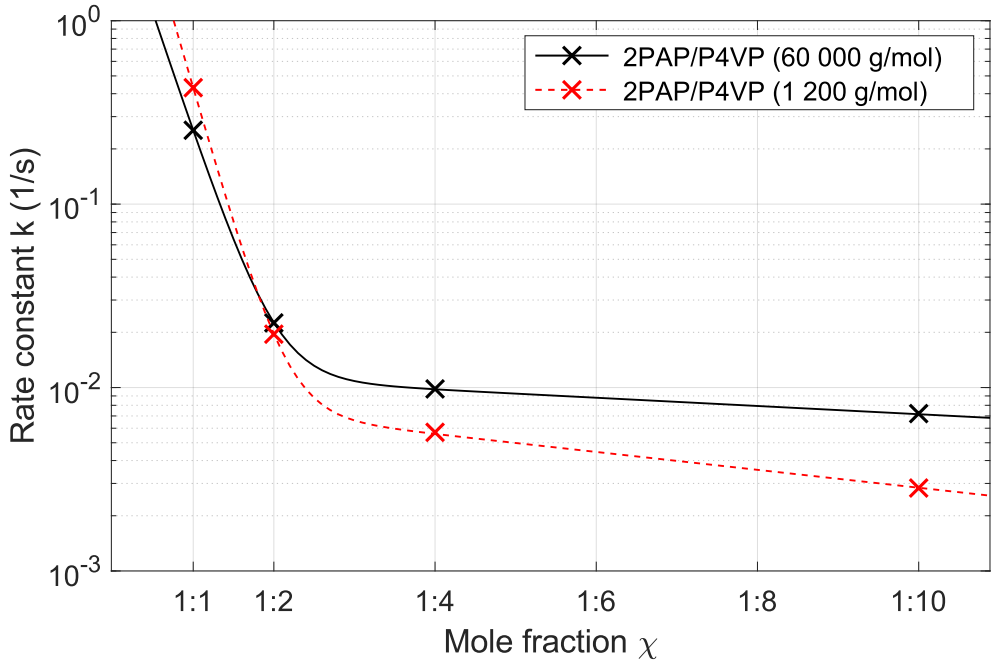

Figure 4.11. Effect of polymer molar mass on isomerisation rate constant. *Data with long-chain polymer (M_w = 60 000 g/mol) and short-chain polymer (M_w = 1 200 g/mol are presented in black and red, respectively. Relaxation rate constants were measured at 23 °C and 50 % RH. The lines are to guide the eye. Standard deviations are not presented as they were in the range of 2–10 % and the resulting error bars would not be visible using the logarithmic scale.*

mole fractions P4VP$_{60k}$ relaxation was faster. Difference in relaxation rate was minor for χ = 1:2 samples with P4VP$_{60k}$ being 15 % faster than P4VP$_{1.2k}$, whereas the difference was more apparent in χ = 1:4 samples with P4VP$_{60k}$ relaxing over fourfold faster than P4VP$_{1.2k}$. Similar difference between light and heavy P4VP was observed with χ = 1:10 samples as P4VP$_{60k}$ relaxation was about fourfold faster than with P4VP$_{1.2k}$ samples.

Experiments revealed the immense impact mole fraction has on azobenzene relaxation. Samples with one 2PAP molecule per two P4VP repeating units (χ = 1:2) exhibited over an order of magnitude slower relaxation compared to equimolar samples: while equimolar samples exhibited lifetime of $\tau_{1:1} \approx$ 2–4 s at 23 °C and 50 % RH, χ = 1:2 sample lifetimes were $\tau_{1:2} \approx$ 45–51 s. As 2PAP ratio to P4VP decreased, steep decline in rate constant ceased and χ = 1:4 samples relaxed only 2 times slower than χ = 1:2 samples for P4VP$_{60k}$ and 5 times slower for P4VP$_{1.2k}$. Despite the substantial change in dye to polymer ratio, χ = 1:10 samples relaxed only about 3 times slower than χ = 1:4 samples for both polymers.

Mole fraction also caused changes in the spectral features presented in Table 4.2. As 2PAP mole fraction reduced from equimolar to χ = 1:10, a red shift of 7–8 nm was observed with absorbance maxima shifting from 353 nm to 361 nm for P4VP$_{60k}$ and from 353 nm to 360 nm for P4VP$_{1.2k}$, respectively. No notable effect of molar weight on spectral features was detected given a $\pm$1 nm tolerance for variation. Similarly minor changes in full width at half maximum could be observed for different mole fraction and molar

χ_{real}	M_w (g/mol)	w_a	τ (s)	β	λ_{max} (nm)	**FWHM** (nm)
1:1,01	60 000	68,1%	3.95 ± 0.04	0.84 ± 0.01	353	71
1:0,99	1 200	68,4%	2.31 ± 0.02	0.92 ± 0.01	353	69
1:2,01	60 000	51,7%	44.5 ± 1.10	0.66 ± 0.01	356	66
1:2,01	1 200	51,7%	51.2 ± 1.35	0.66 ± 0.01	356	65
1:3,98	60 000	35,1%	102 ± 1.81	0.62 ± 0.01	358	65
1:4	1 200	35,0%	175 ± 2.81	0.66 ± 0.01	359	64
1:10	60 000	17,7%	139 ± 3.59	0.56 ± 0.01	361	63
1:9,93	1 200	17,8%	353 ± 3.63	0.59 ± 0.01	360	62

Table 4.2. Summary of molecular environment effects on isomerisation. *Table presents* cis *lifetimes along with other essential parameters related to* cis $\rightarrow$ trans *isomerisation in samples of varying mole fraction and polymer molar mass.*

weight samples: full width at half maximum reduced from about 70 nm for equimolar samples to 62 nm for 1:10 mole fraction samples. Stretching exponent β in fitting parameters presented in equation 3.3 varied as a function of mole fraction: $\beta_{1:1} \approx 0.9$ for equimolar samples, while for $\beta_{1:10} \approx 0.6$, indicating deviation from first order reaction kinetics. Poutanen *et al* reported similar relaxation constant dependence from mole fraction in 2016 [72].

Table 4.2 presents mole fraction χ_{real}, P4VP molar mass M_w, azobenzene mass percentage w_a, *cis* lifetime τ, stretching exponent β, wavelength at absorbance maximum λ_{max} and full width at half maximum FWHM for 2PAP/P4VP samples selected for studying the effects of molecular environment on *cis* $\rightarrow$ *trans* isomerisation.

Overall change in relaxation rate constant was over two orders of magnitude for $P4VP_{1.2k}$ samples and over 35 times for $P4VP_{60k}$ samples, allowing for tuning the *cis* lifetime range of azobenzenes for humidity sensing. Thin films containing the studied molecules presented in section 4.1.1 were fabricated with mole fraction $\chi = 1:4$. For example, by tuning the *cis* lifetime range of the sensitive MeO-OH to lower mole fraction, *e.g.* to $\chi =$ 1:7, *cis* lifetime can be prolonged in high humidity, allowing for high resolution humidity sensing with longer detector signal integration times and thus lower monitoring signal intensity. Moreover, Poutanen *et al* have reported that reducing mole fraction expands the dynamic range rendering the azobenzene more sensitive to RH [101].

Relaxation rate can be engineered to some extent with the selection of polymer molar mass, as well. For $\chi =$ 1:2 molar weight has marginal effect on rate constant, but for lower mole fractions electing heavier polymer results in faster relaxation and vice versa for equimolar films. Further research is needed to determine whether there is a linear dependence between polymer M_w and relaxation rate, but for humidity sensor applications the paramount result is that affordable and widely available $M_w \sim$ 60 000 g/mol P4VP is suitable for azobenzene thin film fabrication and even the preferred choice for lower humidity sensing for lower mole fractions.

4.2 Sample aging

This section involves discussion concerning the results from aging measurements, namely POM images taken periodically from samples selected for aging measurements as well as absorption spectra and rate constants measured on the same day as corresponding POM images.

4.2.1 POM images

Polarised light microscopy (POM) images were taken at regular time intervals from samples chosen for studying aging effects in azobenzene-containing supramolecular polymers. Purpose of the imaging was to investigate possible azobenzene aggregation in films due to insufficient azobenzene immobilisation with hydrogen bonding to P4VP hydrogen bond acceptor pyridyl. As elaborated in sections 2.2.3 and 3.2.1, sufficiently large aggregates would appear as bright spots in POM images due to birefringence emerging from the anisotropy in ordered crystalline structure. Representative POM images from aging samples are presented in Fig 4.12.

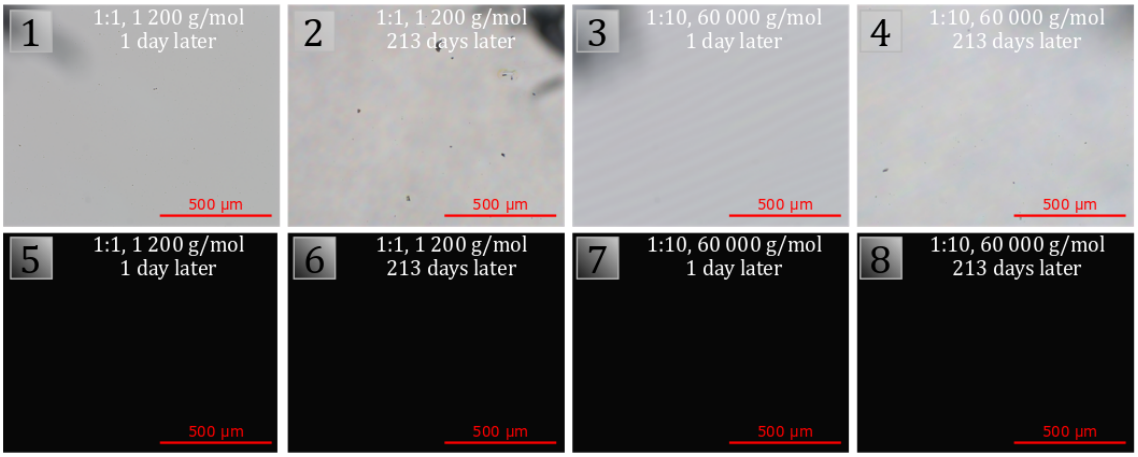

Figure 4.12. Azobenzene aggregation in P4VP/2PAP thin film. *Images 1-4 are POM images taken with bright field illumination with 30 ms exposure while images 5-8 were taken with cross-polarised light with 300 ms exposure. First two columns are from $\chi = 1{:}10$ samples with $\chi = 1{:}1$ samples with $P4VP_{1.2k}$ one day and 213 days after sample fabrication, and the last two columns are from $P4VP_{60k}$ one day and 213 days after sample fabrication, respectively. Microscope images revealed no visible aggregation or phase separation over the 213 days period.*

Images 1–4 in Fig 4.12 were taken without cross-polarised light, in other words with polariser but without analyser, with 30 ms exposure, while images 5–8 were taken with cross-polarised light with 300 ms exposure. Each column represents a given day when the upper image was taken to see if any phase separation visible to the eye occurred and the lower image corresponds to the same spot with cross-polarised light. A small mark was made onto the backside of the glass substrate to indicate the spot so images could be taken from the same spot in the sample over time. Samples chosen to represent the set of aging samples are $\chi = 1{:}1$ samples with $P4VP_{1.2k}$ in the two columns on the left and $\chi = 1{:}10$ samples with $P4VP_{60k}$ in the two columns on the right.

As can be seen from Fig 4.12, no aggregation effects are visible in the bright field or cross-polarised images after 213 days since sample fabrication. In both first day sample images the surface is visibly mostly clean while images from the same spot 7 months later revealed how the surface deteriorated with visible dark spots. These spots are most likely dust particles accruing on the surface instead of aggregation or phase separation as cross-polarised images show no corresponding bright spots.

Despite tenfold longer exposure time with cross-polarised images, no birefringent aggregation was observed. To verify that this was due to intermolecular interaction between azobenzene hydrogen bond donor and P4VP hydrogen bond acceptor, a set of samples was fabricated using poly(methyl methacrylate) (PMMA) as the polymer instead of P4VP. Unlike P4VP, PMMA has no hydrogen bond acceptor group and thus forms weaker intermolecular forces with 2PAP molecules, insufficient to prevent azobenzene aggregation. Corresponding POM images from these PMMA samples are displayed in Fig 4.13.

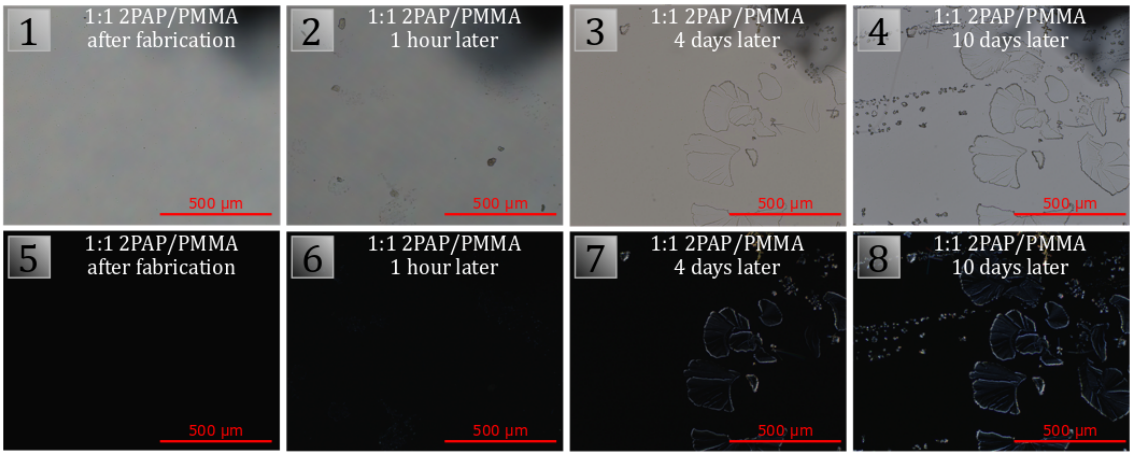

Figure 4.13. Azobenzene aggregation in 2PAP/PMMA thin film. *Images 1-4 are POM images taken with bright field illumination with 30 ms exposure while images 5-8 were taken with cross-polarised light with 300 ms exposure. First column was taken immediately after sample fabrication, second column an hour later, third column 4 days later and fourth column 10 days later. Image 3 is of different colour than other bright field images due to erroneous colour temperature settings.*

Images 1–4 in Fig 4.12 were taken from PMMA samples without crossed polariser and analyser, in other words with linearly polarised light with, 30 ms exposure, while images 5–8 were taken with cross-polarised light with 300 ms exposure. Sample of $\chi = 1{:}1$ was imaged in four instances, each corresponding to one column of images: directly after sample fabrication, 1 hour later, 4 days later and 10 days later from left to right, respectively. Images directly after sample fabrication show no aggregation effects, but already an hour later some initial phase separation is visible in the bright field image. Cross-polarised image does not show birefringent aggregation after an hour, but in the third column azobenzene aggregation is visible in bright field and cross-polarised images.

Lack of strong intermolecular interaction between the polymer and azobenzene in the film leads to eventual phase separation as is evident from Fig 4.12 3–4 and 7–8. Thermal motion brings azobenzenes within interaction distance from one another and aggregate

formation begins as described in section 2.2.3. Further aggregation is witnessed as time passes in the rightmost column: extensive azobenzene aggregation and resulting birefringence 10 days after sample fabrication manifests in shell-shaped regions typical to recrystallisation.

Because no such aggregation is observed in any of the P4VP/2PAP aging samples even 7 months after sample fabrication, good stability can be concluded for azobenzene-containing supramolecular polymers. Ruling out aggregation and phase separation from potential detrimental aging effects is beneficial for any commercial applications as sample stability can be guaranteed in terms of aggregation. However, these results cannot be fully generalised to account for all azobenzene derivatives as changes in substitution pattern affect the dipole moment of the molecule and thus the aggregation behaviour. Further research is needed on especially on the aggregation of push-pull substituted azobenzenes with strong dipole moment to gain a more comprehensive understanding on azobenzene aggregation in supramolecular complexes.

4.2.2 Absorption

As a part of studying the aging effects on P4VP/2PAP samples, absorption spectra were periodically measured from the set of aging samples. Effects of aging were explored in terms of changes in absorption, shape of the spectrum and wavelength of absorbance maxima. Perhaps the most prominent feature in terms of absorption, changes in absorbance maxima at wavelengths λ_{max} indicated in Table 4.1 were resolved from measured spectra and are presented in Fig 4.14.

Absorbance maxima in Fig 4.14 are presented as normalised for absorbance maximum measured on the day of sample fabrication to ease comparison between sample sets. Mean A_{max} from a set of aging measurement samples is presented for P4VP$_{60k}$ samples with black colour and for P4VP$_{1.2k}$ samples in red, including error bars representing standard deviations in each set of measurements. A_{max} over time is divided into four graphs involving data from samples of a given mole fraction indicated in the top left corner of the graph.

As can be seen in Fig 4.14 a), A_{max} reduced over time for equimolar samples fairly linearly by almost 9 % for P4VP$_{60k}$ samples over the timespan of 213 days, whereas P4VP$_{1.2k}$ samples exhibited only about 5 % decrease in A_{max}. Neither set of the equimolar samples showed a saturating trend, possibly indicating a continuous aging effect for a timespan of at least 7 months. Conversely, $\chi = 1{:}2$ samples displayed an entirely different behaviour. A_{max} remained relatively unchanged for P4VP$_{60k}$ samples for the first two months and the began a slight incline, eventually reaching about 1 % higher A_{max} than at the time of sample fabrication. P4VP$_{1.2k}$ samples, on the other hand, demonstrated a slight increase in A_{max} in the first months but eventually reduced to slightly lower A_{max} than initially. Given a $\pm$1 % tolerance for variation, however, $\chi = 1{:}2$ samples remained virtually unchanged in terms of absorption and thus displayed no aging effects.

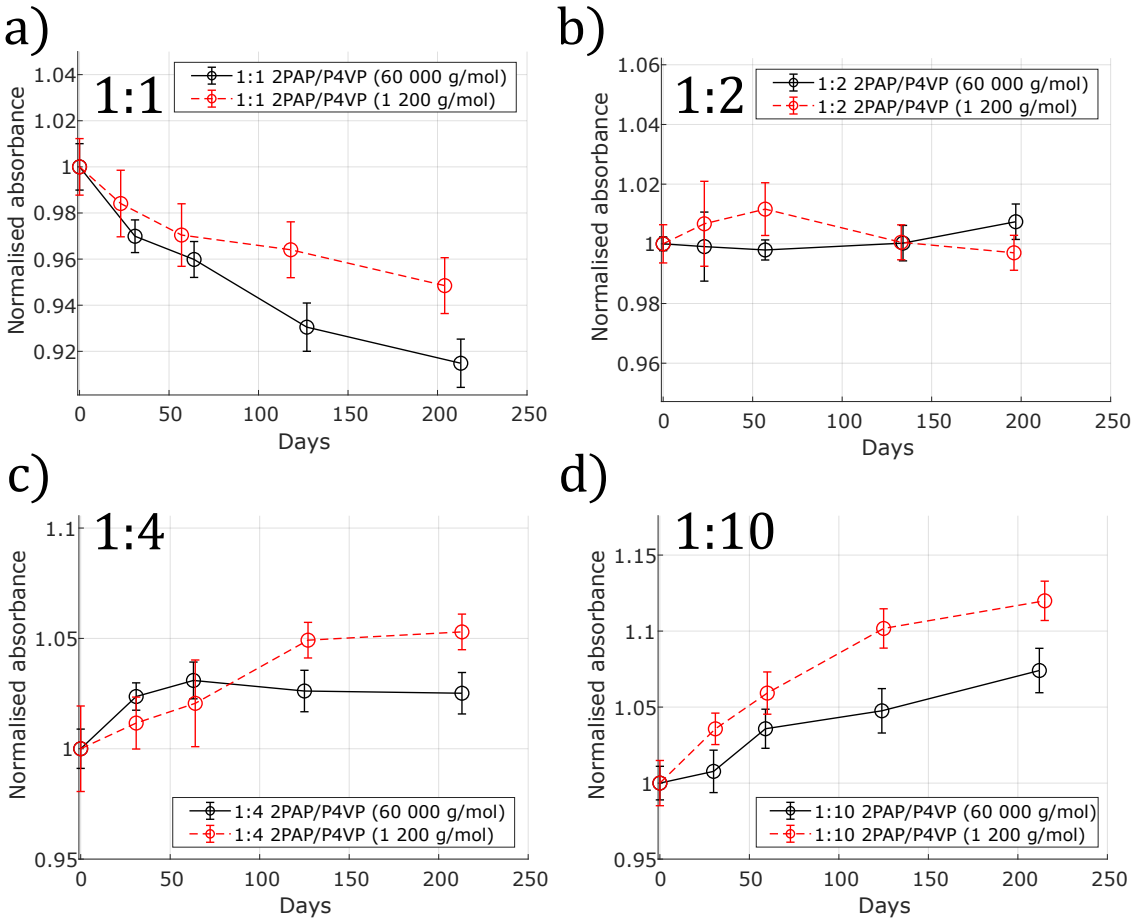

Figure 4.14. Absorbance maxima over time. *Absorbance maxima normalised for A_{max} on the day of sample fabrication are presented as a function of time for a) equimolar samples with mole fraction 1:1 as well as b) 1:2, c) 1:4 and d) 1:10 mole fractions for samples with more P4VP repeating units than 2PAP molecules. P4VP$_{60k}$ samples are presented in black and P4VP$_{1.2k}$ samples in red. The lines are to guide the eye. Error bars represent standard deviations in each set of measurements.*

A notable increase in A_{max} can be observed in both of the lower mole fraction sample sets. $\chi =$ 1:4 samples show a growth of 2–3 % during the first two months after sample fabrication and then saturation to some extent as change in A_{max} diminish over time. P4VP$_{1.2k}$ samples reach a little over 5 % increase while P4VP$_{60k}$ samples saturate notably to about 2 % higher A_{max}. Similar saturation is not observed with $\chi =$ 1:10 samples as A_{max} rises fairly steadily across the studied timespan. P4VP$_{60k}$ samples absorbance grows by 7 % during 7 months whereas P4VP$_{1.2k}$ samples demonstrate greatest change in A_{max} with nearly 11 % increase. Part of this may be caused by dust accruing on the sample surface, causing additional monitoring light attenuation through scattering effects, but it is unlikely dust would account for this significant increase in absorbance. Absorbance change may also result from molecular realignment: slight molecular orientation along the normal of the sample surface gradually deteriorates, or conversely, isotropic alignment changes over time as molecules align along the sample surface.

In contrast with aging effects in POM imaging, changes in absorption over time depend on mole fraction. For equimolar films absorbance will decrease over time, while for lower

mole fraction samples it will decrease. Optimal mole fraction in terms of changes in absorption is χ = 1:2 with marginal changes over the timespan of 7 months. Similarly, P4VP$_{60k}$ films with χ = 1:4 mole fraction appear a viable alternative with A_{max} settling around 2 % higher than on the day of fabrication. To further illuminate these changes in absorption, Fig 4.15 presents absorption spectra for P4VP$_{60k}$ films with χ = 1:1 and χ = 1:10 mole fraction.

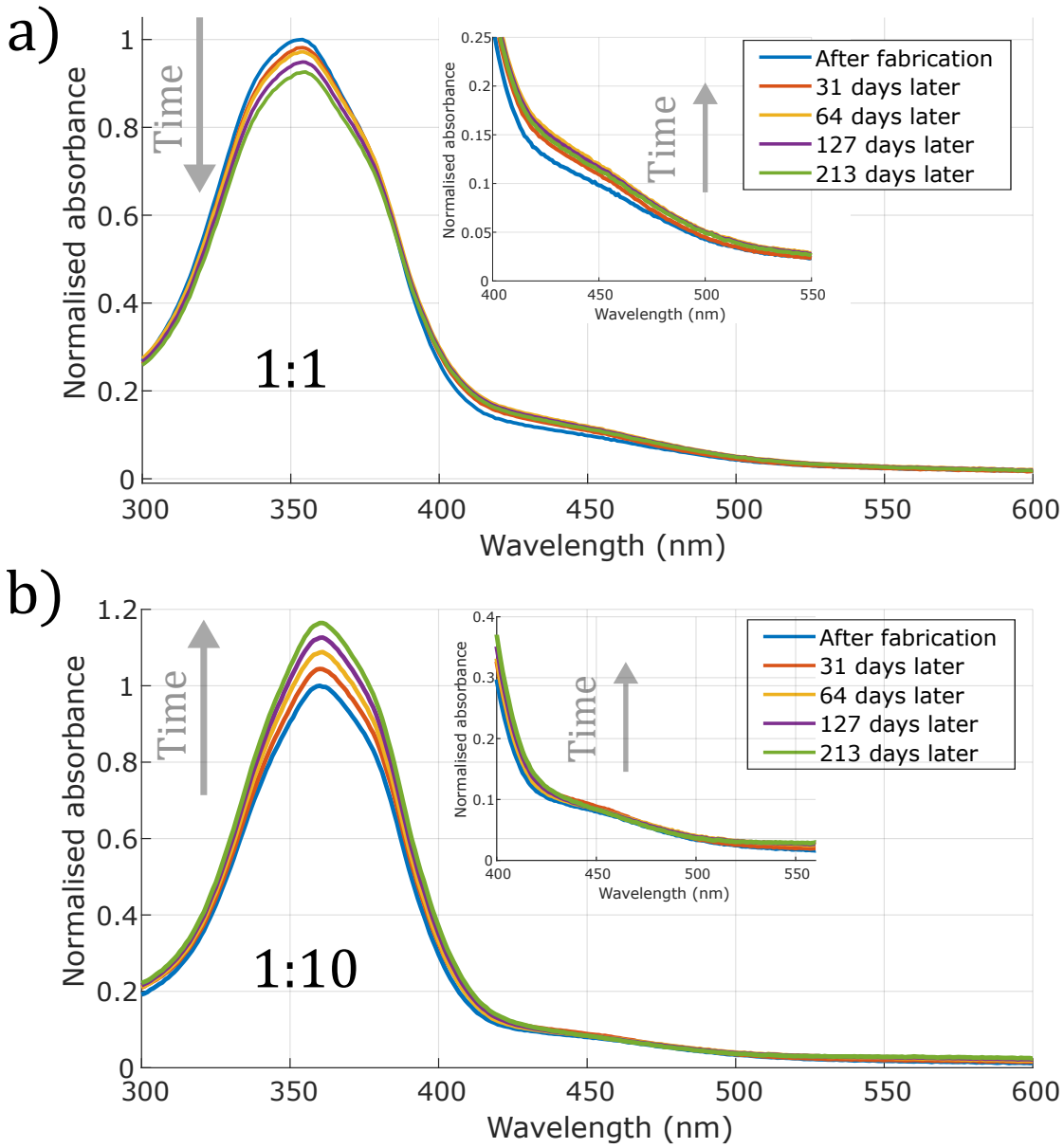

Figure 4.15. Absorption spectra over time. *Spectra represent a) equimolar P4VP$_{60k}$ and b) 1:10 mole fraction P4VP$_{1.2k}$ samples absorption spectra over a timespan of 213 days.* cis *population change is highlighted with inset of $n \rightarrow \pi^*$ band. As shown in Fig 4.14, equimolar samples display a reduction in absorbance over time while 1:10 mole fraction samples increase in absorbance.*

As seen from Fig 4.15 a), changes in absorption are observable across the $\pi \rightarrow \pi^*$ band. However, it is noteworthy that in these spectra absorption in the $n \rightarrow \pi^*$ band increases and consequently decreases in $\pi \rightarrow \pi^*$ band. This could be an indication of *cis* $\rightarrow$ *trans*

isomerisation, although it is not the possible explanation. Another possibility is that some chemical reaction has transformed some 2PAP into molecules with higher absorption in the $n \rightarrow \pi^*$ band. However, similar increase can be observed for $\chi = 1{:}10$ samples, although absorption at $\pi \rightarrow \pi^*$ band increases over time, as well. Therefore both isomerisation and a chemical reaction are unlikely causes of the observed aging effects as they would yield congruent results for samples with different mole fraction. Furthermore, dust would cause apparent increase in absorbance also in near infrared which is not observed in the spectra, thus effectively ruling out dust as a plausible explanation.

Samples were kept in the dark for at least a day prior to measuring absorption spectra and handled in red lighting during measurements so excitation from ambient lighting is unlikely. Absorption spectra were measured in ambient laboratory conditions at 21 ± 0.5 °C, but laboratory humidity was not controlled and varied between 16–35 % RH. Because azobenzenes are constantly in a dynamic equilibrium between *cis* and *trans* populations, variation in A_{max} over time presented in 4.14 may be due to changes in ambient conditions, namely humidity. However, all spectra for aging samples were measured during the same day, so the relative trends still apply: on the day equimolar samples exhibited a decrease in A_{max}, $\chi = 1{:}2$ samples A_{max} remained unchanged while A_{max} decreased for lower mole fraction samples.

Fig 4.15 also demonstrates similar lack of aggregation as seen in POM images. As aggregation would cause blue shift or band broadening in absorption spectra, Fig 4.15 further confirms the observations made from POM imaging concerning azobenzene aggregation. Although some changes in absorption can be seen in Fig 4.15, spectral shape has not changed during the timespan of aging measurements and thus it is unlikely any aggregation has occurred. Similarly, differences in absorbance maxima wavelength were within the ± 1 nm tolerance for variation and hence no substantial $\Delta\lambda_{max}$ was observed.

4.2.3 Rate constant

For humidity sensing purposes, most significant aging effects for azobenzene-containing thin films are changes in *cis* $\rightarrow$ *trans* thermal relaxation rate constant. In order to study these effects, rate of relaxation was measured periodically from the set of aging measurement samples in the Linkam measurement chamber with constant $T = 23 \pm 0.5$ °C and 50 ± 0.5 % RH. Results of these relaxation rate measurements over time are presented in Fig 4.16.

Relaxation rate constants in Fig 4.14 are presented as a function of time along with linear regression fit represented with a dashed line. Data is presented for $P4VP_{60k}$ samples with black colour and for $P4VP_{1.2k}$ samples in red, including error bars representing standard deviations in each set of measurements. Figure is divided into four graphs involving data from samples of a given mole fraction indicated in the top left corner of the graph. In addition to linear regression, a separate shape-preserving interpolar fit is presented for non-linear data from lower mole fraction $P4VP_{60k}$ samples.

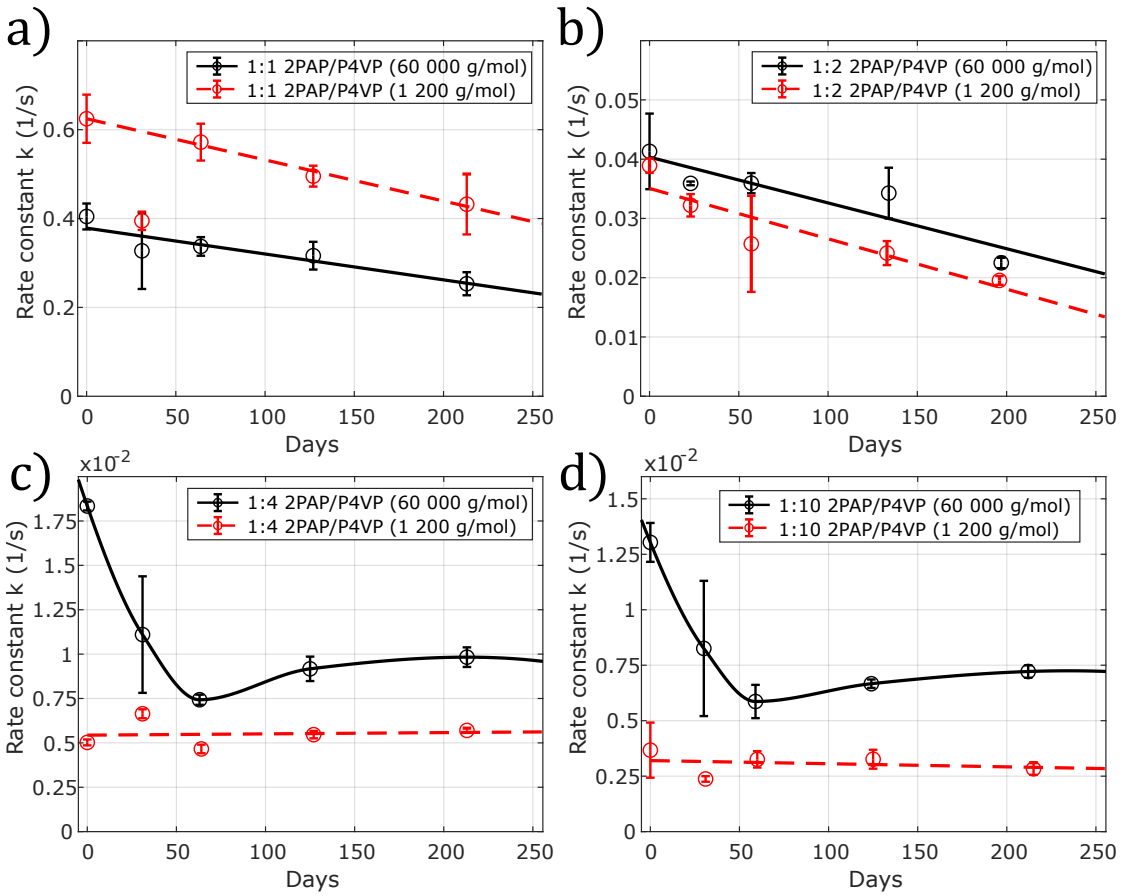

Figure 4.16. Isomerisation rate constants over time. *Rate constants as a function of time are presented for a) equimolar samples with mole fraction 1:1 as well as b) 1:2, c) 1:4 and d) 1:10 mole fractions for samples with more P4VP repeating units than 2PAP molecules. Long-chain polymer samples presented in black with a continuous line fitting and short-chain polymer samples in red with a dashed line fitting. Error bars are standard deviations in each set of measurements. Linear fit is applied to all other data sets except for long-chain samples in c) and d) where a shape-preserving interpolar fit is used to guide the eye.*

Equimolar samples exhibit moderately linear aging effects with relaxation rate over time. As shown in Fig 4.11 a), $P4VP_{1.2k}$ relaxes back to *trans* faster than $P4VP_{60k}$. However, this rate of relaxation slows down for $P4VP_{1.2k}$ over time with 30 % reduction in rate constant, translating to an increase in lifetime from 1.6 s to 2.3 s, whereas $P4VP_{60k}$ demonstrates almost 40 % reduction in rate constant with $\tau_{0\,\mathrm{d}} = 2.5$ s and $\tau_{213\,\mathrm{d}} = 4$ s, respectively. Aging effects for both polymer sample sets give no indication of saturation as the slow decrease in rate constant may continue for far longer than the studied 7-month timespan. Furthermore, clearly some random error occurred during the second set of measurements as rate constants for both sets of samples diverge from the linear regression describing the other measurements adequately.

Similar decrease in rate constants is visible in Fig 4.14 b) with $\chi = 1{:}2$ samples. In polymer sample sets, the rate constant is halved over the timespan of 213 days corresponding to an increase from $\tau_{0\,\mathrm{d}} = 25$ s to $\tau_{213\,\mathrm{d}} = 50$ s for $P4VP_{1.2k}$ and $\tau_{0\,\mathrm{d}} = 30$ s to $\tau_{213\,\mathrm{d}} = 60$ s for $P4VP_{60k}$. Aging effects appear continual and may indicate a longer period of slowing rate of relaxation over time. Also similar to equimolar samples, some mea-

surements involved notable random error. Linear regression for P4VP$_{60k}$ measurements is far from optimal but perhaps a random error occurred with the fourth measurement about 4 months after sample fabrication as the standard deviation is greatest. Random error for P4VP$_{1.2k}$ is easier to specify, however, as the third measurement has relatively massive standard deviation.

Both of the lower mole fraction sample sets reveal anomalous results for relaxation rate over time. While P4VP$_{1.2k}$ results align fairly well with linear regression and exhibit a change of $\Delta k_{1:4} = 10$ % and $\Delta k_{1:10} = 20$ %, P4VP$_{60k}$ samples do not align with the linear regression fit. Moreover, P4VP$_{60k}$ samples exhibit rebound-resembling behaviour in which rate constant decreases for the first two months and then recovers to somewhere close to relaxation rate 1 month after sample fabrication. Therefore, overall decrease in rate constant is only twofold for $\chi = 1{:}4$ and fourfold for $\chi = 1{:}10$, although lowest measured relaxation was four and six times slower, respectively. Prominent standard deviation is visible in the second measurement for both P4VP$_{60k}$ sample sets as well as divergence from linear regression with P4VP$_{1.2k}$ sample, indicating some random error caused significant error in measurements one month after sample fabrication.

In the light of results from Fig 4.16, optimal combination of molecular environment factors to avoid detrimental aging effects would be to use P4VP$_{1.2k}$ with $\chi = 1{:}4$. Alternatively P4VP$_{60k}$ polymer with $\chi = 1{:}4$ or $\chi = 1{:}10$ could prove suitable for commercial use after allowing the aging effects run their course prior to implementation. The effects of annealing on aging effects were also studied in part for $\chi = 1{:}4$ samples and the data suggest that longer annealing periods reduce the aging effects on rate constant over time. A threefold reduction in rate constant standard deviation over the timespan of 140 days was detected for samples that were annealed for 24 hours at 80 °C compared to samples without any annealing, as well as 40 % lower standard deviation compared to samples annealed for an hour prior to storage.

Annealing also halved the total change in rate constant over time for samples annealed for 24 hours with respect to unannealed samples. Rate constant for $\chi = 1{:}4$ samples annealed for 24 hours seemed to stabilise after 28 days with less than 10 % variation in rate constant. Given these results, storing the thin films for 6–8 months should suffice to reach the saturation stage of minor relaxation rate changes without extended annealing as illuminated with blue dashed line in Fig 4.16, and this stabilisation phase may be shortened to a month with sufficient annealing. Other molar weight and mole fraction combinations could also suffice if sensors are programmed to compensate for the change in rate constant due to aging effects. However, extensive further research is needed on the aging effects before existing data can be used to compensate for aging effects in humidity sensing.

4.3 Discussion

Results presented in previous sections affirm the potential azobenzenes hold in humidity sensing. With the proper selection of substituents, polymer, and mole fraction, azobenzene relaxation rate constant can be engineered in terms of stability, *cis* lifetime, dynamic range, and aging effects. Based on these results, we can design the optimal humidity sensor comprising of an azobenzene with hydrogen bond donor group, a hydrogen bond acceptor polymer, and a suitable mole fraction between these.

To avoid detrimental aging effects, mole fraction should not be equimolar. Optimal choice would be $\chi = 1 : 4$ and either $P4VP_{60k}$ or $P4VP_{1.2k}$. Heavier polymer offers affordable and easily available polymer while short-chain polymer promises less uncertainty with aging effects. From single-azobenzene film point of view, optimal sensor material for below 50 % RH measurements would be a NO_2-OH thin film, while measurements above 50 % RH could be conducted with a DMA-OH thin film. Sensor could also involve a MeO-OH thin film for enhanced resolution setting or replace DMA-OH in high RH sensing altogether if measuring relaxation rates up to $k \sim 10^1$ 1/s feasible. For sensors comprising of a single thin film, CN-OH demonstrates tolerable relaxation lifetime in low humidity while remaining below $k \sim 10^1$ 1/s relaxation rate in saturated humidity.

The most viable combination of molecules for sensor applications is DMA-OH, CN-OH and NO_2-NH_2. With conveniently compatible isosbestic points the combination of these three azobenzenes allows for measuring temperature as well as humidity in both low and high humidity. Forming suitable supramolecular complexes in thin films is simple in terms of fabrication, so sensor application is realisable and would serve as a tool for accurate RH sensing in both low and high RH. Future research is best aimed at discovering more alternative humidity-sensitive azobenzenes from push-pull systems as well as double donor systems, as with a more extensive library of humidity-sensitive azobenzenes the range of possible optimal combinations also expands.

Azobenzene-based thin film sensor has multiple angles to enter the humidity sensing market. In terms of humidity sensing range, theoretical capability for sensing extremely low (<10 % RH) or extremely high (>90 % RH) is demonstrated and Poutanen *et al* have reported successfully measuring humidity below (5 % RH) [101], so one definite advantage compared to existing solutions in humidity sensing is the ability to measure at extreme humidity. Similarly, isomerisation-based humidity sensing allows for highly accurate measurements. Using MeO-OH, dynamic range of 5 orders of magnitude can be used to accurately measure RH decimals and therefore compete with existing humidity sensors holding a market share with high accuracy in RH measurements. Undoubtedly further substitution design can yield even more sensitive molecules, and perhaps the leap in Pyr-OH relaxation rate can be harnessed in hypersensitive humidity sensing.

Perhaps the greatest challenge in productisation lies in competitive pricing. Numerous well-established service providers currently dominate the sales and entering the market with a new product and thus with limited testing raises questions of product viability. Given

the vast availability of reagents, thin film fabrication will most likely not be the limiting factor in competitive pricing. Furthermore, other components required for sensor applications presented in Fig 3.5 are common optics components and should be integrable into a sensor setup readily. As long as notable aging effects are avoided and sensor can apply multiple thin films to accommodate for different humidity ranges, azobenzene-based thin film humidity sensing shows great promise for commercial applications in the near future.

5 CONCLUSIONS AND OUTLOOK

This thesis delved into azobenzene thin films in humidity sensing applications. Theory part covered the basics of azobenzenes, photoisomerisation process and various applications of azobenzenes as well as various molecular environments azobenzenes can be studied in, in particular polymers. Additionally, a brief introduction into humidity sensing was given before elaborating how azobenzene photoisomerisation and subsequent thermal relaxation can be used to measure relative humidity.

To determine the parameters affecting azobenzene isomerisation rate and how azobenzene thin films are affected by aging affects, eight molecules were selected for a set of measurements with a spectrophotometer, polarised optical microscope (POM) and a thermal isomerisation setup. Studied molecules were para-substituted azobenzenes with hydrogen bond donor groups with which azobenzenes formed supramolecular polymer thin films with P4VP. Molecules were fabricated into thin films containing P4VP via spin coating, after which azobenzenes in films were photoisomerised from the thermodynamically stable *trans*-form to the metastable *cis*-form. The unstable isomer relaxed over time back to *trans* at a rate highly dependent on temperature and humidity. The rate of relaxation was measured in various humidity and constant temperature to study the humidity sensitivity of the molecules.

In addition to the humidity sensitivity of different azobenzenes, aging and molecular environment effects on relaxation were studied for a previously studied hydroxyazobenzene 2PAP. Sets of samples were fabricated with various mole fractions and polymer molar masses and subsequently studied over time. Absorption spectra, POM images and relaxation rate constants were used to compare aging effects on samples with different mole fraction and polymer molar mass, and the results from these measurements were used to form a basis for the design an optimal azobenzene thin film humidity sensor.

DMA-OH with slower relaxation rate than 2PAP proved to be best suited for high RH measurements, while CN-OH and NO_2-OH were better for low RH measurements faster than 2PAP relaxation rate. MeO-OH proved to be most sensitive with a dynamic range of 10^5, while NH_2-NH_2 and Pyr-OH proved far less humidity sensitive with dynamic range of 10^2. In addition, Pyr-OH demostrated a peculiar humidity sensitivity as the rate constant increases rapidly by over 60 times between 50–55 % RH while exhibiting typical logarithmic humidity dependence elsewhere in humidity range.

Aging effects revealed to be extensive. Although no aggregation or spectral shift was observed during the 213 days of aging study, changes in absorbance maxima and relaxation rate were reported. Furthermore, both mole fraction and polymer molar mass proved to affect the isomerisation rate. In conclusion, optimal combination for humidity sensing is to use 1:4 mole fraction and either molar mass polymer, although 60 000 g/mol is more readily available and affordable. Commercially competitive humidity sensor could be devised from using CN-OH thin film for below 50 % RH measurements, DMA-OH for above 50 % RH and NO_2-NH_2 for temperature sensing. Alternatively, MeO-OH would be best suited for enhanced resolution setting.

As long as notable aging effects are avoided and sensor can apply multiple thin polymer films or multiple azobenzenes in a single thin film to accommodate for different humidity ranges, azobenzene-based thin film humidity sensing shows great promise for commercial applications in the near future. These sensors can compete with existing solutions in humidity sensing range using multiple azobenzenes to measure different humidity ranges, measurement accuracy due to their large dynamic range and cost-effective reagents and optical components to ensure competitive pricing.

This thesis unravelled a myriad of interesting topics for further research with potential commercial applications. Firstly, aging effects in azobenzene thin films are still not fully understood. Gaining a comprehensive understanding of the factors affecting especially azobenzene relaxation rate over time would solidify the potential for commercial applications. With the aging effects still in part uncertain, reliability of humidity sensing can be questioned. Moreover, this thesis confirmed the effect of polymer molar mass on azobenzene isomerisation rate. It remains to be studied to what extent there is a relationship between isomerisation rate and molar mass of the polymer in the molecular environment of the azobenzene in the thin film.

Lastly, further research on alternative substituents and their effect on humidity sensitivity would most certainly uncover new azobenzenes with superior humidity sensitivity. Similarly valuable would be to study which substituents enable humidity sensing in azobenzenes as working hypothesis is that azobenzene must be able to tautomerise. Particularly interesting would be to discover why NO_2-NH_2 lacks humidity dependence, if the humidity insensitivity extends to other pseudostilbenes and how the Pyr-OH humidity dependence is between 50–55 % RH and whether its immense dynamic range could be utilised in low or high humidity sensing. In any event, this thesis is yet another demonstration that azobenzenes are still and will be relevant for cutting-edge photonics research and applications for years to come.

REFERENCES

[1] Soref, R. Silicon photonics: a review of recent literature. *Silicon* 2 (2010), 1–6.

[2] Clark, J. and Lanzani, G. Organic photonics for communications. *Nature photonics* 4 (2010), 438–446.

[3] IUPAC. "Azo compounds", Compendium of Chemical Terminology, 2nd ed. (the "Gold Book"). Compiled by A. D. McNaught and A. Wilkinson. Online version (2019-) created by S. J. Chalk. (2014).

[4] Demselben. Ueber das Stickstoffbenzid. *Annalen der Pharmacie* 12 (1834), 311–314.

[5] Noble, A. III. Zur Geschichte des Azobenzols und des Benzidins. *Justus Liebigs Annalen der Chemie* 98 (1856), 253–256.

[6] Hunger, K. *Industrial dyes: chemistry, properties, applications*. Druckhaus Darmstadt GmbH, Darmstadt: John Wiley & Sons, 2007.

[7] Griffiths, J. II. Photochemistry of azobenzene and its derivatives. *Chem. Soc. Rev.* 1 (1972), 481–493.

[8] Kumar, G. S. and Neckers, D. Photochemistry of azobenzene-containing polymers. *Chemical Reviews* 89 (1989), 1915–1925.

[9] Bléger, D. and Hecht, S. Strategies for Switching with Visible Light, Chapter 4 in Photon-Working Switches by Yokoyama, Y. and Keitaro N. *Photon-Working Switches*. Springer, 2017, 93–114.

[10] Zhang, H., Jiang, X., Wu, W. and Mo, Y. Electron conjugation versus π–π repulsion in substituted benzenes: why the carbon–nitrogen bond in nitrobenzene is longer than in aniline. *Phys. Chem. Chem. Phys.* 18 (2016), 11821–11828.

[11] Law, J. and Rennie, R. *Aromatic compound*. Oxford University Press. 2020. Read 12.4.2020, available at https://www.oxfordreference.com/view/10.1093/acref/9780198841227.001.0001/acref-9780198841227-e-315.

[12] Yager, K. and Barrett, C. Azobenzene polymers for photonic applications, Chapter 1 in Smart Light-Responsive Materials: Azobenzene-Containing Polymers and Liquid Crystals by Y. Zhao and T. Ikeda. (2009).

[13] Peretti, J., Biteau, J., Boilot, J.-P., Chaput, F., Safarov, V., Lehn, J.-M. and Fernandez-Acebes, A. Remanent photoinduced birefringence in thin photochromic sol–gel films. *Applied physics letters* 74 (1999), 1657–1659.

[14] Sekkat, Z. and Knoll, W. *Photoreactive organic thin films*. Amsterdam, Academic Press: Elsevier, 2002.

[15] Yager, K. and Barrett, C. Azobenzene Polymers as Photomechanical and Multifunctional Smart Materials, Chapter 17 in Intelligent Materials by Shahinpoor, M. and Schneider, H.-J. Cambridge: Royal Society of Chemistry, 2008, 424–446.

[16] Bandara, H. D. and Burdette, S. C. Photoisomerization in different classes of azobenzene. *Chemical Society Reviews* 41 (2012), 1809–1825.

[17] Priimägi, A. *Polymer-azobenzene complexes: from supramolecular concepts to efficient photoresponsive polymers*. TKK dissertations. Teknillinen korkeakoulu, Espoo., 2009.

[18] Yager, K. G. and Barrett, C. J. Novel photo-switching using azobenzene functional materials. *Journal of Photochemistry and Photobiology A: Chemistry* 182 (2006), 250–261.

[19] Watson, L. *Azobenzene: Aspects, Applications, and Research*. Nova Science Publishers, New York, 2017.

[20] Daley, R. *Organic Chemistry, Part 1 of 3*. Lulu.com, Online, 2005.

[21] Johnson, C. D., Johnson, C. D. et al. *The Hammett Equation*. Cambridge University Press; 1 edition, Cambridge, 1973.

[22] Chiu, K. Y., Tran, T. T. H., Wu, C.-G., Chang, S.-H., Yang, T.-F. and Su, Y. O. Electrochemical studies on triarylamines featuring an azobenzene substituent and new application for small-molecule organic photovoltaics. *Journal of Electroanalytical Chemistry* 787 (2017), 118–124.

[23] Hansch, C. and Leo, A. *Substituent Constants for Correlation Analysis in Chemistry and Biology*. Wiley, Michigan, 1979.

[24] Hansch, C., Leo, A. and Taft, R. A survey of Hammett substituent constants and resonance and field parameters. *Chemical reviews* 91 (1991), 165–195.

[25] Favre, H. and Powell, W. *Nomenclature of Organic Chemistry: IUPAC Recommendations and Preferred Names 2013*. Royal Society of Chemistry, Cambridge, UK, 2013.

[26] Hartley, G. S. The cis-form of azobenzene. *Nature* 140 (1937), 281–281.

[27] Henzl, J., Mehlhorn, M., Gawronski, H., Rieder, K.-H. and Morgenstern, K. Reversible cis–trans isomerization of a single azobenzene molecule. *Angewandte Chemie International Edition* 45 (2006), 603–606.

[28] Sekkat, Z., Wood, J. and Knoll, W. Reorientation mechanism of azobenzenes within the trans→cis photoisomerization. *The Journal of Physical Chemistry* 99 (1995), 17226–17234.

[29] Koshima, H., Ojima, N. and Uchimoto, H. Mechanical motion of azobenzene crystals upon photoirradiation. *Journal of the American Chemical Society* 131 (2009), 6890–6891.

[30] Matharu, A. and Ramanujam, P. Photochromic Polymers for Optical Data Storage: Azobenzenes and Photodimers, Chapter 6 in Photochemistry and photophysics of polymeric materials by Allen, N. S. John Wiley & Sons, Hoboken, New Jersey, 2010, 209–234.

[31] Towns, A. Industrial Photochromism, Chapter 5 in Applied Photochemistry: When Light Meets Molecules by Bergamini, G. and Silvi, S. Springer International Publishing Cham, Switzerland, 2016.

[32] Taketsugu, T. and Harabuchi, Y. Ab Initio Molecular Dynamics Study on Photoisomerization Reactions: Applications to Azobenzene and Stilbene, Chapter 18 in Frontiers of Quantum Chemistry by Wójcik, M., Nakatsuji, H., Kirtman, B.and Ozaki, Y. Singapore: Springer Singapore, 2018, 431–453.

[33] Sindhu, A., Pradhan, R., Lourderaj, U. and Paranjothy, M. Theoretical investigation of the isomerization pathways of diazenes: torsion vs. inversion. *Physical Chemistry Chemical Physics* 21 (2019), 15678–15685.

[34] Lednev, I. K., Ye, T.-Q., Hester, R. E. and Moore, J. N. Femtosecond time-resolved UV- visible absorption spectroscopy of trans-azobenzene in solution. *The Journal of Physical Chemistry* 100 (1996), 13338–13341.

[35] Russew, M.-M. and Hecht, S. Photoswitches: from molecules to materials. *Advanced Materials* 22 (2010), 3348–3360.

[36] Renth F. Bahrenburg, J. and Temps, F. Ultrafast Photoswitching Dynamics of Azobenzenes with Intraand Intermolecular Constraints, Chapter 12 in Photon-Working Switches by Yokoyama, Y. and Keitaro N. *Photon-Working Switches*. Springer, Japan, 2017, 237–259.

[37] Siewertsen, R., Schönborn, J. B., Hartke, B., Renth, F. and Temps, F. Superior Z $\rightarrow$ E and E $\rightarrow$ Z photoswitching dynamics of dihydrodibenzodiazocine, a bridged azobenzene, by S 1 (n π*) excitation at λ= 387 and 490 nm. *Physical Chemistry Chemical Physics* 13 (2011), 1054–1063.

[38] Garcia-Amoros, J., Diaz-Lobo, M., Nonell, S. and Velasco, D. Fastest thermal isomerization of an azobenzene for nanosecond photoswitching applications under physiological conditions. *Angewandte Chemie International Edition* 51 (2012), 12820–12823.

[39] Shiraishi, Y., Itoh, M. and Hirai, T. Thermal isomerization of spiropyran to merocyanine in aqueous media and its application to colorimetric temperature indication. *Physical Chemistry Chemical Physics* 12 (2010), 13737–13745.

[40] Hatano, S., Horino, T., Tokita, A., Oshima, T. and Abe, J. Unusual negative photochromism via a short-lived imidazolyl radical of 1, 1'-binaphthyl-bridged imidazole dimer. *Journal of the American Chemical Society* 135 (2013), 3164–3172.

[41] Helmy, S., Leibfarth, F. A., Oh, S., Poelma, J. E., Hawker, C. J. and Read de Alaniz, J. Photoswitching using visible light: A new class of organic photochromic molecules. *Journal of the American Chemical Society* 136 (2014), 8169–8172.

[42] Helmy, S., Oh, S., Leibfarth, F. A., Hawker, C. J. and Read de Alaniz, J. Design and synthesis of donor–acceptor stenhouse adducts: a visible light photoswitch derived from furfural. *The Journal of organic chemistry* 79 (2014), 11316–11329.

[43] Bléger, D., Schwarz, J., Brouwer, A. M. and Hecht, S. o-Fluoroazobenzenes as readily synthesized photoswitches offering nearly quantitative two-way isomerization with visible light. *Journal of the American Chemical Society* 134 (2012), 20597–20600.

[44] Ahmed, Z., Siiskonen, A., Virkki, M. and Priimagi, A. Controlling azobenzene photoswitching through combined ortho-fluorination and-amination. *Chemical communications* 53 (2017), 12520–12523.

[45] Dabrowa, K., Niedbała, P. and Jurczak, J. Engineering Light-Mediated Bistable Azobenzene Switches Bearing Urea D-Aminoglucose Units for Chiral Discrimination of Carboxylates. *The Journal of organic chemistry* 81 (2016), 3576–3584.

[46] Dong, L., Feng, Y., Wang, L. and Feng, W. Azobenzene-based solar thermal fuels: design, properties, and applications. *Chemical Society Reviews* 47 (2018), 7339–7368.

[47] Irie, M., Fukaminato, T., Matsuda, K. and Kobatake, S. Photochromism of diarylethene molecules and crystals: memories, switches, and actuators. *Chemical Reviews* 114 (2014), 12174–12277.

[48] Andersson, J.-Å., Petterson, R. and Tegnér, L. Flash photolysis experiments in the vapour phase at elevated temperatures I: spectra of azobenzene and the kinetics of its thermal cis-trans isomerization. *Journal of Photochemistry* 20 (1982), 17–32.

[49] Homocianu, M., Fifere, N. and Airinei, A. Azobenzene: research progress and its reflections in applications, Chapter 1 in Azobenzene Aspects, Applications and Research by Watson, L. Nova Science, New York, 2017, 1–27.

[50] Whitten, D. G., Wildes, P. D., Pacifici, J. and Irick Jr, G. Solvent and substituent on the thermal isomerization of substituted azobenzenes. Flash spectroscopic study. *Journal of the American Chemical Society* 93 (1971), 2004–2008.

[51] Cusati, T., Granucci, G. and Persico, M. Photodynamics and time-resolved fluorescence of azobenzene in solution: a mixed quantum-classical simulation. *Journal of the American Chemical Society* 133 (2011), 5109–5123.

[52] Yoon, J. H. and Yoon, S. Photoisomerization of azobenzene derivatives confined in gold nanoparticle aggregates. *Physical Chemistry Chemical Physics* 13 (2011), 12900–12905.

[53] Titov, E., Lysyakova, L., Lomadze, N., Kabashin, A. V., Saalfrank, P. and Santer, S. Thermal cis-to-trans isomerization of azobenzene-containing molecules enhanced by gold nanoparticles: an experimental and theoretical study. *The Journal of Physical Chemistry C* 119 (2015), 17369–17377.

[54] Chu, Z., Han, Y., Bian, T., De, S., Král, P. and Klajn, R. Supramolecular control of azobenzene switching on nanoparticles. *Journal of the American Chemical Society* 141 (2018), 1949–1960.

[55] Hashim, A. A. *Polymer thin films*. IntechOpen, Online, 2010.

[56] Stachurski, Z. H. *Fundamentals of amorphous solids: structure and properties*. Weinheim, Germany: John Wiley & Sons, 2015.

[57] Kasha, M., Rawls, H. R. and El-Bayoumi, M. A. The exciton model in molecular spectroscopy. *Pure and Applied Chemistry* 11 (1965), 371–392.

[58] Hestand, N. J. and Spano, F. C. Molecular aggregate photophysics beyond the Kasha model: novel design principles for organic materials. *Accounts of chemical research* 50 (2017), 341–350.

[59] Jelley, E. E. Spectral absorption and fluorescence of dyes in the molecular state. *Nature* 138 (1936), 1009–1010.

[60] Delaire, J. A. and Nakatani, K. Linear and nonlinear optical properties of photochromic molecules and materials. *Chemical Reviews* 100 (2000), 1817–1846.

[61] Wang, K., Yin, L., Miu, T., Liu, M., Zhao, Y., Chen, Y., Zhou, N., Zhang, W. and Zhu, X. Design and synthesis of a novel azobenzene-containing polymer both in the main-and side-chain toward unique photocontrolled isomerization properties. *Materials Chemistry Frontiers* 2 (2018), 1112–1118.

[62] Weber, C., Liebig, T., Gensler, M., Pithan, L., Bommel, S., Bléger, D., Rabe, J. P., Hecht, S. and Kowarik, S. Light-controlled “molecular zippers” based on azobenzene main chain polymers. *Macromolecules* 48 (2015), 1531–1537.

[63] Lehn, J.-M. Towards complex matter: supramolecular chemistry and self-organization. *European Review* 17 (2009), 263–280.

[64] Schneider, H.-J. Supramolecular Polymers, Chapter 12 in Applications of supramolecular chemistry. CRC Press, USA, 2012.

[65] Hu, D., Hu, Y., Huang, W. and Zhang, Q. Two-photon induced data storage in hydrogen bonded supramolecular azopolymers. *Optics Communications* 285 (2012), 4941–4945.

[66] Kuo, S.-W. Hydrogen-bonding in polymer blends. *Journal of Polymer Research* 15 (2008), 459–486.

[67] Ji, G., Yang, Z., Zhang, H., Zhao, Y., Yu, B., Ma, Z. and Liu, Z. Hierarchically Mesoporous o-Hydroxyazobenzene Polymers: Synthesis and Their Applications in CO2 Capture and Conversion. *Angewandte Chemie International Edition* 55 (2016), 9685–9689.

[68] Vapaavuori, J., Grosrenaud, J., Siiskonen, A., Priimagi, A., Pellerin, C. and Bazuin, C. G. Photocontrol of Supramolecular Azo-Containing Block Copolymer Thin Films during Dip-Coating: Toward Nanoscale Patterned Coatings. *ACS Applied Nano Materials* 2 (2019), 3526–3537.

[69] Garcia-Amorós, J. and Velasco, D. Understanding the fast thermal isomerisation of azophenols in glassy and liquid-crystalline polymers. *Physical Chemistry Chemical Physics* 16 (2014), 3108–3114.

[70] Antonov, L. *Tautomerism: methods and theories*. Weinheim, Germany: John Wiley & Sons, 2013.

[71] Alkorta, I., Goya, P., Elguero, J. and Singh, S. P. A simple approach to the tautomerism of aromatic heterocycles. *National Academy Science letters* 30 (2007), 139.

[72] Poutanen, M., Ikkala, O. and Priimagi, A. Structurally controlled dynamics in azobenzene-based supramolecular self-assemblies in solid state. *Macromolecules* 49 (2016), 4095–4101.

[73] Rosales, A. M., Rodell, C. B., Chen, M. H., Morrow, M. G., Anseth, K. S. and Burdick, J. A. Reversible control of network properties in azobenzene-containing hyaluronic acid-based hydrogels. *Bioconjugate chemistry* 29 (2018), 905–913.

[74] Bahram, M., Mohseni, N. and Moghtader, M. An introduction to hydrogels and some recent applications, Chapter 2 in Emerging concepts in analysis and applications of hydrogels by Majee, S. B. IntechOpen, Online, 2016.

[75] Puntoriero, F., Ceroni, P., Balzani, V., Bergamini, G. and Vögtle, F. Photoswitchable dendritic hosts: a dendrimer with peripheral azobenzene groups. *Journal of the American Chemical Society* 129 (2007), 10714–10719.

[76] Koskela, J. E., Liljeström, V., Lim, J., Simanek, E. E., Ras, R. H., Priimagi, A. and Kostiainen, M. A. Light-fuelled transport of large dendrimers and proteins. *Journal of the American Chemical Society* 136 (2014), 6850–6853.

[77] Mosciatti, T., Bonacchi, S., Gobbi, M., Ferlauto, L., Liscio, F., Giorgini, L., Orgiu, E. and Samori, P. Optical input/electrical output memory elements based on a liquid crystalline azobenzene polymer. *ACS applied materials & interfaces* 8 (2016), 6563–6569.

[78] Fuhrmann, T. and Tsutsui, T. Synthesis and properties of a hole-conducting, photopatternable molecular glass. *Chemistry of materials* 11 (1999), 2226–2232.

[79] Virkki, M., Tuominen, O., Kauranen, M. and Priimagi, A. Photoinduced nonlinear optical response in azobenzene-functionalized molecular glass. *Optics express* 24 (2016), 4964–4971.

[80] *Humidity*. Encyclopaedia Britannica, Online, 2020.

[81] Wernecke, R. and Wernecke, J. *Industrial moisture and humidity measurement: a practical guide*. Weinheim, Germany: John Wiley & Sons, 2013.

[82] Lee, C.-Y. and Lee, G.-B. Humidity sensors: a review. *Sensor Letters* 3 (2005), 1–15.

[83] Buck, A. L. New equations for computing vapor pressure and enhancement factor. *Journal of applied meteorology* 20 (1981), 1527–1532.

[84] Lide, D. R. *CRC handbook of chemistry and physics*. Vol. 85. CRC press, USA, 2004.

[85] Morris, A. S. and Langari, R. Summary of Other Measurements, Chapter 21 in Measurement and instrumentation: theory and application 2nd Edition. Academic Press, Amsterdam, 2016, 633–672.

[86] Chen, Z. and Lu, C. Humidity sensors: a review of materials and mechanisms. *Sensor letters* 3 (2005), 274–295.

[87] Scholz, G. Marktanalyse: Sensoren und Meßgeräte für Gasfeuchte/Market analysis: Sensors and instruments for gas humidity. *tm-Technisches Messen* 59 (1992), 88–109.

[88] Yang, H., Ye, Q., Zeng, R., Zhang, J., Yue, L., Xu, M., Qiu, Z.-J. and Wu, D. Stable and fast-response capacitive humidity sensors based on a ZnO nanopowder/PVP-RGO multilayer. *Sensors* 17 (2017), 2415.

[89] Boudaden, J., Steinmaßl, M., Endres, H.-E., Drost, A., Eisele, I., Kutter, C. and Müller-Buschbaum, P. Polyimide-based capacitive humidity sensor. *Sensors* 18 (2018), 1516.

[90] Qi, R., Zhang, T., Guan, X., Dai, J., Liu, S., Zhao, H. and Fei, T. Capacitive humidity sensors based on mesoporous silica and poly (3, 4-ethylenedioxythiophene) composites. *Journal of Colloid and Interface Science* 565 (2020), 592–600.

[91] Park, K.-J. and Gong, M.-S. A water durable resistive humidity sensor based on rigid sulfonated polybenzimidazole and their properties. *Sensors and Actuators B: Chemical* 246 (2017), 53–60.

[92] Burman, D., Santra, S., Pramanik, P. and Guha, P. K. Pt decorated MoS2 nanoflakes for ultrasensitive resistive humidity sensor. *Nanotechnology* 29 (2018), 115504.

[93] Ascorbe, J., Corres, J. M., Arregui, F. J. and Matias, I. R. Recent developments in fiber optics humidity sensors. *Sensors* 17 (2017), 893.

[94] Luo, Y., Chen, C., Xia, K., Peng, S., Guan, H., Tang, J., Lu, H., Yu, J., Zhang, J., Xiao, Y. et al. Tungsten disulfide (WS 2) based all-fiber-optic humidity sensor. *Optics express* 24 (2016), 8956–8966.

[95] Foskett, L. W. and Foster, N. B. A spectroscopic hygrometer. *Bulletin of the American Meteorological Society* 24 (1943), 146–153.

[96] Sorli, B., Pascal-Delannoy, F., Giani, A., Foucaran, A. and Boyer, A. Fast humidity sensor for high range 80–95% RH. *Sensors and Actuators A: Physical* 100 (2002), 24–31.

[97] Buchberger, A., Peterka, S., Coclite, A. M. and Bergmann, A. Fast Optical Humidity Sensor Based on Hydrogel Thin Film Expansion for Harsh Environment. *Sensors* 19 (2019), 999.

[98] Squillaci, M. A., Zhong, X., Peyruchat, L., Genet, C., Ebbesen, T. W. and Samori, P. 2D hybrid networks of gold nanoparticles: mechanoresponsive optical humidity sensors. *Nanoscale* 11 (2019), 19315–19318.

[99] Chen, M., Xue, S., Liu, L., Li, Z., Wang, H., Tan, C., Yang, J., Hu, X., Jiang, X.-F., Cheng, Y. et al. A highly stable optical humidity sensor. *Sensors and Actuators B: Chemical* 287 (2019), 329–337.

[100] Xu, J., Bertke, M., Li, X., Gad, A., Zhou, H., Wasisto, H. S. and Peiner, E. Gravimetric humidity sensor based on ZnO nanorods covered piezoresistive Si microcantilever. *Smart Sensors, Actuators, and MEMS VIII*. Vol. 10246. International Society for Optics and Photonics. 2017, 10246–11.

[101] Poutanen, M., Ahmed, Z., Rautkari, L., Ikkala, O. and Priimagi, A. Thermal isomerization of hydroxyazobenzenes as a platform for vapor sensing. *ACS macro letters* 7 (2018), 381–386.

[102] Caron, S. Electrophilic Aromatic Substitution, Chapter 5 in Practical synthetic organic chemistry: reactions, principles, and techniques. John Wiley & Sons, USA, 2020, 255–277.

[103] Pohanish, R. P. *Sittig's handbook of toxic and hazardous chemicals and carcinogens*. William Andrew, USA, 2017.

[104] Li, M.-J. and Zeng, T. The deleterious effects of N, N-dimethylformamide on liver: A mini-review. *Chemico-biological interactions* 298 (2019), 129–136.

[105] *Chloroform Safety Data Sheet*. Global Safety Management Inc., Online, 2015.

[106] *N,N-Dimethylformamide Safety Data Sheet*. Thermo Fisher Scientific, Online, 2018.

[107] Dahman, Y. *Nanotechnology and functional materials for engineers*. Amsterdam, Netherlands: Elsevier, 2017.

[108] Tuziuti, T. Influence of sonication conditions on the efficiency of ultrasonic cleaning with flowing micrometer-sized air bubbles. *Ultrasonics sonochemistry* 29 (2016), 604–611.

[109] Yilbas, B. S., Al-Sharafi, A. and Ali, H. Surfaces for Self-Cleaning, Chapter 3 in Self-Cleaning of Surfaces and Water Droplet Mobility. Elsevier, Amsterdam, Netherlands, 2019, 45–98.

[110] Ossila. *Spin Coating: Complete Guide to Theory and Techniques.* Ossila, 2020. Online, read on 26.04.2020. Available at https://www.ossila.com/pages/spin-coating.

[111] Mishra, A., Bhatt, N. and Bajpai, A. Nanostructured superhydrophobic coatings for solar panel applications, Chapter 12 in Nanomaterials-Based Coatings by Tri, P., Rtimi, S. and Plamondon, C. Elsevier, Amsterdam, Netherlands, 2019, 397–424.

[112] Zhang, J. X. and Hoshino, K. *Molecular Sensors and Nanodevices: Principles, Designs and Applications in Biomedical Engineering*. Academic Press, USA, 2018.

[113] Kohli, R. and Mittal, K. *Developments in Surface Contamination and Cleaning, Volume 8 - Cleaning Techniques*. Elsevier, Oxford, UK, 2015.

[114] Sinturel, C., Vayer, M., Morris, M. and Hillmyer, M. A. Solvent vapor annealing of block polymer thin films. *Macromolecules* 46 (2013), 5399–5415.

[115] Embar-Seddon, A. and Pass, A. *Forensic Science*. v. 3. Salem Press, Ipswich, Massachusetts, 2015.

[116] *Fiber-Coupled LEDs*. Thorlabs, Inc., Online, 2020, read on 26.04.2020. Available at https://www.thorlabs.com/newgrouppage9.cfm?objectgroup_id=5206.